Center of Excellence for Explosive Detection, Mitigation and Response

Center of Excellence for Explosive Detection, Mitigation and Response

A Department of Homeland Security

Center of Excellence

University of Rhode Island (URI);

California Institute of Technology; Purdue University

New Mexico State University; University of Illinois

Florida International University Hebrew University, Jerusalem Israel

Weizmann Institute of Science

Fourth Annual Report

July 2012-September 2013

DHS agreement number: 2008-ST-061-ED0002

Table of Contents

Introduction 1

Characterization

1.1 Characterization of Homemade Explosives 8
Jimmie Oxley & James Smith (URI)

1.2 Theoretical Projects 12
Ronnie Kosloff (Hebrew U) & Yehuda Zeiri (BGU)

1.3 Characterization of Non-Ideal Explosives
S. F. Son, L. J. Groven, D. R. Guildenbecher and R. S. Janesheski 19

1.4 Simulants for Canines & IMS Explosive Detection Systems 21
Jose Almirall (FIU)

1.5 Adhesion Studies 23
Merav Zeira, Boris Israel, Yehuda Zeiri (Ben Gurien U)

Detection

2.1 Explosives Sensor Enhancement
William Euler (URI) 29

2.2 Detection of Explosives and Explosives Precursors 31
Otto Gregory (URI)

2.3 Development of Resonating Nanocantilever Chemical Vapor Sensors and Thiol Encapsulated Gold Nanoparticle Chemiresistors 38
Nathan S. Lewis (Cal Tech)

2.4 Gas Phase Ion Chemistry and Non-Contact Sampling of Explosives 44
Gary Eiceman (NMSU)

2.5 Shaped Femtosecond Pulses for Remote Chemical Detection 48
Yaron Silberberg (Weizmann)

2.6 SERS Method for Detection of Ultra-Low Levels of Explosives in Complex Matrices 52
Radha Narayanan (URI)

2.7 X-ray Bottle Screener Simulant Project 59
Jimmie Oxley, James Smith

Mitigation

3.1 Development of Novel Composite Materials & Structures for Blast Mitigation
Arun Shukla (URI) 63

3.2 Development of Structural Steel with Higher Blast/Thermal Resistance 69
H. Ghonem (URI)

3.3 Structural Response to Non-ideal Explosions 78
J. E. Shepherd, J. Damazo, N. Bitter, J. Odell (California Institute of Technology)

3.4 Stress Attenuation by Means of Particulates 87
Carl Rousseau (URI)

3.5 Self-Healing Materials for Autonomic Mitigation of Blast Damage 90
Sottos & White (U Illinois)

3.6 Self-Healing Concrete 100
Arijit Bose (URI)

3.7 Water Blast Mitigation
S. F. Son, A. Zakrajsek, L. Groven, D. Guildenbecher 102

Appendices (available in separate file: 2012.CEEDMR.Report.pdf)

5.1.1.1 Synthesis and Characterization of Urea Nitrate and Nitro Urea
Jimmie Oxley, James Smith

5.1.1.2 Characterization and Analysis of Tetranitrate Esters
Jimmie Oxley, James Smith

5.1.1.3 Factors Influencing Triacetone Triperoxide (TATP) and Diacetone Diperoxide (DADP) Formation: Part I
Jimmie Oxley, James Smith

5.1.2.1 Role of Metal Ions in the Destruction of TATP: Theoretical Considerations
Ronnie Kosloff, Jimmie Oxley, James Smith, and Yehuda Zeiri

5.1.2.2 Density-Dependent Liquid Nitromethane decomposition: Molecular Dynamics Simulations on ReaxFF
Yehuda Zeiri, Ronnie Kosloff

5.1.2.3 Molecular Dynamics Simulations of Weak Detonations
Yehuda Zeiri, Ronnie Kosloff

5.1.3 Detonation Failure Characterization of Non-Ideal Explosives
Steven Son

5.1.4 Fast Detection of Triacetone Triperoxide (TATP) from Headspace Using Planar Solid-phase Microextraction (PSPME) Coupled to an IMS Detector
James Smith, Jimmie Oxley, Jose Almirall

5.1.5 The Adhesion of Particles of Standard Explosives to Model Surfaces
Yehuda Zeiri

5.2.3 Composites of Carboxylate-capped TiO_2 Nanoparticles and Carbon Black as Chemiresistive Vapor Barriers
Nathan Lewis

5.2.4 The Kinetics of the Thermal Decomposition of the Chloride Adduct of Ethylene Glycol di-nitrate: An Ion Mobility Spectrometry and *ab initio* Calculation Study
G. Eiceman

5.2.5 Solution-based Direct Readout Surface Enhanced Raman Spectroscopic (SERS) Detection of ultra-low Levels of Thiram with Dogbone Shaped Gold Nanoparticles
Radha Narayanan

5.2.6 Standoff Detection via Single-beam Spectral Notch Filtered Pulses
Yaron Silberberg

5.3.1 Development of Novel Composite Materials & Structures for Blast Mitigation
Arun Shukla

5.3.3 Boundary Layer Profile Behind Gaseous Detonation as it Affects Reflected Shock Wave Bifurcation
Joseph Shepherd

5.3.7 Appendix: Experiments and Analysis of Water-sheet Breakup and Mitigating Potential Under Blast Loading
Steven Son

Center of Excellence Explosives
Fourth Annual Report

The goal of this CoE in Explosives is to mitigate the worldwide explosive threat, both today and in the future. To reach that goal, URI has maintained four thrust areas Characterization, Detection, Mitigation, and Education. In addition, one project has been designated as E-2-E. A second one awaits funding for such designation E-2-E.

Characterization

For the present and near term, studies are aimed at physical characterization of novel explosives and explosives signatures, along with determination of thermal stability and sensitivity (1.1). This information is available to the community within weeks by publication on the URI Explosive Database, journal publication, and classes. Beyond that is the need to understand the mechanism of material formation and destruction with the goal of hindering or facilitating these events (1.1). Looking to the future we believe it is high priority to identify and prioritize the list of potential threats. Therefore, we are taking two approaches to identifying potential explosives—a comprehensive theoretical approach which involves prediction of physical properties and hazards (1.2) and an experimental approach (1.3). Enhanced sample collection is addressed both by an experimental approach based on micro-extraction for the capture of extremely small quantities of the volatile compounds (1.4) and a survey of potential materials using atomic force microscopy (1.5).

Detection

Vapor: Progress continues towards development of sensors that are sensitive, selective and able to detect trace levels of explosives. A number of novel sensors are being developed. The sensors employ two orthogonal spectral techniques; surface enhanced Raman scattering (SERS) and metal enhanced fluorescence (MEF). Due to the light absorbing properties of TNT and its quenching capabilities the MEF component was shown to be particularly sensitive to TNT (2.1, 2.6). Another approach is detecting explosive vapors via use of a nano-cantilever (2.3). The response of these sensors is due to two mechanisms; one that affects mass accumulation to the sensor and another that affects its stiffness. Modeling studies suggest that the response of the nano-cantilever to vapor appears to be due more to change in the sensor spring constant rather than accumulation of mass. Also investigated are nano-particle chemi-resistor sensors. Applications of organic capping groups impart electrical conductivity to the films on these sensors.

Standoff: "Shaper-less" standoff remote detection from distances of up to 50 meters has been demonstrated using fempto-second pulses shaped by a photonic crystal filter. Progress continues in the effort to improve the detection scheme (2.5).

Particulate: The fundamental behavior of ions in ion mobility spectrometers (IMS) continues to be studied. To this end a kinetic dual shutter IMS with a gas chromatograph interface was constructed. This instrument successfully characterized ion lifetimes, energies, and kinetics of decomposition of gas phase ions of energetic materials. Studies are in progress on as many explosives in the nitro-alkane and nitro-aromatic family as possible (2.4)

Bulk: Initial focus was on creating simulants for a particular X-ray detection instrument, an AS&E bottle screener. Success in that endeavor resulted in a shift of emphasis from creating simulants to creating a simulant development method. Recent efforts have focus on acquiring routine access to x-ray instruments (2.7).

Mitigation

In the mitigation thrust area the approach is diverse from technologies that mitigate the effect of the blast (3.7) to new sandwich compounds and functionally graded materials that more readily withstand blast (3.1). New metrics of assessing material stress (3.4) as well as non-ideal explosive events (3.3) are under development. Already to the commercialization stage are techniques for manufacturing self-healing materials polymers (3.5) and cements (3.6).

Engage to Excellence

An outstanding success has been achieved in our **E-2-E** project (3.2)—the development of a new steel with a significantly high blast resistance. This has been accomplished through a systematic numerical/analytical/experimental approach carried out by Professor Hamouda Ghonem and his research group over four years of funding. First, they established metrics for rating the residual strength of steel under post blast conditions. For this purpose, they built an advanced gas gun capable of delivering a blast pressure of 25 GPa at 1000 m/s. Joining this unique gas gun with Split-Hopkinson Pressure Bar and ECAP severe plastic deformation system, blast testing of steel with different microstructures and compositions could be routinely accomplished in the URI-Mechanics of Materials Research lab. These testing facilities coupled with numerical simulation techniques are used to develop pre-strained steel with a blast resistance up to 12 GPa of blast pressure as opposed to that of present steels which is best assessed as 4 GPa. These efforts in the DHS Center have been assisted by FM Global and US Steel. The application significance of this steel is its potential in retrofitting of tunnels and doming of nuclear reactors with a steel fiber mesh to act as self-sustained blast protection shields.

Education

Our work in this field to date is as follows. Each University project in the Center supports one or more graduate students. (See listing on the projects.) This is their best learning experience. Undergraduates are also supported on the projects as their class schedules permit. In addition, URI has traveling magic shows for elementary and junior high students. For two summers we hosted Minority Scholars and for the last three summers we have hosted high school science teachers. In the summer of 2012 our Center supported eleven high school teachers to conduct research at University of Rhode Island (URI). Four teachers of physics were placed in URI engineering departments; and four teachers of chemistry, in the URI chemistry department. The teachers worked fulltime for 6-8 weeks. They were required to prepare a poster and give a brief presentation of their work at the end of their tenure. The purpose of this program is to provide high school teachers with an opportunity to gain research experiences they can take back to the classrooms. Over twenty professional classes were offered this year, providing training for well over 400 professionals. For over a decade we have offered classes to DHS and its components. This year we began week-long courses with lectures and labs. Since May we have offered 4 weeks of such classes and trained 48 TSA explosive specialists as well as NYPD forensic lab personnel. The next TSA class will be offered at the end of September.

Terrorism Issues	April 26-27, '11	18
Fundamentals of Explosives	May 3-5, '11	22
Combustion	May 9-10, '11	18
Insensitive Munitions	May 10-11, '11	26
Det'n & DDT	June 7-9,'11	20
Mat'l Response	July 21-22, '11	15
Protocols	Aug 2-3, '11	16
Det'n & DDT	Sept 6-8, '11	35
Dynamic Diagnostics	Sep. 28-29, '11	15
Stability	Jan 18-19, '12	16
Air Blast	Feb 14-16, '12	10
Fundamentals	Feb 27-29, '12	25
Nanoenergetics	Mar 12-13, '12	15
Explosive Devices & Firing Trains	April 10-12, '12	12
Fundamentals of Explosives LANL	April 24-25, '12	42
Fundamentals of Explosives	May 1-3, '12	38
Warhead	May 8-12, '12	13
Fundamentals & Forensic Analysis	May 7-18, '12	9
Fundamentals of Explosives for TSA	May 21-25, '12	24
Fundamentals of Explosives Dugway	July 10-12, 2012	7
Fundamentals of Explosives	July 17-19, 2012	24
		420

Characterization of Homemade Explosives

Jimmie C. Oxley; James L Smith
with Patrick Bowden; Lucus Steinkamp; Guang Zhang; Ryan Rettinger; Matt Porter; Austin Porter

Objective: Our objective is a thorough understanding of the synthesis, characteristics, and performance of explosives presently in use and those potentially used in the future. For example, this group's first publication on ammonium nitrate (AN) was in 1988. In line with the approach outlined below that publication addressed thermal stability. AN-based explosives did not make it to U.S. consciousness until the Murrah Federal Building bombing in 1995. We were already investigating ways to reduce explosivity of AN. A long-term goal is to recognize explosive potential in chemicals not yet classified as explosives. There is precedence for this approach. There were decades between the discovery of the following chemicals and their recognition as explosives: picric acid, PETN, TATB, tetrazole.

Approach:

For monomolecular explosives, such as erythritol tetranitrate (**ETN**), our approach is assess ease of synthesis; physical properties; and, after the standard safety tests are performed, determine long term thermal stability. (See summary below, attached paper and URI database entry http://expdb.chm.uri.edu.)

With triacetone triperoxide (**TATP**) and diacetone diperoxide (**DADP**) we continue studies to understand mechanisms of formation and, specifically, the effect of water. The reason is two-fold: 1) develop a rational approach to thwart their synthesis; 2) understand the effect of reagent concentration (hydrogen peroxide and acid) and, thus, how precursor control might be effectively applied. (See papers)

We have previously reported moderate success in thwarting the synthesis of urea nitrate (**UN**). Now in direct response to law-enforcement requests we have characterized the more powerful dehydration product nitrourea (**NU**). (See papers)

Results for DADP, ETN, and NU have been added both to the URI database, and to vendor detection instruments such as the Thermo Scientific First DefenderRM (Ahura, Raman).

Among the homemade explosives (HME) which are "mix-and-shoot," we have multiple papers on **AN-based** explosives, and therefore, have pursued thwarting of those HME outside the Center. With Center funding we have focused on explosives made with hydrogen peroxide (**HP**). We are in the process of writing a permanent patent on chemicals which destroy HP during its concentration by heating HP-ethanol is a thermally stable liquid explosive which we have a number of years experience using on the firing range. Now we are initiating a study of the stability of HP with other fuels.

In terms of recognizing explosive potential we have initiated a course of study and have asked two other groups (Purdue and LANL) to join us in this effort. Both groups have been visited during this reporting period.

Relevance: We work on a daily basis with personnel from TSA ESS-Ts, bomb squads, transportation police, and vendors of explosive detection instrumentation.
Representative questions over the last few months:
TSA: How much oxidizer (permanganate) and fuel (glycol) do I need to initiate TATP?
TSL: What is the best way to determine HP and sugar kinetics? (They did a good job on this one without us, but now wish to use some of our instrumentation.)
TMA: Do products designed for masking human odor for purposes of hunting prevent dogs or instruments from finding explosives?
TSA: Why does toilet paper sensitize nitromethane?
Vendor: Our facility can't handle explosives; how can I show my instrument works?
TSA/Bomb Squads: Will my Ahura (Raman) initiate….?
Bomb Squad: What's the safe way to transport TATP or HMTD? Safe way to destroy it?

Erythritol Tetranitrate (ETN)

Our lab first encountered ETN was during the bust of a home lab of a 17-year-old Massachusetts boy. Since then due to the widespread availability of erythritol, for low carb diets, ETN has been used in a number of incidents. Our URI lab was one of the first to characterize this material, and our advice has been sought by a number of agencies, including Sandia National Lab, on handling of this reportedly highly sensitive material. Thermal behaviors, vapor pressures, densities, and drop weight impact results, as well as analytical protocols, were reported for three tetranitrate esters: erythritol tetranitrate (ETN), 1,4-dinitrato-2,3-dinitro-2,3bis(nitrato-methylene) butane (SMX), and pentaerythritol tetranitrate (PETN). ETN and SMX both melt below 100^{o}C and have ambient vapor pressures comparable to TNT. While LC/MS was shown to be a viable technique for analysis of all three tetranitrate esters, only ETN was successfully analyzed by GC/MS. Performance of these nitrate esters as evaluated in lab using the small-scale explosivity device (SSED) suggested RDX >> DNTN > PETN > ETN. Detonation velocities were calculated using Cheetah 6.0. Since the starting material is now widely available, it is likely that law enforcement will find ETN in future improvised explosive devices. This paper with its analytical schemes should prove useful in identification of this homemade explosive.

Peroxide Explosives

Organic peroxides generally find use as polymerization catalysts or bleaching agents. However, a few with high ratios of peroxide functionalities to organic species have found use as illicit explosives, specifically TATP (Triacetone Triacetone), DADP (diacetone diperoxide), HMTD (hexamethylene triperoxide diamine), and MEKP (methyl ethyl ketone peroxide). We have reported attempts to prevent synthesis of TATP in an improvised setting (see paper). That work pointed out the need for a detailed mechanistic study. Some of the questions of interest in studying TATP formation/destruction were the conditions under which TATP and DADP form, the mechanisms of formation and destruction, whether DADP could be formed directly or only through a TATP intermediate. These questions were addressed using TATP in d^6 acetone; d^{18}-TATP in proteo-acetone; and TATP with dichloroacetone. Nuclear magnetic resonance spectroscopy (NMR) and gas chromatography/mass spectrometry (GC-MS) were used to examine acetone exchange during TATP synthesis asa well as effects of reaction conditions on intermediates and products and factors which affect destruction. Formation and destruction mechanisms are postulated. In addition we are developing non-explosive canine aids for both TATP and HMTD. In the case of TATP issues with packaging and shipping are being pursued with the aim of creating a commercial product. In the case of HMTD long-term stability is being determined.

Urea Nitrate and Nitrourea

Urea nitrate (UN) has been popular as an improvised explosive. More powerful is the dehydration product of UN--nitrourea (NU). While there has, as yet, been no terrorist use of this material, this year law enforcement asked how to distinguish between UN and NU. A study was undertaken to characterize NU and to determine distinguishing characteristics. While both white solids melt around 160°C, all other properties contrast significantly as might be expected from an inorganic salt (UN) and an organic compound (NU). See table below and paper.

	UN	NU
melting point °C	157-159	153-155
density g/cm^3	1.67±0.011	1.73±0.026
DSC 20°/min dec °C	~160, ~380	~140
DSC J/g	~500, small	1000
TGA dec at °C, % wt loss	160°C, 40%	160°C, 100%
	250°C, 40%	
IR cm^{-1}	3500, 3200, 2410 broad	3400-2700 mult peaks
	1704, 1568, 1426, 1298	1605, 1305
^{1}H NMR d^6-acetone ppm	8	7,12
^{13}C NMR d^6-DMSO ppm	163	151
MS negative	nitrate	NU-H$^+$
MS negative with CCl4	urea + Cl$^-$ or 2 urea + Cl$^-$	NU + Cl$^-$
MS positive	urea + H$^+$	methyl carbonate+NH$_4^+$
		cyanic acid+NH$_4^+$
solubility mg/mL:		
Water	167.2±0.5	20±2
Ethanol	14.2±0.1	17.2±0.6
Methanol	54.8±0.9	43±8
Acetone	10.4±0.2	41±5

Future Work: With the long-term goal of reducing the effectiveness of chlorate explosives we have initiated a literature study to determine what is known about their reactivity with various fuels. Where information is lacking studies will be initiated.

Graduate Students (partially supported)





Morgan Turano Ryan Rettinger Jon Canino Lucus Steinkamp Austin Brown

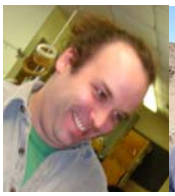


Joe Brady Pat Bowden
PhD Jul 2011 PhD Dec 2011
Brookhaven NL Los Alamos NL

Publications:

Oxley; J.C.; Smith, J.L.; Bowden, P.R.; Rettinger, R.C. "Factors Influencing Triacetone Triperoxide (TATP) and Diacetone Diperoxide (DADP) Formation: Part I" accepted to PEP attached

Oxley, J.C.; Smith, J.L. Vadlamannan, S.; Brown, A.C.; Zhang, G.; Swanson, D.; Canino, J "Synthesis and Characterization of Urea Nitrate and Nitrourea" accepted to PEP attached

Oxley, J.C.; Smith, J.L.; Brady, IV, J.E.; Brown, A.C. Characterization and Analysis of Tetranitrate Esters, *Propellants, Explosives, Pyrotechnics*, **2012**, 37(1), 24-39. Attached

Oxley, J.C.; Smith, J.L.; Brady, J.E.; Hart, C.E. Estimating Ambient Vapor Pressure of Low Volatility Explosives by Rising-Temperature Thermogravitmetry; Propellants, Explosives, Pyrotechnics, accepted

Wilson' S.A.; Brady, J.E.; Smith, J.L.; Oxley, J.C. The Risk of Mixing Dilute Hydrogen Peroxide and Acetone Solutions *J of Chemical Health & Safety*, **2012**, *19(2)*, 27-33.

Dubnikova, F.; Kosloff, R.; Oxley, J.C.; Smith, J.L.; Zeiri, Y. Role of Metal Ions in the Destruction of TATP: Theoretical Considerations; *J. Phys. Chem. A*, **2011**, *115*, 10565-10575.

Theoretical Projects within the Center of Excellence

Ronnie Kosloff and Yehuda Zeiri
Hebrew University Jerusalem, Israel

I. Objective

The goal is to establish and apply theoretical methods that will be able to predict the sensitivity and detonatability of energetic materials. This is in response to the proliferation of the threat of improvised explosives and the growing threat of the proliferation of military type explosives. The list of threats has increased substantially. As a result it becomes very difficult and time consuming to study each of the variants experimentally. We therefore want to establish a comprehensive theoretical modeling protocol which will be able to predict the hazard of new materials. In addition we want to calculate physical properties such as spectrum, density and energetics. Finally we intend to suggest methods to dispose safely such materials.

II Significance to DHS

Our theoretical modeling bridges the gap between the microscopic world of chemical reactions and the bulk properties of explosive. Using modeling methods we are able to asses and predict properties of undocumented materials. Our computations supply the basic spectroscopic assignments which is a major input in remote detection. We can calculate stability and final products of improvised explosives.

III. Accomplishments

We published a comprehensive study of the properties of the decomposition of liquid Nitromethane. Our study employed reactive (REAXFF) molecular dynamics simulations under various conditions of constant temperature and compression. We have identified a change of mechanism of decomposition between low and high density. In low density at elevated temperatures the first step in decomposition is the breakup of the nitrogen carbon bond. At high density there is a transition to bimolecular reaction with a proton transfer. This may explain the large difference between detonation in liquid and solid form of Nitromethane. This study is an important step in establishing a computational method for predicting the initiation and detonation properties of liquid explosives. We are currently extending these studies to liquid TNT.

We have published an extensive theoretical study on the disposal of TATP. This study is in collaboration with the experiments carried out of URI. The theory calculates the properties of ion TATP complexes with the purpose to identify a catalyst for safe disposal. We suggest an additional role of high ion concentrations as a means to screen van der Waals forces and allow dissolution of TATP.

IV. Details

Molecular dynamics simulations of weak detonations [3]

Detonation of a three-dimensional reactive nonisotropic molecular crystal was modeled using molecular dynamics simulations. The detonation process is initiated by an impulse, followed by the creation of a stable fast reactive shock wave. The terminal shock velocity is independent of the initiation conditions. Further analysis shows supersonic propagation decoupled from the dynamics of the decomposed material left behind the shock front. The dependence of the shock velocity on crystal nonlinear compressibility resembles solitary behavior. These properties categorize the phenomena as a weak detonation. The dependence of the detonation wave on microscopic potential parameters was investigated. An increase in detonation velocity with the reaction exothermicity reaching a saturation value is observed. In all other respects the model crystal exhibits typical properties of a molecular crystal.

Explosives are characterized by a detonation wave which propagates through the material. After initiation, the velocity of the detonation front reaches a steady state that exceeds the speed of sound in the material. The present paper is devoted to the analysis of a model solid explosive with the purpose of correlating the microscopic structure and interatomic forces to the bulk detonation properties. The investigation is based on a classical molecular dynamics simulation with a simple force field. The initial goal was to construct a first-principle model that is able to qualitatively reproduce a stable detonation wave. The microscopic parameters considered are the crystal structure, the intermolecular forces that stabilize this structure, and the intramolecular potentials that yield the driving chemical reaction. The present investigation unravelled a new type of a solitary-like detonation wave that is directly driven by the one-step exothermic chemical decomposition. From a hydrodynamical perspective it can be classified as a weak detonation.

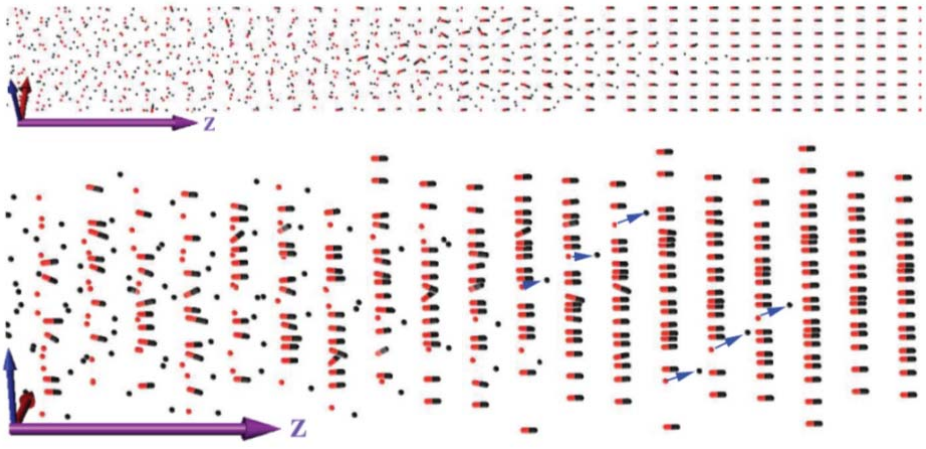

A snapshot of the detonation wave. The propagation axis is the Z direction. Periodic boundary condition are used in the X, Y directions. The right-hand side shows the unperturbed crystal structure. The red (gray) objects represent the heavy particles (N).

The black objects represent the light particles (C). On the left-hand side of the image one can observe the burnt material after the passage of the shock wave. The shock front is characterized by pilot cascades of light particles that are emitted from the decomposed molecules and initiate the next layer in a domino-like effect. The lower panel is an enlarged viewpoint of the detonation front. The arrows indicate decomposed N-C pairs, corresponding to the pilot cascade.

The purpose of this study was to bridge the gap between a first-principle microscopic model of detonation and bulk hydrodynamical theories. The first task was to obtain a stable detonation wave independent of initial conditions. For this task we constructed a reactive molecular crystal mode characterized by pair potentials. The equilibrium properties of the crystal are typical. It is stable at low temperatures and melts at temperatures that scale with the binding energy. The model crystal also possesses linear elastic waves. The detonation potential was added by making the molecule metastable to dissociation releasing a significant amount of energy. The model fulfilled the expectations and a stable detonation wave was identified. Further analysis, which compared the results obtained in the simulations to hydrodynamical theory, revealed a puzzling picture. The detonation wave did not have the characteristics of the common solutions of the ZND model. Some of the differences are the following:

(1) The compression at the shock front was minor.

(2) The chemical reaction coincided with the shock front.

(3) The shock velocity was supersonic with respect to the burnt material left behind.

Searching for a meeting point with hydrodynamical theory we conclude that the phenomenon we observed in the MD simulation is a weak detonation. Weak detonation is a possible hydrodynamical solution in which the shock wave is supersonic with respect to the material left behind. The characteristics of weak detonations are different from normal detonations: The weak detonation velocity is higher, and the detonation pressure after completion of the reaction is smaller than in the normal detonation case. Also, in weak detonations there is no compression of the material before the reaction. Zel'dovich argues that such solutions are usually unattainable for substances that are initially inert. However, he points out that weak detonations might occur if the chemical reaction would start in the initial state without preliminary heating of the substance by the shock wave.

Why are weak detonations attainable and stable in our case The answer is in the kinematic behavior of the crystal? The shock propagates with characteristic of a nonlinear solitary wave. The propagation velocity is determined by the repulsive part of the interatomic potential which is similar to solitons on a Toda lattice. The other kinematic property is the mass of the group that emitted from the dissociating molecule. When the shock front comes from the heavy side, the light particle is breaking out with the majority of the kinetic energy, initiating the reaction on the next

crystal plane. This can be imagined as a shock propagation by the domino effect which never looks back. The ideal domino effect has no change in the density after the front. This is accompanied by a negligible increase in the mass velocity. The melting of the crystal and the equilibration of the burnt material lag behind the shock front and are decoupled from it due to the supersonic velocity. Remarkably when the molecule orientation is the opposite (heavy particle is placed ahead of the light one in the shock direction), then the detonation does not reach a steady state. It explains the details of the solitary wave ignition mechanism. If the light particle is pushed forward at the high (supersonic) velocity after the decomposition, it quickly hits another molecule in the next crystal plane, allowing the reaction to propagate at supersonic speed due to the domino effect. On the contrary, if the heavy particle is placed ahead, it breaks out at much slower delaying the propagation of the decomposition reaction: These observations pose additional questions

(1) What are the conditions that are necessary to observe weak detonation in experiments.
What are the conditions that an MD simulation will reconstruct the standard solutions of the ZND model

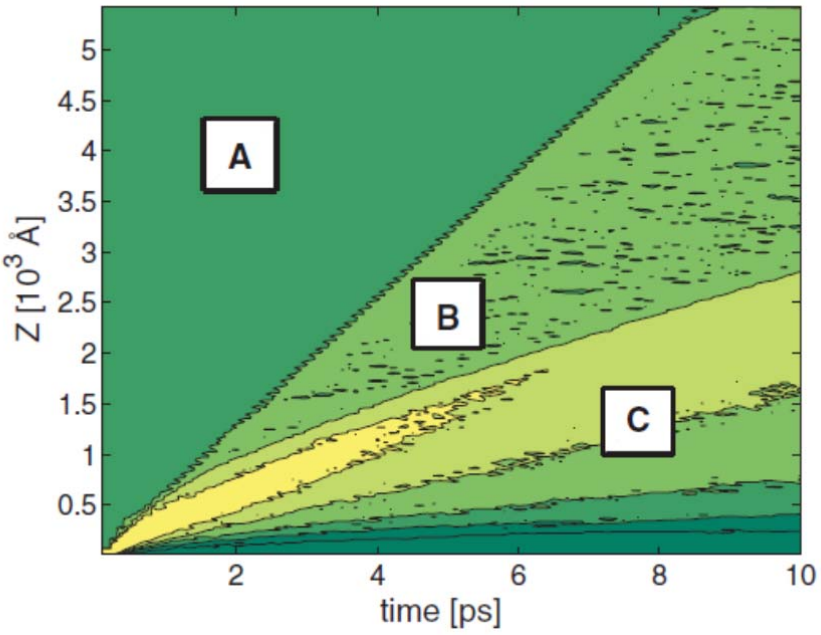

Contour plot of mass velocity along the Z direction. Three regions are marked in the plot: Region A is the preshocked material. The mass velocity here is 0. Region B is the material after the reaction wave. The decomposition front and the discontinuity of the mass velocity coincide, characterizing the reaction wave. Region C is the material after the compression wave

Role of Metal Ions in the Destruction of TATP: Theoretical Considerations [2]

The safe decomposition of solid TATP (triacetone triperoxide) explosive is examined theoretically. The route to destruction starts with formation of metal complexes between a metal ion and the TATP molecule. The second step is decomposition of the molecules into stable final products. We examined the structure and stability of both metal ion (including Na+, Cu+, Cu2+, Co2+, and Zn2+) and proton complexes with TATP using quantum chemical calculations at the DFT-PBE0 level of theory. In addition, for each ion complex, we determined the initial steps in the pathway to decomposition together with the associated transition states. We find that the products of decomposition, in particular, acetone, are also stabilized by ion metal complexes. In agreement with experiment, we find the best candidates for metal ion induced decomposition are Cu2+ and Zn+2/

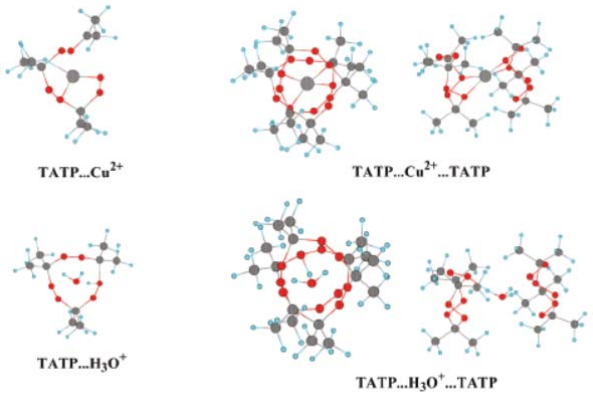

Optimized structures of ion-TATP (left column) and TATP-ion-TATP (right set of four pictures) complexes for Cu2+ and H3O+. In the case of sandwich-type complexes, the right column corresponds to the side view, while the left column corresponds to the top view

Density-Dependent Liquid Nitromethane Decomposition: Molecular Dynamics Simulations Based on ReaxFF [1]

The decomposition mechanism of hot liquid nitromethane at various compressions was studied using reactive force field (ReaxFF) molecular dynamics simulations. A competition between two different initial thermal decomposition schemes is observed, depending on compression. At low densities, unimolecular C_N bond cleavage is the dominant route, producing CH3 and NO2 fragments. As density and pressure rise approaching the Chapman-Jouget detonation conditions (□30% compression, >2500 K) the dominant mechanism switches to the formation of the CH3NO fragment via H-

transfer and/or N_O bond rupture. The change in the decomposition mechanism of hot liquid NM leads to a different kinetic and energetic behavior, as well as products distribution. The calculated density dependence of the enthalpy change correlates with the change in initial decomposition reaction mechanism.
It can be used as a convenient and useful global parameter for the detection of reaction dynamics. Atomic averaged local diffusion coefficients are shown to be sensitive to the reactions dynamics, and can be used to distinguish between time periods where chemical reactions occur and diffusion dominated, nonreactive time periods.

Nintro-Methane Crystal. (a) unitcell (b) 5 - 4 - 3 energy minimized supercell, and (c) liquid Nintro Methane supercell at ambient conditions.

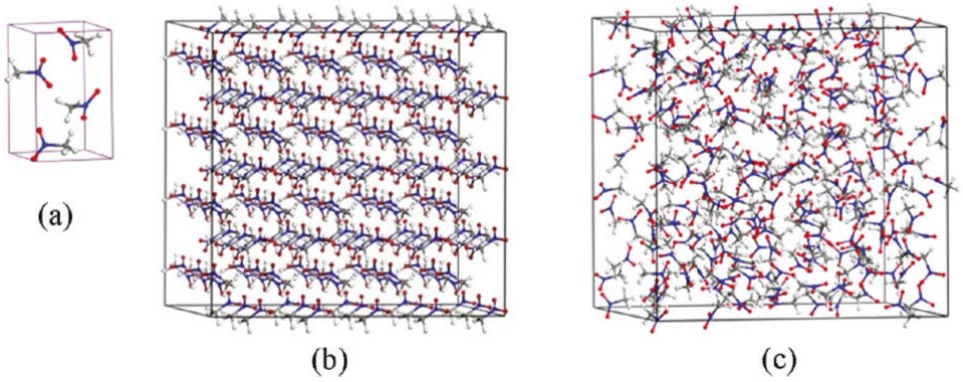

IV. Students Supported

Morag Am Shalem: PhD. Subject: Molecular dynamics simulations of weak detonation waves. 

Ido Shefer: MsC. Subject: Molecular dynamics simulations of THz spectroscopy of TATP. 

David Furmann MsC. Subject Molecular dynamics simulation of reactive materials.

V. Conference & Journal Publication

[1] Density-Dependent Liquid Nitromethane Decomposition: Molecular Dynamics Simulations Based on ReaxFF
Naomi Rom, Sergey V. Zybin, Adri C. T. van Duin, William A. Goddard, Yehuda Zeiri, Gil Katz, and Ronnie Kosloff
J. Phys. Chem. 115, 10181 (2011).
[2] Role of Metal Ions in the Destruction of TATP: Theoretical Considerations
Faina Dubnikova, Ronnie Kosloff, Jimmie C. Oxley, James L. Smith, Yehuda Zeiri,
J. Phys. Chem. 115, 10565 (2011).
[3] Density dependent liquid Nitromethane decomposition: MD simulations based on REAXFF Nomi Rom, **APS Shock Compression of Condensed Matter 2011, Dates and Location: June 26 - July 1, Chicago.**
[4] Molecular dynamics simulations of weak detonations, Morag Am-Shallem, Yehuda Zeiri, Sergey V. Zybin, and Ronnie Kosloff, **Phys. Rev. E 84 061122 (2011).**

Characterization of Non-Ideal Explosives

S. F. Son (PI), L. J. Groven, D. R. Guildenbecher and R. S. Janesheski
School of Mechanical Engineering, Purdue University

1. Objective

The goal of this experimental work is to characterize non-ideal explosives on a small-scale. The need of characterized non-ideal explosives has seen an increase due to the constituent materials used and relatively low costs that allow terrorist to obtain and use them. However, there is an insignificant amount of experimental data available due to the large-scale setup that is required for characterization. The main restraint is due to the large critical diameters needed to sustain a steady detonation in a non-ideal explosive. We are performing small-scale experiments in tubes with small diameters relative to the expected critical diameter and anticipating unsteady detonations that are likely to fail in many cases. Using a microwave interferometer, a highly time resolved profile of the location of the detonation front is measured. The failure dynamics measured with the interferometer allows for the characterization of the non-ideal explosive over a wide parameter space (from overdriven to failure). A simulation of the experimental results is being pursued using CTH, a shock physics hydrocode, to calibrate a reaction model of the non-ideal explosive. The small-scale nature of the experiment allows for various parameters to be changed quickly that include chemical composition, non-ideal explosive density, and confiner thickness. The final goal of this work is to demonstrate that the calibrated model obtained from the small-scale experiment calibration is able to predict the results of large scale experiment.

2. Summary

A unique method for characterizing non-ideal explosives on a small-scale has been achieved. This experiment has also been successful at evaluating the relative detonability of different mixtures with only a few grams of material. Successful experiments have been performed using the microwave interferometer to measure the detonation front's position profile of non-ideal explosives. Different compositions of AN with either diesel fuel, mineral oil, or sugar have been used as non-ideal explosives. The failure dynamics between the compositions were measurably different. The amount of fuel in the non-ideal explosive affected the distance the detonation was able to sustain itself as well as the rate at which it decreased in velocity and eventually reached complete failure. Experiments showed different failure dynamics among a single composition when the thickness of the confinement was changed. It was seen that lateral losses of energy occur in the thin-walled confiners and reduces the reaction zones ability to sustain the detonation. The thick-walled confiner sees minimal deformation, which allows for the much slower rate of deceleration of the detonation front as it is failing.

This year we used PMMA attenuators with different lengths. Detonation of the non-ideal explosive occurred as long as the shock transferring through the PMMA if it was thin enough. The goal was to see the initiation of the detonation within the non-ideal explosive from the overdriven shock and how the weakened shock through the attenuator affects the failure dynamics. A clear effect was quantified. We also varied the density of the non-ideal explosive and measured how it altered the failing detonation front. A very dense non-ideal explosive may limit the hot-spot formation that is required to sustain the reaction zone developed as the shock travels through the material. Material properties such as particle size are also of potential interest and will be examined this next year. Modeling of the non-ideal explosives is underway using CTH. Working simulations have been developed and parameters are currently being tuned to fit the experimental data. Once the data has been fit, the calibrated model will then be compared to results reported from large scale experiments.

3. Accomplishments

Highly time resolved measurements of the detonation front failing within non-ideal explosives have been successfully performed. Experiments have been completed that investigated the various factors such as composition and confiner thicknesses have on the failure dynamics of non-ideal explosives. All tests performed have showed the ability of the microwave interferometer technique to successfully measure different failure characteristics among different non-ideal explosive configurations. Simulating the experimental results using CTH has begun. It is our goal to use to tune the parameters of a suitable model to calibrate our experimental data. We are collaborating with ERDC with their modeling and large scale experiments. We have also begun discussions with Prof. Jack Yoh about modeling issues. If successful, this experimental technique will allow for a much cheaper and less time consuming method of calibrating currently needed models of non-ideal explosives.

4. Details

This past year our focus has been mainly on varying the materials tested more and varying the applied shock strength (using PMMA barriers) and these results were reported in a journal submission. They also appear in Robert Janesheski's 2012 M.S. thesis. This work is summarized in the Appendix that follows.

5. Students Supported

Robert Janesheski

6. Conference & Journal Publications

Paper submitted for publication (in review).

7. Future Directions

This year we are considering a wider range of materials, including those that have been tested at large scale by ERDC and others. A new PhD student has been trained on CTH and also the experiments.

Development of Simulants of Hydrogen Peroxide Based Explosives for use by Canine and IMS Detectors

José Almirall, Ph.D., D*epartment of Chemistry and Biochemistry and International Forensic Research Institute, Florida International University, Miami, FL*

I. Objective

The objective of this effort is to develop an improved field instrument system for the detection of explosive odors based on ion mobility spectrometry (IMS). The PI and co-workers have previously described the composition of the volatile and semi-volatile chemical compounds that are characteristic of several drugs of abuse and chemical explosives in order to assist the design and application of canine detection training aids. The PI has also developed ***pre-concentration*** and ***sampling*** devices based on Solid Phase Microextraction (SPME) for the capture of extremely small quantities of the volatile compounds (on the order of ng) for subsequent detection using IMS using an in-house developed interface (patent pending). The current effort investigates home-made explosives (HME) detection, particularly explosives based on hydrogen peroxide (HP). This proposal aims to characterize the odor signatures of a set of samples from HP-based explosives, some of which will be provided by the University of Rhode Island Center of Excellence, in order to improve the detection of this threat using IMS instruments. The existing large installed base of > 12,000 IMS instruments make this technology viable as a crime scene detection tool and the already proven use of detection canine teams also makes this approach a viable alternative to instrumental detectors. The project team will continue to characterize the odor signature compounds of HP-based explosives and provide the chemical data to the URI center collaborators. The results will also be used to target compounds that can be used for 1) IMS detection and 2) canine detection. The identification of these compounds will assist future researchers interested in detection of HP-based explosives. Additionally, the effort will continue to develop a planar-SPME device specifically designed and optimized to extract the volatile odor signature compounds associated with HP-based explosives. Finally, the existing IMS operating parameters will be investigated to work towards an unambiguous identification of the target compounds of the HP-based explosives by coupling an IMS instrument with a mass spectrometer of high sensitivity to better investigate the composition of the ion swarms in the IMS experiment. An already existing ESI-IMS-MS instrument in our laboratory will be used in this research along with the more traditional techniques of SPME-GC-MS and SPME-IMS already developed in our lab.

II. Accomplishments

A manuscript describing the results of the analysis of TATP using PSPME coupled to IMS was published in a very good quality analytical chemistry journal (attached).

W Fan, M Young, J Canino, J Smith, J Oxley**,** and **JR Almirall*,** Fast Detection of Triacetone Triperoxide (TATP) from Headspace using Planar Solid Phase Microextraction (PSPME) Coupled to an IMS Detector, *Anal. and Bio. Chem.* **2012,** DOI 10.1007/s00216-012-5878-x.

III. Students Supported

Mimy Young: PhD in Chemistry
Wen Fan: PhD in Chemistry

IV. Conference Presentations

April 2012. Field Detection of Hydrogen Peroxide Based Explosives Using SPME-GC-MS and PSPME-IMS, Department of Homeland Security Center of Excellence at the University of Rhode Island, Providence, RI (PA, **Invited Oral**)

March 2012. Rapid Instrumental Detection of Explosives and Drugs in the Field, in New Developments in Forensic Chemistry for use at the Crime Scene and in the Laboratory Symposium, Pittsburgh Conference, Orlando, FL (PA, **Invited Oral** and Symposium Organizer)

February 2012. Field Detection of Drugs and Explosives by SPME-IMS and PSPME-IMS, Forensic Science Without Borders Symposium - NIJ Grantees Meeting, American Academy of Forensic Sciences Meeting, Atlanta, GA (PA, **Invited Oral**)

September 2011. NFSTC Technology Transition Workshop; PSPME for the Analysis of Drugs and Explosives, Largo, FL (PA, **Workshop Organizer**)

June 2011. Performance Evaluation and Calibration of Planar Solid Phase Microextraction (PSPME) Using Vapors of Standards Followed by Ion Mobility Spectrometry (IMS) Detection, Gordon Research Conference on the Analysis of Illicit Substances, Lucca, Italy (PA, Poster)

June 2011. Headspace Profiling of Volatile Compounds from Explosives Using Planar Solid Phase Microextraction (PSPME) Followed by Ion Mobility Spectrometer (IMS) Detection Gordon Research Conference on Illicit Substances, Lucca, Italy (SP, Poster)

June 2011. Fast Detection of Triacetone Triperoxide (TATP) from Headspace using Planar Solid Phase Microextraction (PSPME) Coupled to an Ion Mobility Spectrometer Detector, Gordon Research Conference on Illicit Substances, Lucca, Italy (SP, Poster)

Adhesion Studies

Merav Zeira, Boris Israel, Yehuda Zeiri; Ben Gurion University

Objective

During the last year the research at BGU was pursued in two directions, measurements of particle adhesion using both atomic force microscopy (AFM) and the aerodynamic approaches. In both research directions the main objectives were to develop improvements that will allow to perform measurements that could not be carried out. For details of these improvements see description below.

In addition, we devoted much time to the analysis of AFM data that accumulated during the previous year experiments and to write the papers. The first paper that summarizes the results of adhesion experiments of explosive particles to self assembled monolayers (SAM) was submitted for publication to the Journal of Physical Chemistry (see enclose manuscript) and the second paper, related to adhesion of explosive particles to different substrates, is being written at present.

Accomplishments

AFM measurements: The main goal in improvement of AFM measurements was to develop a simple device that will allow to perform force measurements between explosive particles and "soft" substrates such as cloth, polymers, elastomers, skin and hair. Force measurements on these type of substrates are complex due to the compressibility of the substrate. The device developed aims to minimize the effect of the compressibility on the results. In addition, we are developing at present a data analysis algorithm that will allow to take into account the substrate compressibility. Experiments of explosive adhesion forces onto cloth, polymers and hair will be carried out during the next year.

Aerodynamic measurements: In the aerodynamic measurements of particle adhesion we had to rebuild the system to improve its accuracy, control and repeatability. To achieve these tasks we included a programmable accurate gas flow control and a fast electric valve, both controlled by a LabView program. In addition we extended the optical system to allow the attachment of a fast camera to the microscope to allow rapid photography of the experiments. These modifications lead to more accurate and repeatable experiments and allow us to control the length of the air jet pulse between 1-10,000 msec. At present we are working on the development of a numerical code that will allow detailed statistical analysis of the frames obtained by the rapid photography.

Details

AFM measurements:

The contribution of chemical interactions to the adhesion forces were studied by AFM force measurements between explosive particles and different end groups attached to SAM. The results of this investigation were summarized in a paper that was submitted to the Journal of Physical Chemistry. The manuscript is enclosed and sent with this report.

Results of experiments aimed to study the adhesion of explosive particles to various common substrates is being summarized at present. For example, the adhesion of three explosives to glass and stainless steel (SS) surfaces are presented in Fig. 1 below. The experiments were performed in ambient air and under water environments. The main difference in these two environments is the existence and contribution of capillary forces in the ambient air experiments while they are eliminated in the under water experiments.

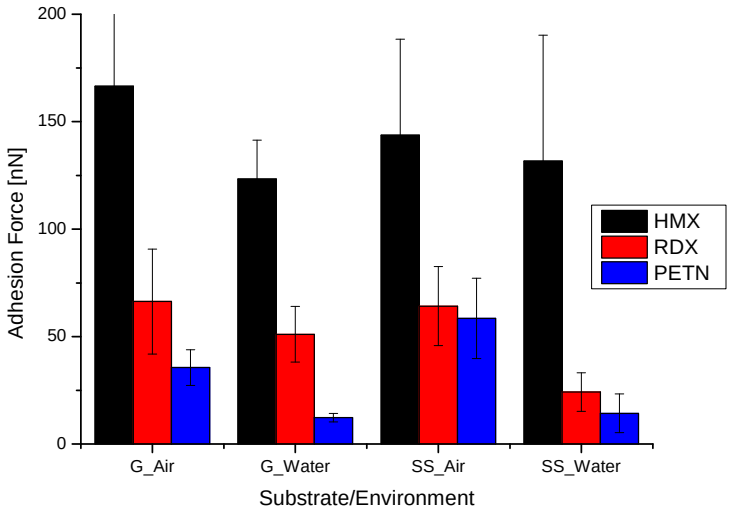

Fig. 1: Adhesion force of explosive particles onto glass and SS substrates. The experiments were carried out in two environments: ambient air and under water.

These results clearly show that the contribution of capillary forces to adhesion are relatively small, however, they exist and lead to increased adhesion in ambient air by about 10-20%. These results clearly show that adhesion of HMX to the two substrates is much larger that that of RDX and PETN. We tried to examine the influence of finger prints on the adhesion of RDX particles to Perspex and glass substrate. Pictures of clean Perspex surface and one with finger prints as well as a glass surface with finger print are shown in Fig. 2.

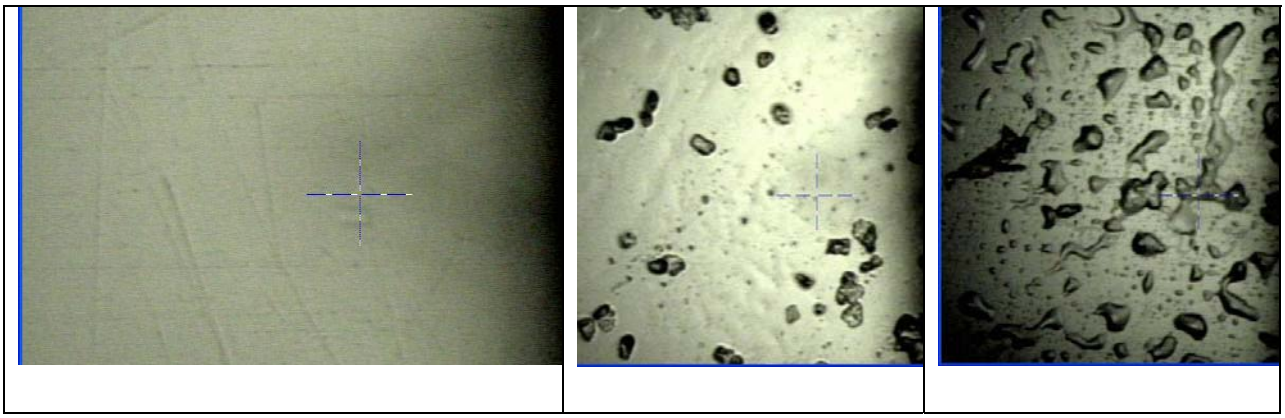

Fig. 2: Images of clean Perspex surface (left); finger print on Perspex (middle) & on glass (right).

It is clear from these pictures that the finger prints do not wet the two substrates examined. We tried to measure force curves for RDX adhesion onto a site on the substrate covered with a drop of finger print. The measurement could not be completed since he adhesion force was too high and we could not perform the regular approach and retraction rout of the particle glued to the tip. Moreover, once the particle was exposed to the drop of finger print oils, it became covered with it and attempts to measure adhesion of the particle to clean site on the surface resulted in "contamination" of the substrate surface by finger print liquid. A series of such "contaminated" site are shown in Fig. 3 below.

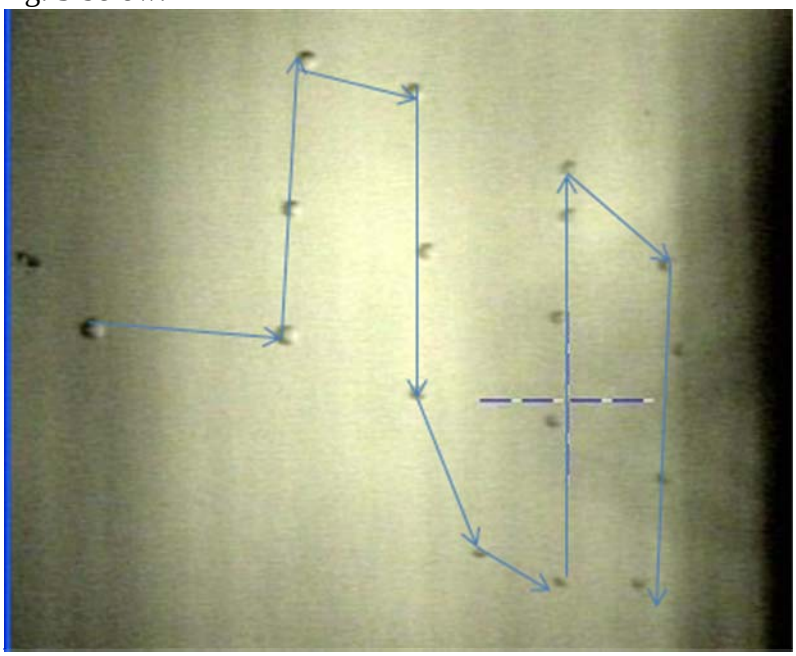

Fig. 3: A sequence of "contaminate" sites on a glass surface following attempt of adhesion measurement with a particle that touched a drop of finger print oil.

During the coming year we shall try again to carry out adhesion force measurements to finger prints on various substrates. We plan to use in these experiments tips with 2-3 orders of magnitude larger force constants that may allow completion of the force measurement using the AFM.

Aerodynamic measurements:

The preliminary results for measurement of alumina particles on glass substrate are shown in Fig. 4 below. These measurements were performed using the upgraded system. The experiments used to sizes of particles: 5 and 22.5 μm (average size according to manufacturer). The experiment were performed using two very different air jet duration, 5 and 1000 msec respectively. Each experiment was repeated three times and the error bars show represent the standard deviations obtained. These preliminary results clearly indicate that one need more repetitions to obtain a more accurate average value with reduced error. In addition, these results clearly show that the smaller particles are removed more efficiently than the larger particles. Moreover, it seems that most of the particle removal process occurs at the stage where a well developed steady state flow is achieved.

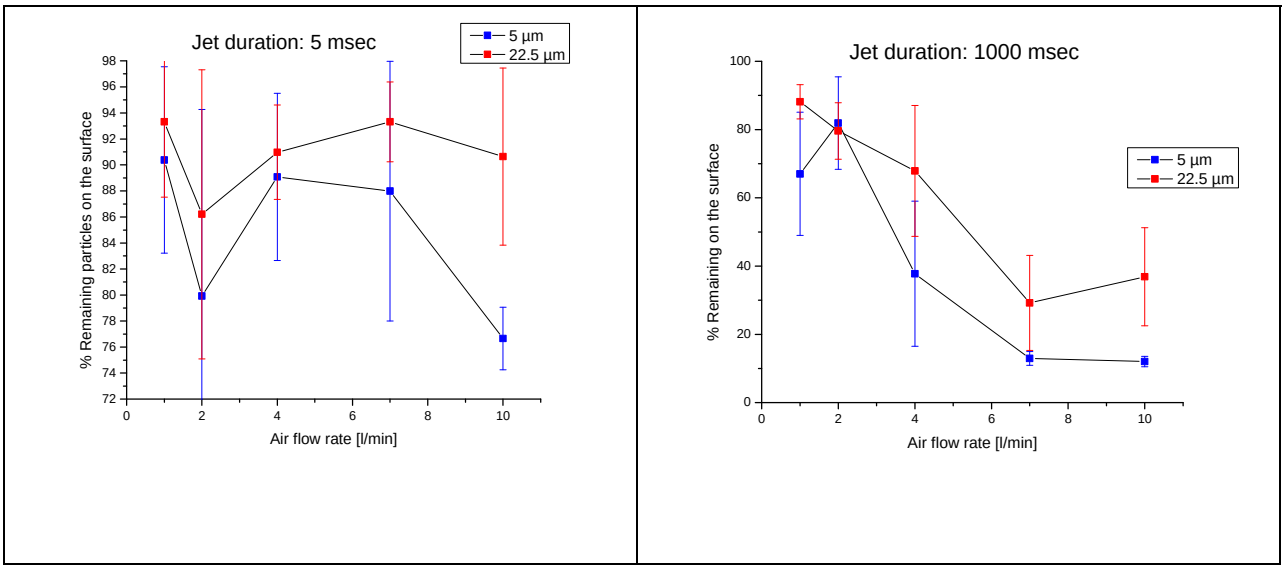

Fig. 4: Percentage of particle removal by an air jet of duration 5 msec (left) and 1000 msec (right) using 5 and 22.5 µm particles (blue and red respectively).

We have recorded a few experiments using a rapid camera (the movies are too big to send by email). At present we are in a process of data analysis to obtain the statistical behavior of the system during the exposure to the air jet. The statistical analysis will follow the particle number, particle-particle distance and particle size distribution as a function of time during the jet operation.

Students Supported

Merav Zeira – is a new undergraduate student who started to work on AFM measurements a few weeks ago. She will perform the adhesion force measurements on compressible substrates. She works three day every week during the summer and will continue to work for 2 days a week next year.

Merav next to the system used to glue the explosive particles to the cantilever for the AFM measurements.

Raya Zach – A retired technician who work in my laboratory 2-3 days a week. She is involved in the preparation of explosive coated particles and measurements using: HPLC and DMS.

Raya standing next to the stand alone DMS system.

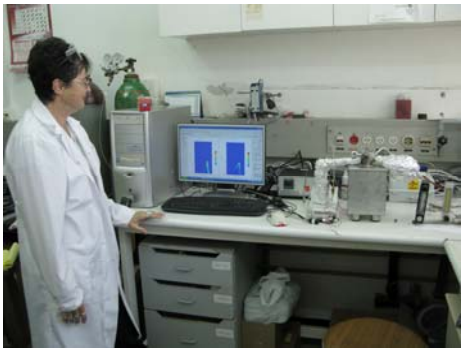

Yossi Matana - A retired technician who works in my laboratory 3-4 days a week. Yossi is the person who is in charge of development of system and maintenance of chromatography systems. He is performing at present research related to the use of DMS to detect explosives.

Yossi standing next to the GC-DMS system used in the explosive detection study.

Boris Israelov - is an undergraduate student working for 3 days a week during the summer and for 2 days a week next year on the aerodynamic approach to study adhesion.

Boris standing next to the aerodynamics system use for the adhesion measurements.

Yonathan Schwartz - is an undergraduate student working for 2 days a week during the summer and during next year. He is working on ion chemistry of explosives using a commercial IMS system.

Yonathan standing near the IMS system (not seen in the picture).

Conference & Journal Publications

1. I participated and gave an oral presentation on AFM force measurements in the " Trace Explosives Detection Workshop" in Boston during April 2012.
2. The paper on the role of different end groups of a SAM on adhesion was submitted to the Journal of Physical Chemistry. The manuscript is enclosed.
3. A second paper related to AFM measurements of explosive particles to various substrates is being written at present and will be sent for publication in about 1-2 month.

Explosive Sensor Enhancements

William Euler, Chemistry Dept; University of Rhode Island

1. Objective

The objective of the work is to develop new sensors able to sensitively, selectively, and broadly detect explosives at trace levels.

2. Summary

A dual sensor using metal-enhanced fluorescence (MEF) and surface enhanced Raman scattering (SERS) capable of providing sensitivity, selectivity, and the ability to identify multiple types of explosives has been studied. The MEF portion of the sensor has exceptional sensitivity to TNT for two reasons: more light is absorbed to give a stronger signal and also induces a stronger quench by the analyte. SERS spectra have been obtained for model compounds.

3. Accomplishments

A major discovery was made in preparing the MEF sensor. Typical enhancements for the fluorescence intensity in MEF are 10 – 50. By using a polymer spacer we were able to increase these enhancements by a factor of 10 to ~400 (unoptimized!). There is no reported mechanism for such a large enhancement so significant effort is being made to understand this new physics.

4. Details

A survey of solution phase rhodamine and fluorescein dyes was made to identify interactions with a suite of explosives or common impurities in explosives (including TNT, PETN, RDX, HMX, TATP, and a number of nitrotoluenes). Ultimately, this will lead to array sensors that will use pattern recognition techniques to identify the analyte. A collaboration with David Castañon has been initiated to develop machine-learning algorithms to accomplish this task.

In the solution phase studies, a new reactivity pattern was found for TNT and trinitrobenzene (TNB) that was studied. It appears that a Meisenheimer complex can form between TNT and TNB and that this sigma-adduct is fluorescent. We hope to be able to exploit this chemistry in sensor development.

Sol-gel substrates are being prepared as a porous host for the sensor materials. Protocols for optically clear samples containing fluorescent dyes and polymers have been established. Further, proof of concept experiments successfully showed that the fluorescent dyes in the sol-gels can be quenched by TNT.

5. Students Supported

Graduate Students: Emily Hall, Christopher Latendresse, Meredith Matoian
Undergraduate Students: Syrena Fernandes, JungMin Hwang, Alessandra Lonardo, Courtney McGowan, Sangmin You, Hui Qi Zhang

From left to right: Chris, Meredith, JungMin (aka Alex), Hui Qi (aka Vicky), Bill, Alessandra, Emily, Courtney, Sangmin (aka Jessie), and Syrena.

Detection of Explosives and Explosive Precursors

Otto Gregory; Chemical Engineering; University of Rhode Island

1. Objective: The early detection of explosives and explosive precursors in environments targeted by terrorists for the deployment of improvised explosive devices (IED's) is the overall goal of this project. The significance of this work was first highlighted by the failed attempt of "Shoe Bomber" Richard Reid to deploy an IED on an American Airlines jet in 2001 and later on a Northwest Airlines jet in 2009. In both cases, a triacetone triperoxide (TATP) trigger was intended to initiate an explosive device containing pentaerythritol tetranitrate (PETN). Having the ability to detect energetic materials such as TATP and PETN at trace concentrations in confined spaces or more specifically deploy sensor arrays that could "sniff" for explosives is particularly important in scenarios that could threaten public safety. Therefore, a continuous, on-line monitoring system for both nitrogen and non-nitrogen based explosives without generating false positives continues to be our primary goal. Other explosives such as ammonium nitrate, 2,6-DNT, diacetone diperoxide (DADP) and hexamethylene triperoxide diamine (HMTD) are either being tested or are being considered for testing using our sensor platform in the near future.

2. Project Summary: Our initial focus this past year was the detection of TATP and its precursors at trace levels, which was later expanded to include 2,6-DNT, urea and ammonium nitrate. Since the peroxide based compounds are generally harder to detect than the nitrogen based compounds used in IED's and there are more mature technologies for the detection of nitrogen based explosives, we focused our efforts on the compounds TATP initially. Towards that end, we developed a small footprint, robust sensor that can reliably detect TATP at the part per million level without any pre-concentration steps (i.e. detection in a single pass). Our thermodynamic based sensor can continuously monitor the environment for explosives by measuring the heat generated or absorbed by a catalyst in the presence of a target molecule (or molecules). The technique employs a digital control system which enables a microheater coated with a catalyst, to be scanned over a selected temperature range. The electrical power difference due to catalytic activity (power difference between the target molecule and an inert reference) is measured similar to that in a microcalorimeter.

By utilizing arrays of such microheater sensors with different catalysts, it will be possible to uniquely identify target molecules of interest, thus further minimizing false positives. In this way, those energetic materials having sufficient vapor pressure are ideally suited for our thermodynamic based sensor platform. Since we did not see any evidence of acetone in the output signal of our sensor when exposed to TATP and the output signal closely tracked that of hydrogen peroxide, we concluded that we were sensing the catalytic decomposition products of TATP. Further evidence of this was provided by Oxley et al who found that under ambient conditions, TATP primarily decomposes into acetone. Therefore, we believe that the catalytic decomposition of TATP was facilitated by our detection scheme, which is a much more specific reaction or "tag" than the decomposition of TATP to acetone in air ambient. This specific reaction mechanism should help mitigate false positives. Furthermore, the responses (signatures) generated from multiple signals will be used to uniquely characterize the target molecules of

interest when incorporated into sensor arrays comprised of different catalysts. As a result of this work, we have pursued a number of explosives that could potentially be detected by similar mechanisms such as DADP. In addition, we have identified both selective and sensitive catalysts for our sensor template and pursued new sensor templates that will ultimately reduce the frequency of false positives. For example, we have combined a thermodynamic sensor with a conductometric sensor to simultaneously interrogate catalysts exposed to explosive vapors at trace levels. By combining protocols, better sensor selectivity and sensitivity can be realized in the same sensor footprint. In addition, a microelectromechanical systems (MEMS) based sensor has been developed to improve sensor selectivity, sensitivity and response time.

3. Year 4 Accomplishments: Our primary focus this past year was the detection of the more commonly used explosives such as TATP and their precursors acetone and hydrogen peroxide. Unlike many other explosives, TATP contains neither metallic elements nor nitro groups, and therefore, has no significant absorption in the ultraviolet region and does not fluoresce making it very difficult to detect with conventional spectroscopy techniques. Since its precursors (acetone, hydrogen peroxide and a strong acid) are readily available and its preparation is relatively simple, TATP is an explosive of choice for terrorists. Towards that end, we have identified catalysts and developed sensor protocols for the detection of TATP at the ppm level. The response of our sensor to TATP using a number of different catalysts is shown in Figure. 1. Here, the response to 0.685 μg/mL TATP as a function of temperature using several catalysts including WO_3–TiO_2, V_2O_5, SnO_{2-x}, Nb_2O_3 and ZnO was measured. Each of the five oxide catalysts show a unique response as a function of temperature, and show features ranging from almost no peak response for Nb_2O_3 to well defined peaks for ZnO. Since we demonstrated that we can detect hydrogen peroxide at comparable levels using the same metal oxide catalysts, we compared the TATP and peroxide responses to determine if the TATP was decomposing in the vicinity of the microheater as it was being detected. Based on the responses of V_2O_5 and SnO catalysts to TATP and peroxide, it appears that the response of each catalyst to these target molecules occurs at the same temperature and the signatures have a similar shape. From Figure 2, it can be seen that the relative response to acetone is considerably greater than that of H_2O_2, which is consistent with other investigations using thermodynamic based gas sensors for detection. These studies support our findings that significant exothermic heat effects are observed for hydrocarbons. Not only is the magnitude of the response to acetone for Cu_2O significantly greater than that of hydrogen peroxide but it is also of opposite sign, which implies that the sensitivity of our thermodynamic sensor platform to acetone is significantly greater than that of the other products derived from the decomposition of TATP.

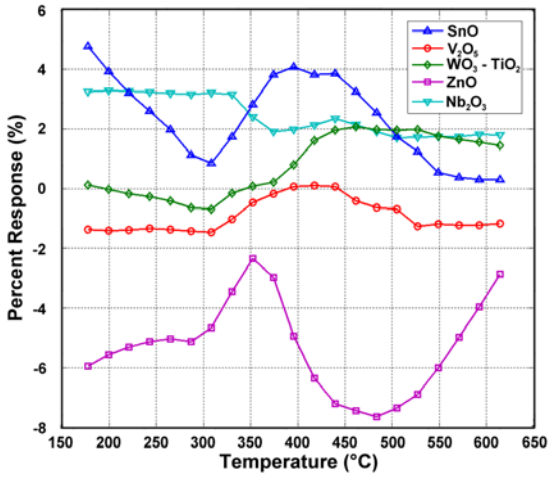

Figure 1 Response of various catalysts to 0.685 µg/mL TATP as a function of temperature

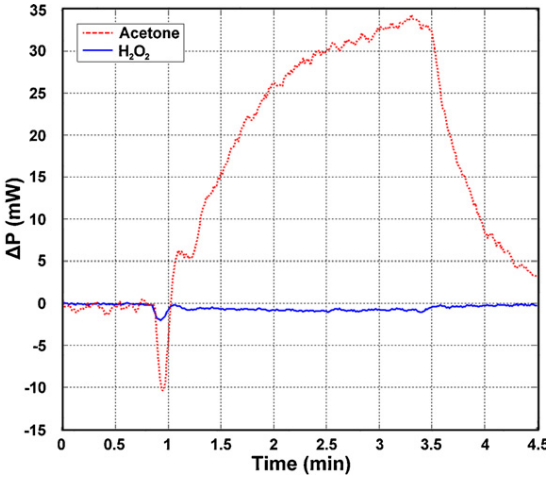

Figure 2. Response of Cu_2O catalyst to acetone and hydrogen peroxide.

Even though we successfully demonstrated a sensor that was capable of detecting TATP at trace levels, relatively poor selectivity between TATP and hydrogen peroxide was observed. Therefore, we incorporated palladium nanoparticles into a SnO_2 catalyst to improve both the sensitivity and selectivity to H_2O_2 over TATP. A Pd:SnO_2 nanocomposite catalyst containing 8 wt% Pd yielded the greatest selectivity (H_2O_2 relative to TATP) as shown in Figure 3. Not only was the selectivity to TATP increased using this approach but the sensitivity to TATP was increased by more than 60% and the sensitivity to H_2O_2 was increased by more than 160%. As a reference, the selectivity improvement relative to urea was also demonstrated in Figure 3. A series of concentration tests to determine the effect of concentration of TATP in the vapor phase on the response of a Pd:SnO_2 nanocomposite catalyst is shown in Figure 4. SEM and TEM micrographs of a Pd:SnO_2 nanocomposite catalyst containing 12 wt% Pd is shown in Figure 5. Microscopy was used to determine the palladium loading in the Pd:SnO_2 nanocomposite catalyst being developed for better selectivity and sensitivity.

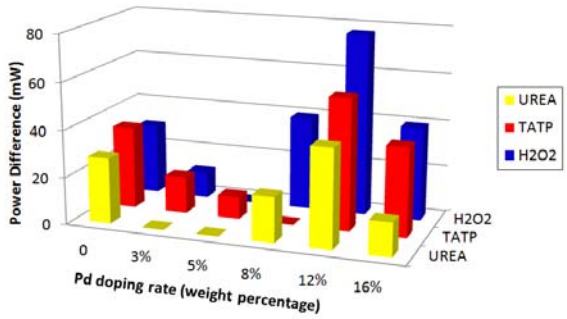

Figure 3. Selectivity of various Pd doped SnO_2 catalysts to urea, H_2O_2 and TATP.

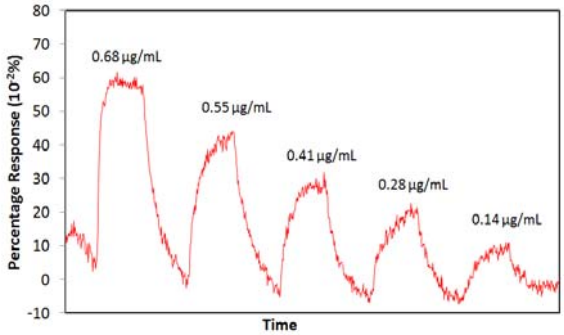

Figure 4. Effect of TATP concentration on the response to a Pd:SnO_2 catalyst (8% Pd)

We have also pursued new sensor templates that will ultimately reduce the frequency of false positives. One novel approach to mitigate false positives was to combine multiple

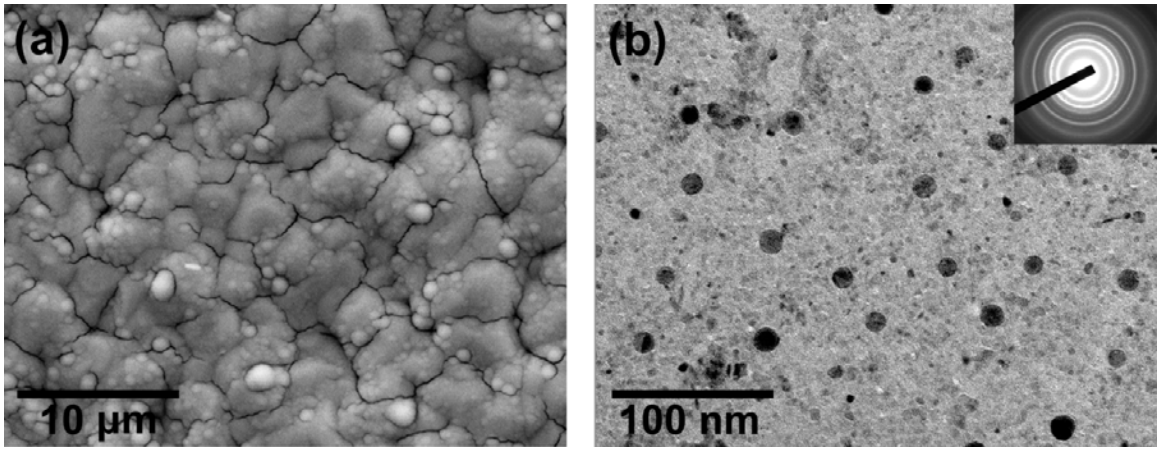

Figure 5. SEM (a) and TEM (b) micrographs of an annealed catalyst with a 12 wt% palladium loading.

sensor platforms to make a more unique signature; i.e. by combining a thermodynamic response with a conductometric response, we can simultaneously interrogate catalysts on the same sensor template by relying on these very different sensing mechanisms. Most conductometric sensors are highly sensitive to oxidizing and reducing species, but other than that difference, target molecules are not readily identified. Thus, conductometric sensors on their own merit have poor selectivity. Thermodynamic based sensors, however, have much greater selectivity, since target molecules react with a particular catalyst, the sensor can accurately measure the heat effects caused by decomposition or detect the decomposition products. In order to minimize the detection of a false positive a conductometric platform for testing was successfully paired with a thermodynamic platform for the first time. This provides a redundancy to mitigate false positives and can lower the detection limit for target molecules at the same time.

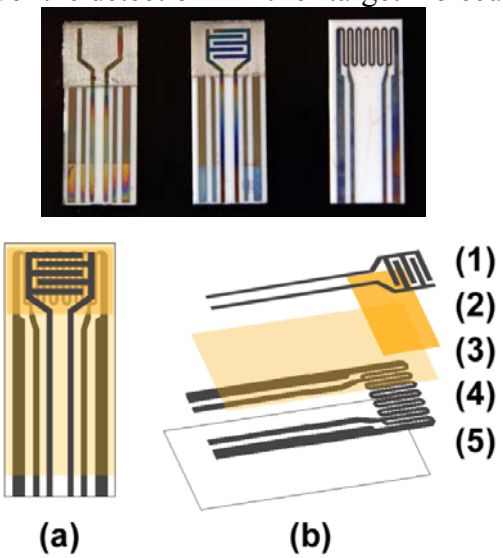

Figure 6. Schematic of conductometric/ thermodynamic sensor showing the top view (a) and expanded views (b) of a sensor consisting of top electrode (1), catalyst layer (2) and alumina passivation layer (3)

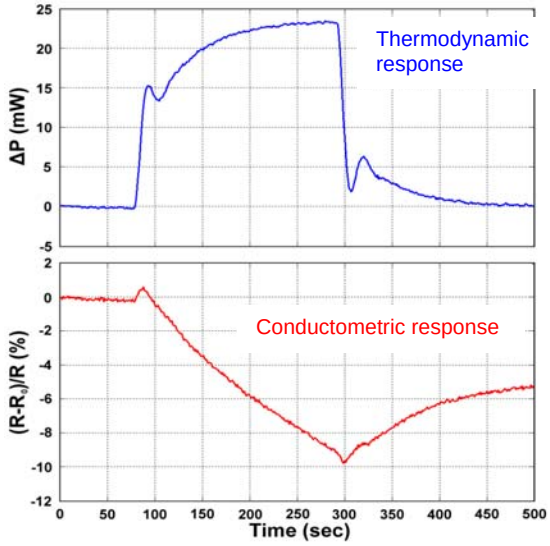

Figure 7. Simultaneous conductometric and thermodynamic response to 58 µg/mL acetone using a SnO_2 catalyst

We have also developed a microelectrochemical (MEMS) based sensor platform that utilizes our novel thermodynamic and conductometric platform on a much smaller scale. A suspended membrane MEMS sensor is being developed at URI to replace the existing alumina substrate solid state sensor (Figure 8). First and second generation devices have been fabricated and tested. They show more than a 60% and 90% reduction in power requirement relative to the existing solid state sensors. Based on our most recent fabrication results, we have reduced the size of the existing heater platform even further and in the process reduced its thermal mass and power consumption. To fabricate a sensor with the desired characteristics, a silicon wafer is etched to form a thin suspended membrane onto which the microheaters and catalyst are deposited, which greatly reduces the thermal mass of the sensor. With this size reduction comes a reduction in power requirements relative to our current sensor platform, leading to an increase in sensitivity to target molecules and a decrease in response time. The smaller length scales achieved with the MEMS platform also creates the possibility of forming microarrays of sensors containing a library of different catalysts, which will increase selectivity and sensitivity for target explosives while eliminating false positives. Due to the ease of integration, the ability to form large sensor arrays and their utility in a fast responding, single pass continuous monitoring system. The MEMS platform being developed at URI is shown in Figure 9 and has considerable potential for commercialization.

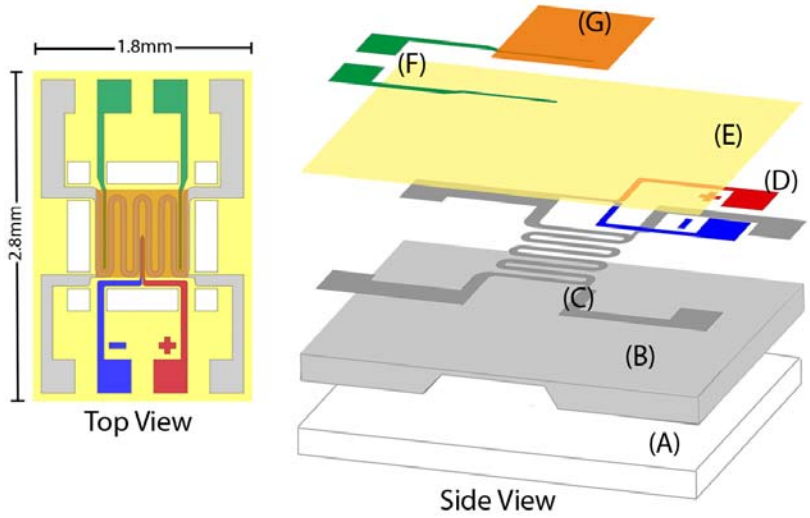

Figure 8. Left is the top view of a URI MEMS sensor and the right is a side view illustrating the layers including: (A) pyrex glass, (B) silicon wafer with an KOH etched cavity on the underside, (C) platinum microheater, (D) Type K thermocouple, (E) silicon dioxide dielectric layer, (F) platinum conductometric electrodes and (G) a metal oxide catalyst layer placed over the coils of the microheater.

A critical component of our detection system for "sniffing" explosives is the acquisition, reduction, and signal processing of the raw data collected from our thermodynamic based measurements. When an inert is passed over the sensor, a baseline electrical analog response is generated. When the sensor is exposed to the target molecule, a signal corresponding to the heat effect is measured and recorded. That is, the analog signal is sampled using an A/D converter and the data stored in a text file. To efficiently analyze

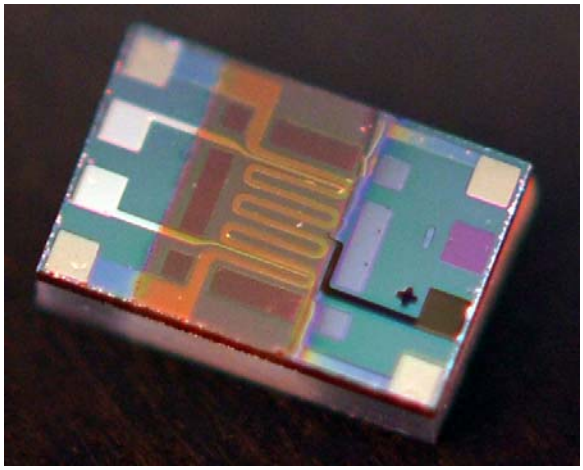

Figure 9. Photograph of a MEMS sensor developed at URI.

this data, a graphical user interface (GUI) using MATLAB was developed. This MATLAB code performs the data reduction function. The acquired digitized signal data is usually over 100,000 sampling points per run. The GUI digitally samples the data and reduces this to between 100 and 2000 data points. It also enables the user to perform some graphical manipulation of the data. Once stored, the data can be easily analyzed or plotted using a broad array of mathematical and graphical tools. A second GUI was developed using MATLAB to perform signal processing functions. This program loads the original data, reduced data, or reduced data that has been truncated. The data can be digitally filtered to minimize random noise either using automatic or manual selection controls depending on user input. The program also enables the user to calculate and subtract out any signal drift either automatically or manually. Our high school chemistry and physics teacher, Mr. Anthony Fascia, was largely responsible for this task, which was successfully integrated into our working sensor platform.

5. Students Supported

<u>Undergraduate Students Supported</u>
Caitlin Hurley; Chemical Eng.
Bisola B. Bruno; Chemical Eng.
Benjamin Jaques, Chemical Eng.
Matin Amani, Electrical Eng.

<u>Graduate Students Supported</u>
Yun Chu; Chemical Eng, PhD
Dan Mallin; Chemical Eng, MS
Carson Pryde; Chemical Eng, MS

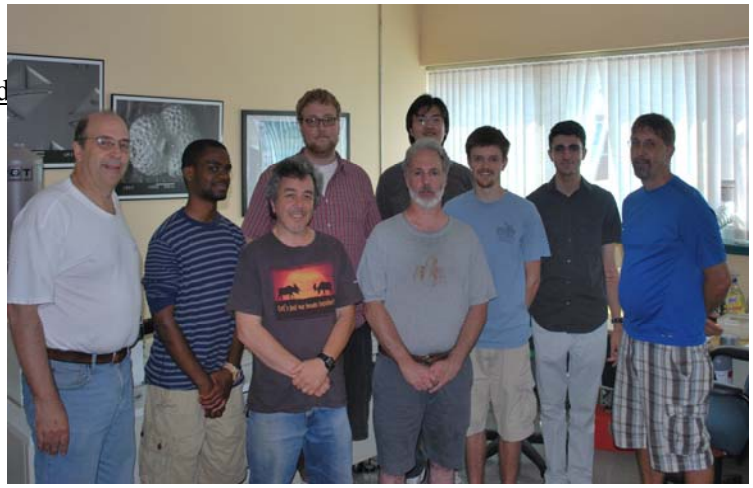

6.Transition Partners
SensorTech, Inc., Savannah, GA and NUWC Middletown, RI

7. Publications / Patents

Y. Chu, C. Pryde, C. Hurley, M. Amani, M. Platek, A. Davis and O.J. Gregory, "Detection of Peroxides Using Pd/SnO_2 Nanocomposite Catalysts", submitted to IEEE Sensors.

M. Amani, Y. Chu, K. Waterman, C. Hurley, M. Platek and O.J. Gregory, "Detection of Triacetone Triperoxide (TATP) Using a Thermodynamic Based Gas Sensor", Sensors and Actuators B: Chemical, Vol. 162, p.7-13 (2012).

K. Maciejewski, Y. Sun, O. J. Gregory and H. Ghonem, "Time-dependent Deformation of Low Carbon Steel at Elevated Temperatures", Materials Science and Engineering: A, Volume 534, p.147–156 (2012).

W. Visser, Y. Sun, O. Gregory, G. Plume, C-E. Rousseau, H. Ghonem, "Deformation characteristics of low carbon steel subjected to dynamic impact loading", Material Science and Engineering A, 528, p. 7857– 7866 (2011).

O.J. Gregory, H. Ghonem, M.J. Platek, J. Oxley, J. Smith, M. Downey, C. Cummiskey and E. Bernier, "Microstructural Characterization of Pipe Bomb Fragments", Materials Characterization, Vol.61, No. 3, p.347-354, (2010).

"A Thermodynamic Based Gas Sensor for the Detection of TATP", O.J. Gregory, M. Platek, M. Amani and A. Cote, URI Patent disclosure filed 2011.

8.Presentations:

221st Electrochemical Society Meeting, Seattle, Washington, May 2012, "Catalyst Development for Thermodynamic Based Gas Sensors Using Combinatorial Chemistry", Y. Chu, C. Hurley, C. Pryde, M. Amani, M.Platek and O.J. Gregory.

RICC Research 2 Reality 2011, Northeastern Univ, Boston, MA, Oct 2011, "Thermodynamic Based Sensors for the Detection of Explosives and Explosive Precursors", O.J.Gregory

219th Electrochemical Society Meeting, May 2011, Montreal, Canada, "Detection of TATP Using Thermodynamic Based Gas Sensors with Metal Oxide Catalysts", Y. Chu, K. Waterman, C. Hurley, M. Amani and O.J. Gregory.

Microscopy and Microanalysis 2010, Portland , OR, "Characterization of Pipe Bomb Fragments using Optical Microscopy and Scanning Electron Microscopy", M.J. Platek, O. J. Gregory, T. Duarte, H. Ghonem, J. Oxley, J. Smith, E. Bernier.

Development of Resonating Nanocantilever Chemical Vapor Sensors and Thiol Encapsulated Gold Nanoparticle Chemiresistors

Nathan S. Lewis

I. Objective

We aim to develop new classes of chemiresistive sensors capable of detecting light gases and vapors, including explosives. These cheap to fabricate and easy to multiplex chemiresistive sensors will improve sensitivity and range of electronic noses, enabling them to detect a wider range of threats to security. Further, we are working toward the realization of a nanoscale electronic nose, which could be embedded in everyday devices like cell phones or incorporated into lab-on-a chip systems such as micro-gas chromatographs, through the development of resonating nanocantilever sensors.

II: Summary

This year we have continued to study the response mechanisms of nanocantilever chemical vapor sensors to determine the optimal polymer coating techniques to maximize sensitivity and minimize response time.

III: Accomplishments

We published one study on carboxylate-capped TiO_2 nanoparticle chemiresistor sensors. The TiO_2 acted as an inorganic support phase for the swellable, organic capping groups of the NPs, and the CB imparted electrical conductivity to the film. Such sensor composite films exhibited a reproducible, reversible change in relative differential resistance upon exposure to a series of organic test vapors. The response of such chemiresistive composites was comparable to, but generally somewhat smaller than, that of thiol-capped Au NPs. We also produced one conference presentation on using surface initiated polymerization to grow thick sorptive films on nanocantilever chemical vapor sensors. Masking and passivation were used to localize polymer growth to specific areas of the nanocantilevers, elucidating the role of competing response mechanisms in observed frequency shifts. The effect of localizing polymer growth on sensor behavior varied depending on whether glassy or rubbery polymer films were employed. Modeling of the nanocantilever responses to analyte vapors revealed that the observed sensor responses are primarily due to changes in sensor spring constant rather than accretion of mass.

Progress Toward Nanoscale Electronic Nose

Heather McCaig, Ed Myers, Derrick Chi, Xinchang Zhang, Nathan S. Lewis, Michael L. Roukes

1) Variation in Glass Transition Temperature of Sorptive Polymer Films Grown by Surface Initiated Polymerization for Sensitising Resonant Nanocantilever Chemical Vapor Sensors

Vapor sorption onto nanocantilevers affects both the mass and the stiffness of the sensors, leading to shifts in the resonance frequency.[1] Mass accretion drives resonance frequency lower while an increase in effective spring constant (due to polymer film swelling or other surface stress changes) drives the resonance frequency higher, such that these two response mechanisms are capable of cancellation under certain conditions. Even if frequency shifts are observed upon exposure to a chemical vapor, the magnitude of the response can be depressed by these competing mechanisms. By utilizing a polymer that maintains a very low glass transition temperature (T_g) in a surface-bound 100 nm thick film, the affects of polymer-induced mechanical strain on the nanocantilever sensor is minimized. Thus the observed response is strongly enhanced.

In this study the performance of nanocantilevers functionalized with SI-ATRP grown films of poly(methyl methacrylate) (PMMA, bulk T_g ~ 70 °C),[2] poly(methyl acrylate) (PMA, bulk T_g ~ 10 °C), and polymer(butyl methacylate, bulk T_g ~ 15 °C)[3] were compared. Films ranged from approximately 90-100 nm thick, and were grown from the top, Au coated, surface of the nanocantilevers. The two methacrylate polymers produced smooth films, while the acrylate polymer, for which a new polymerization procedure was developed, produced rough films due to the higher rate of chain termination during polymerization. SEM images of representative examples of nanocantilevers with each type of coating are shown in Figure 1. The sensors were then exposed to a series of analyte vapors at concentrations ranging from 0.005 – 0.08 P/P^O (where P and P^O are the partial pressure and saturated vapor pressure, respectively). The responses of the nanocantilevers to 400 s vapor exposures are shown in Figure 2. The PMMA-coated nanocantilever exhibited positive shifts in relative resonance frequency upon exposure to analyte vapors, illustrating the effects of sensor stiffening on response. Conversely, the nanocantilevers coated with the low T_g polymers, PMA and PBMA, exhibited negative shifts in resonance frequency upon exposure to analyte vapors, indicating that sensor response was dominated by mass loading or sensor softening. The PBMA coated nanocantilevers exhibited the best sensitivity to analyte vapors, and further was shown to provide linear responses to all vapors tested up to 0.08 P/P^o. The nanocantilevers coated with low T_g polymers also exhibited greatly reduced response times compared to the PMMA-coated sensor, as shown in Figure 3. These results indicate the model for an optimal polymer can include a stiff methacrylate group, which readily polymerizes from surfaces at room temperature without dramatic chain termination, if bulky side chains, such as n-butyl, are incorporated to lower the T_g and facilitate diffusion of analyte vapors.

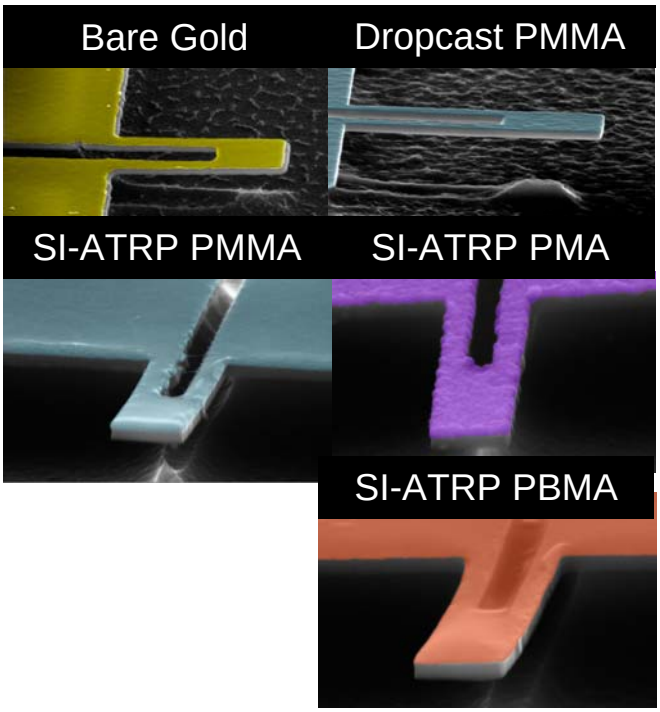

Figure 1: False-color SEM images of nanocantilevers with five different surface chemistries. The dropcast PMMA film is <10 nm thick, while the SI-ATRP grown

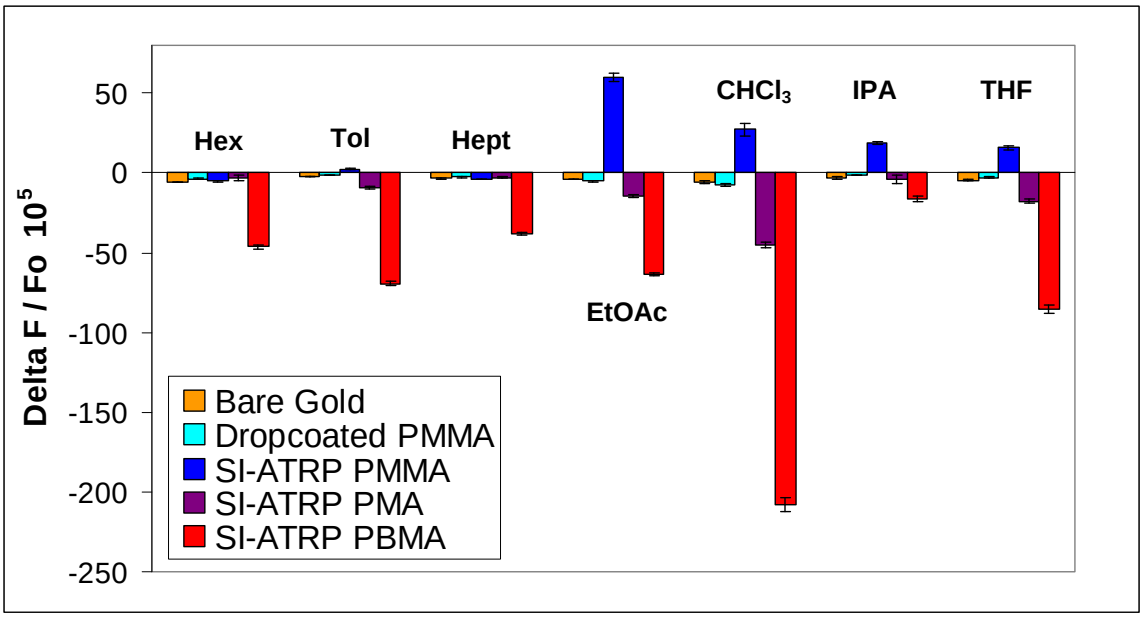

Figure 2: Relative frequency shift of nanocantilevers with various coatings upon exposure to 0.02 P/P^o of a series of volatile organic compounds. This figure has been updated with new SI-ATRP PMA sensor response data.

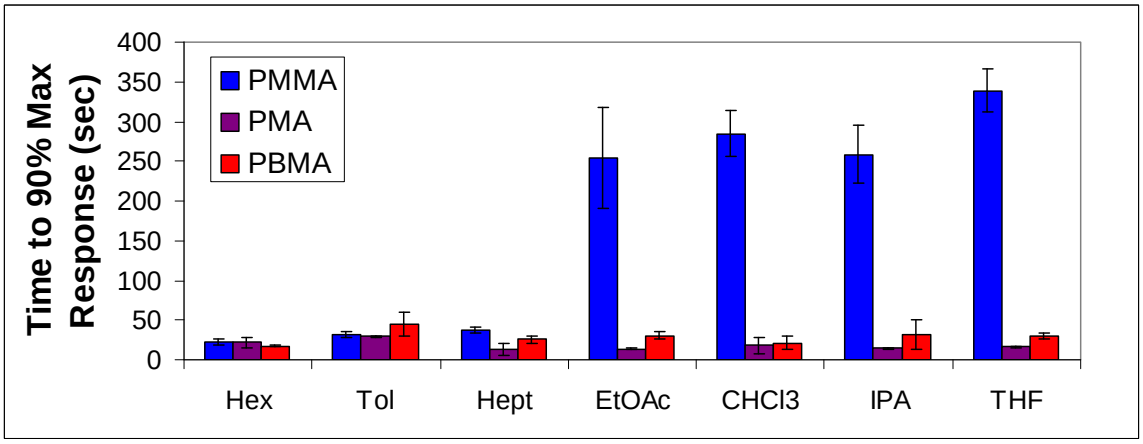

Figure 3: Sensor response time of nanocantilevers coated with thick films of low glass transition temperature PMA and PBMA is much faster than for sensors with a PMMA film. This figure has been updated with new SI-ATRP PMA sensor response data.

2) Enhancing Sensitivity of Nanocantilever Chemical Vapor Detectors Through Localized Surface Functionalization

Nanocantilever chemical vapor sensors respond to the presence of analyte vapor through multiple competing mechanisms including mass loading, which induces a negative shift in resonance frequency, stiffening, which induces a positive shift in resonance frequency. To investigate these mechanisms and enhance sensitivity, we have developed a method to grow thick polymer films on isolated areas of the nanocantilevers. Sections of the cantilever were masked by chromium, and then thiol chemistry along with atom radical polymerization (SI-ATRP) of methyl methacrylate (MMA), methyl acrylate (MA), and n-butyl methacrylate (BMA) was used

to produce films as thick as 80 nm on the gold portions of the nanocantilevers. Polymer films of this thickness sorb significant quantities of vapor and overwhelm the effect non-specific physisorption of vapor molecules onto non-gold surfaces. SEM images of the various chromium-masked cantilevers, pre- and post-polymerization, as shown in Figure 4.

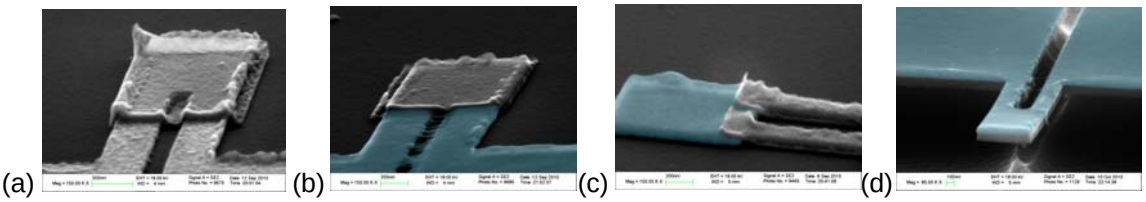

Figure 4: SEM images of (a) bare unsuspended nanocantilever; gold legs and chromium masked tip. (b) PMMA growth is isolated to exposed gold areas of an unsuspended nanocantilever. (c) PMMA only film isolated to Au tip of a Cr-masked cantilever. (d) PMMA grown on the entire surface of an unmasked, suspended cantilever.

The sensors were then exposed to 400 s pulses of a series of analyte vapors at concentrations ranging from 0.005 – 0.08 P/P^O (where P and P^O are the partial pressure and saturated vapor pressure, respectively). The responses of the chromium-masked nanocantilevers coated with SI-ATRP PMMA films (see Figure 5) show that sensor response magnitude is enhanced if vapor sorption on the cantilever tip is prevented (Cr Tip) relative to a gold-only sensor. This provides further evidence of the potential for competing mass-loading and stiffening response mechanisms occurring on a single sensor, and indicates that the optimal coating geometry for a high Tg polymer film minimizes mass-loading.

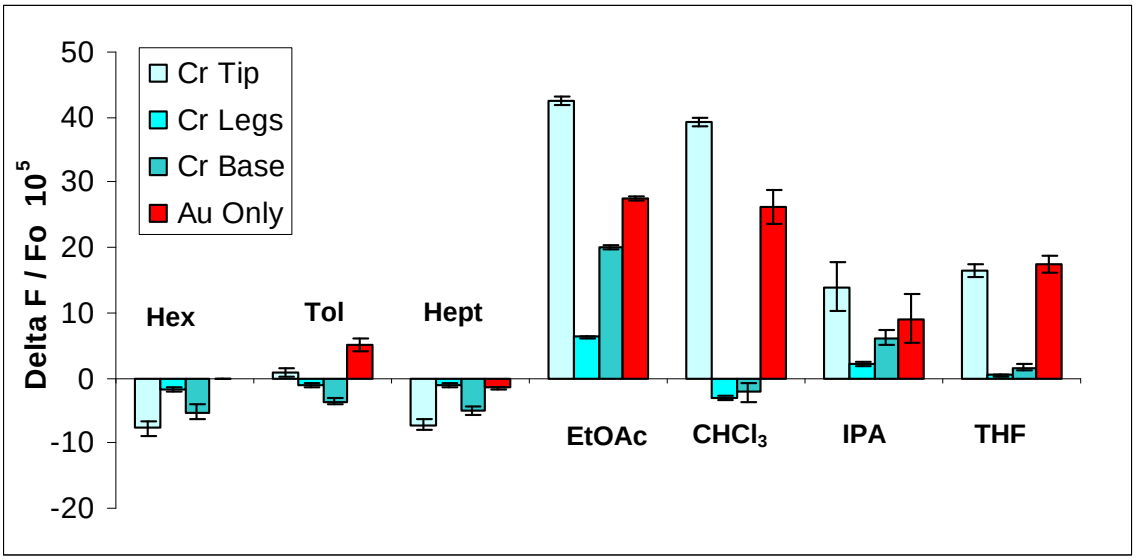

Figure 5: Localization of SI-ATRP PMMA film to the nanocantilever legs enhances sensor response magnitude.

The chromium-masked nanocantilevers coated with the low T_g polymer films PBMA and PMA exhibited much different response behavior from the PMMA-coated sensors. The results of vapor exposures to chromium-masked PBMA-coated nanocantilevers (see Figure 6) reveal that sensor responses are minimized when vapor absorption occurs only on the cantilever tip. This indicates that the large negative shifts in resonance frequency observed for the other sensor geometries is induced by vapor sorption on the legs and base of the nanocantilevers. To further analyze these results, the nanocantilever resonance behavior was modeled (using polymer/vapor partition coefficients calculated from quartz crystal microbalance experiments) to determine the expected resonance frequency shift due to mass-loading only. Due to the shape of the first

resonant mode, mass-loading at the cantilever tip effects frequency one hundred times as strongly as mass-loading on the legs and base of the device. In addition, the calculated resonance frequency shift of a gold-only nanocantilever due to mass-loading was an order of magnitude smaller than the observed responses of gold-only sensors. This indicates that the strong negative shifts in resonance frequency observed for the Cr-Tip, Cr-Base, and Au Only sensors are not due to mass-loading. Instead, these strong responses can be attributed to the softening (decreased spring constant) of the PBMA-coated nanocantilever upon exposure to analyte vapors.

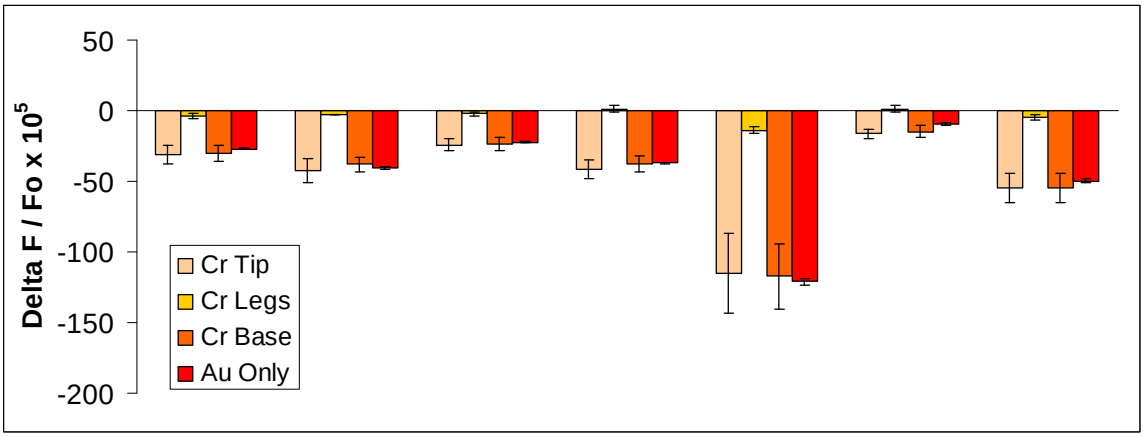

Figure 6: Localization of SI-ATRP PBMA revealed that sensor response was primarily due to vapor sorption on the legs and base of the nanocantilever, and thus was caused by softening of the resonator, rather than mass loading.

No discernible trend in sensor response could be determined for PMA-coated nanocantilevers (see Figure 6) due to insufficient localization of the polymer film (likely due to the failure passivation monolayer on the chromium during the 48 hr, 50 °C polymerization reaction), and the low response magnitude. This result further illustrates the benefit of using monomers capable of polymerizing at room temperature.

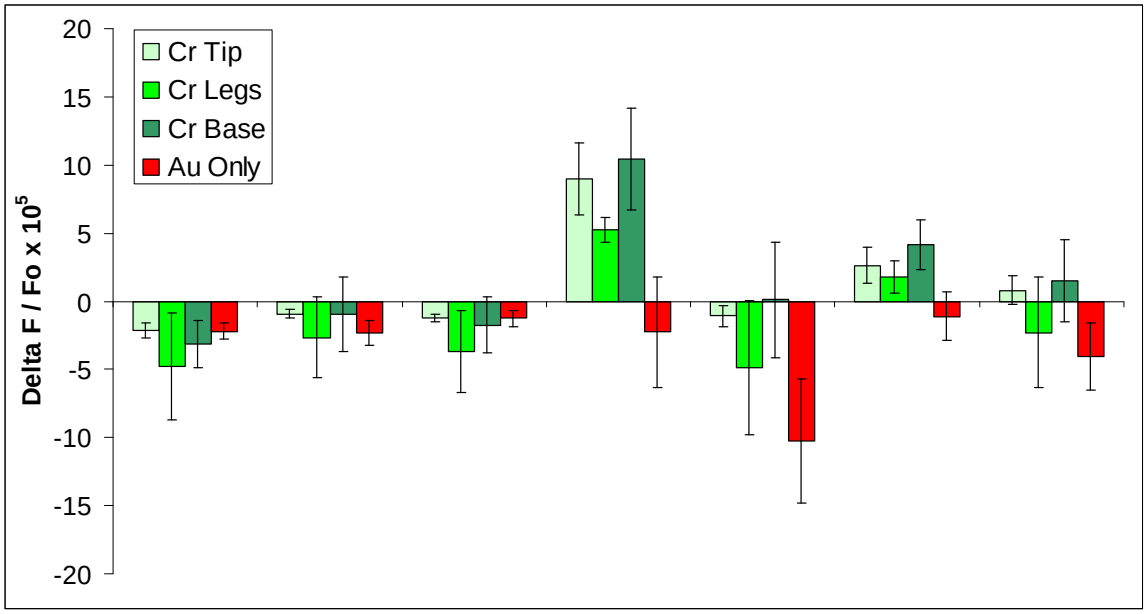

Figure 7: Localization of SI-ATRP PMA did not produce a clear trend due to low response magnitude and insufficient selectivity of polymer deposition area.

References
1. Eom, K.; Park, H. S.; Yoon, D. S.; Kwon, T., Nanomechanical resonators and their applications in biological/chemical detection: Nanomechanics principles. *Phys. Rep.-Rev. Sec. Phys. Lett.* **2011,** *503* (4-5), 115-163.
2. Jones, D. M.; Huck, W. T. S., Controlled surface-initiated polymerizations in aqueous media. *Adv. Mater.* **2001,** *13* (16), 1256-1259.
3. Xu, C.; Wu, T.; Drain, C. M.; Batteas, J. D.; Fasolka, M. J.; Beers, K. L., Effect of block length on solvent response of block copolymer brushes: Combinatorial study with block copolymer brush gradients. *Macromolecules* **2006,** *39* (9), 3359-3364.

V. Students Supported

Heather McCaig: PhD Subject: Resonating nanocantilever chemical vapor sensors.

VI. Journal Publications

1. Garcia-Berrios, E.; Gao, T.; Walker, D.; Brunschwig, B. S.; Lewis, N. S., Composites of carboxylate-capped TiO2 nanoparticles and carbon black as chemiresistive vapor sensors. *Sensors and Actuators B-Chemical* **2011,** *158* (1), 17-22.

VII. Conference Presentations

1. McCaig, H.C.; Myers, E.B.; Chi, D.; Lewis, N.S.; Roukes, M.L. *Probing the Response Mechanisms of Resonating Nanocantilever Chemical Vapor Sensors by Tailoring the Properties and Location of Sorptive Films through Surface Initiated Polymerization.* 243rd ACS National Meeting Spring 2012.

Gas Phase Ion Chemistry and Non-Contact Sampling of Explosives

Gary A. Eiceman; Chemistry Dept; New Mexico State University
575-646-2146; geiceman@nmsu.edu

General

Instruments that are used as trace detectors of explosives at airports worldwide today are based on ion mobility spectrometry (IMS) and these analyzers provide high-speed response (<8s) to nanogram and sub-nanogram amounts of high explosives. Apart from concerns surrounding the actually step of collecting sample, the performance of these instruments is governed by a combination of gas phase ion-molecule chemistry and characterization of ions for mobility in a drift tube at ambient pressure. Significant deficiencies exist in both the technology and in our understandings of principles. Such deficiencies limit the practice of trace detection with the current generation of analyzers, hinder new and next embodiments of these principles, and limit long-range vision for how these principles might be favorably arranged for new capabilities in explosives detection. The overall objective of this work has been to clarify the central and fundamental issue in ion based methods of explosive determinations, namely, the stability and lifetime of ions of explosives in air at ambient pressure. A second and essential aspect of trace detection concerns sample collection and we wish to explore a new concept in surface sampling which might provide a next generation capability for automated screening of items, some of which may have irregular surfaces.

In Year 1, a refined design to measure the stability of gas phase ions was constructed and demonstrated and shown to provide kinetic information on the decomposition of gas phase ions without the failures of all prior designs where entry of sample neutrals into the kinetic region corrupted measurements.

In Year 2, the gas chemistry of explosives or explosive related materials nitrotoluene (NT), dinitrotoluene (DNT), trinitrotoluene (TNT) and Pentaerythritol tetranitrate (PETN) were observed.

In Year 3. The Kinetics of the decomposition of explosives or explosive related adducts materials of Ethylene glycol di-nitrate (EGDN) and tri-nitroglycerine (NG) were experimentally obtained by a dual shutter ion mobility spectrometer. Characterization of other explosives is in progress though not completed at the end of Year 3.

Negative chloride adduct ions of EGDN and NG undergo decomposition at temperatures as early as 80°C suggesting that gas phase ions were more unstable than anticipated. These studies were made using chloride ion chemistry as practiced in current trace detector technologies. For both adducts ions of EGDN and NG, the range of decomposition temperature is as narrow as 10-20°C. The area under the elevated baselines between the adduct peak and the decomposed product ion peak is normally used to derive the rate constants in air at ambient pressure with our method.

In 2012, we added the second dual shutter ion mobility spectrometer for these studies with an electrospray ion source. This instrument will be mainly used to study thermal fragile explosives in parallel to the other instrument. Studies with 1,2-NG, 1,3-NG, PETN, ETND, EGDN and TEGDN are underway with these instruments and will be continued in 2012 to 2013.

RESULTS AND DISCUSSION

Ion Kinetic Studies with EGDN

In Figure 1, a 3-D plot is shown of the results of a temperature study for EGDN and chloride dopant with the gas chromatograph kinetic ion mobility spectrometer. The plot shows the formation of EGDN·Cl^- adduct and the decomposed product ion (NO_3^-), well separated from an impurity peak by gas chromatograph pre-fractionation.

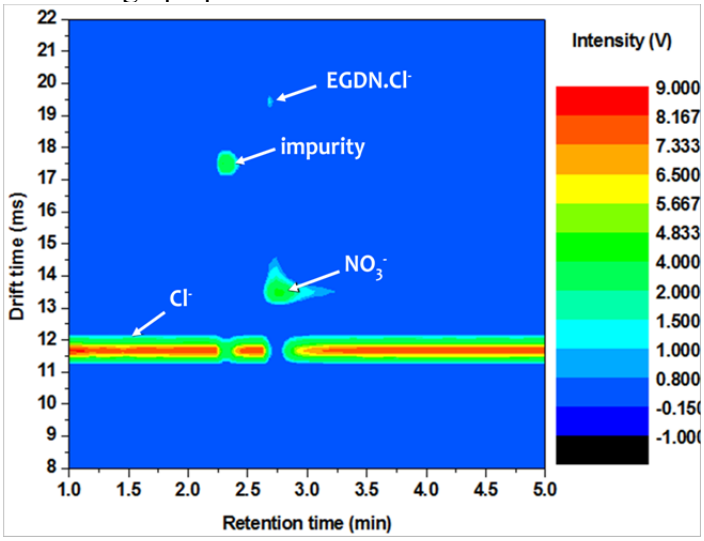

Figure 1. Contour plot for the thermal decomposition of EGDN·Cl^- adduct ion at 88°C.

Figure 2 shows the decomposition of EGDN·Cl^- adduct with the first shutter operation of the mobility spectrometer. The baseline elevation between the EDGN·Cl^- and NO_3^- peaks suggest the decomposition of the adduct giving off NO_3^- .Some off the EDGN·Cl^- gated into the drift region decompose while they travel from shutter to the detector. These ions have drift times in between the drift times of EDGN·Cl^- and NO_3^- ions. Thus, they elevated the baseline. This is a 1st order reaction and the decomposition is higher at the shutter compared to the detector side. Therefore, the baseline elevation has a slope from NO_3^- peaks towards the EGDN·Cl^- peak. However, NO_3^- ion intensity may not be exactly due to the decomposition of the EDGN·Cl^- adduct ions in the drift region. To ensure that EDGN·Cl^- adduct ions were injected (isolated) into the drift region of the mobility spectrometer by operating both shutters.

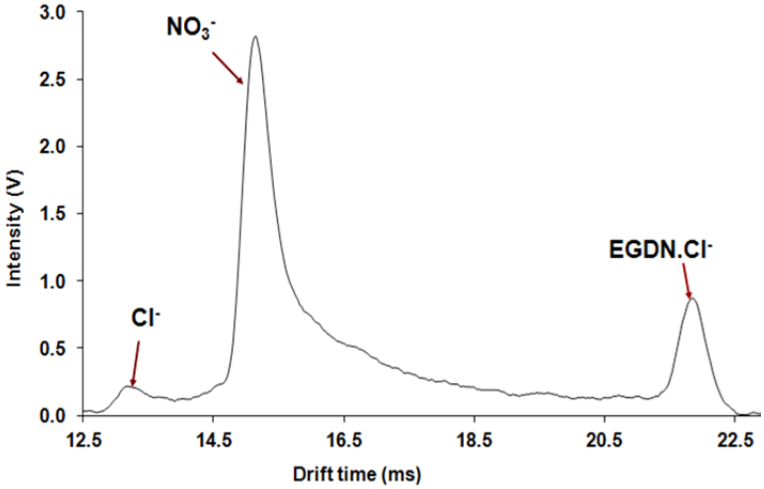

Figure 2 The decomposition of EGDN·Cl^- adduct with the first shutter operation at 84°C.

Figure 3 shows the decomposition of the isolated EGDN·Cl^- ions within the drift region of the mobility spectrometer. The area under the elevated baseline can be used to calculate the kinetics (rate constant) for the decomposition. By obtaining the rate constants for several temperatures within a narrow temperature range, an Arrhenius relationship can be derived to obtain the activation energy and pre-exponential factor for the reaction. Figure 4 shows the Arrhenius plot obtained from the experimental rate constants.

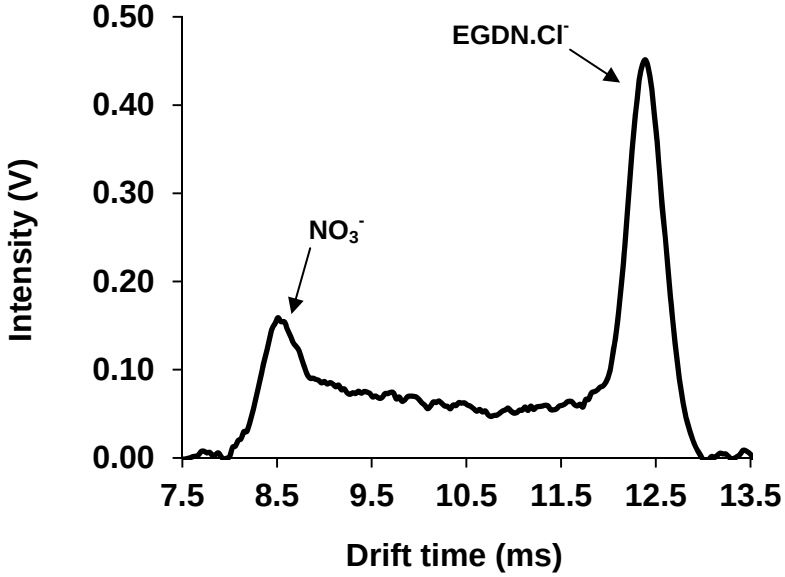

Figure 3 The decomposition of the isolated EGDN·Cl^- ions within the drift region of the mobility spectrometer at 88°C.

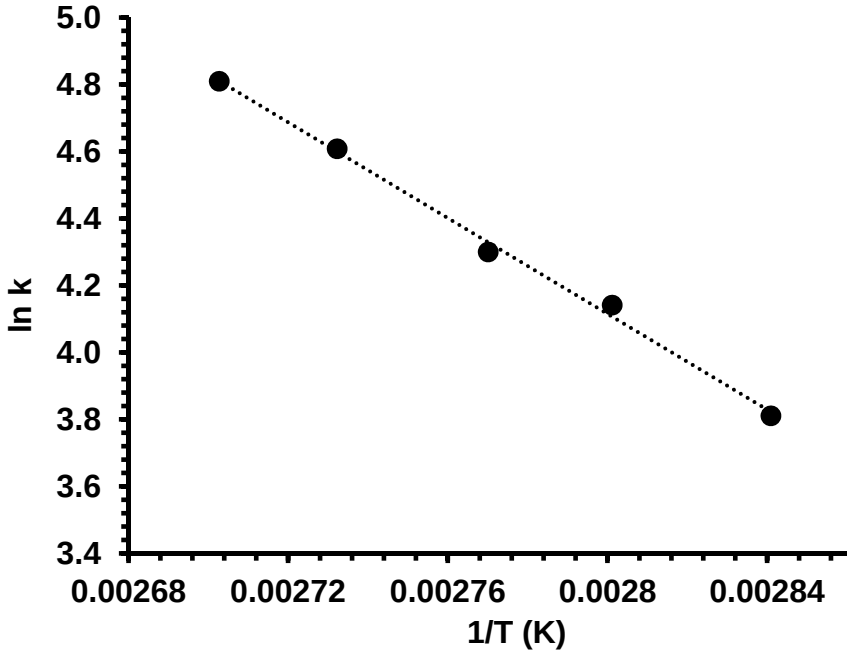

Figure 4. Arrhenius plot for the thermal decomposition of EGDN·Cl^- adduct.

Ion kinetic studies with NG

Thermal decomposition of $NG{\cdot}Cl^-$ adduct was observed over a temperature range of 112 to 123°C by the same technique. Spartan 10 was used for *ab-initio* calculations to determine the kinetics and the reaction path for the thermal decompositions of both EGDN and NG adducts. It was found that both decompositions are displacement reactions where chloride ion displaces one of the nitrates and forms a neutral molecule. *ab-initio* calculation of dissociation gives an enthalpy change for decomposition by loss of NO_3^- from $EGDN{\cdot}Cl^-$ as 61 kJ mol^{-1}. The experimentally obtained enthalpy change for the above mention dissociation was 62 kJ mol^{-1}. The *ab-initio* calculation of dissociation gives an enthalpy change for decomposition by loss of NO_3^- from $NG{\cdot}Cl^-$ as 76 kJ mol^{-1}. The experimentally obtained enthalpy change for the above mention dissociation was 82 kJ mol^{-1}.

CONCLUSIONS

A kinetic dual shutter ion mobility spectrometer with a gas chromatograph as a sample pre-fractionation inlet was built and characterized successfully to determine ion lifetimes, energies, and kinetics of decomposition of gas phase ions of energetic materials. The thermal dissociation of $EGDN{\cdot}Cl^-$ adduct showed a displacement reaction as shown; $EGDN{\cdot}Cl^- \rightarrow (EGDN\text{-}NO_3+Cl) + NO_3^-$. The dissociation of $EGDN{\cdot}Cl^-$ adduct was observed in the temperature range of 79°C to 97°C at ambient pressure. Thermal dissociation of NG·Cl- follows the same reaction path that of $EGDN{\cdot}Cl^-$. The dissociation of $NG{\cdot}Cl^-$ adduct was observed in the range of 112-123°C at ambient pressure. Kinetics for the thermal dissociations of chloride adducts of EGDN and NG were experimentally determined and the difference in experimental and *ab-initio* calculations for ΔH^o were found to be as low as ~1-5 kJ/mole.

Future Work

The instrument is in superb operating condition and studies are being made on as many explosives in the nitro-alkane and nitro-aromatic family as possible.

Publications

1. Two journal articles in preparation
2. One presentation at the 20th International Conference on Ion Mobility Spectrometry, July 2012, Orlando, FL (copy attached).

Shaped Femtosecond Pulses for Remote Chemical Detection

Yaron Silberberg, Weizmann Institute of Science, Rehovot, Israel

I. Objective

Our goal is to develop nonlinear spectroscopic methods for the remote detection of hazardous materials in general and explosives in particular, using the vibrational spectrum of molecules as a fingerprint for chemical species identification. The main approach we have been taking employs carefully tailored ultrashort laser pulses for Stimulated Raman Scattering (SRS) and Coherent Anti-stokes Raman Spectroscopy (CARS).

II. Accomplishments

We have demonstrated a "Shaper-less" standoff remote detection from distance of up to 50 meters, using femtosecond pulses shaped by a photonic crystal filter, results now published in Appl. Phys. Lett. (attached).

We have continued our effort to improve detection scheme. In particular, we have been investigating methods for fast pulse shaping to detect simultaneously several species by forming lock-in detection on temporally modulated pulse shapes as described below.

III. Details

Fast pulse shaping techniques for rapid tunability of excited Raman levels

Standoff detection often calls for simultaneously probing multiple Raman levels or the collection of a full Raman spectrum. Particularly, the ability to rapidly tune the specific Raman mode under interrogation could determine the applicability of a particular method [1]. In conventional multi-beam approaches, the speed of a spectral scan is therefore limited by the desired resolution, ie number of spectral acquisitions, and dictated by the time required to detune the pump and stokes beams (seconds). In single-beam selective excitation approaches, based on pulse shaping, the speed is also limited by the resolution, however dictated by the ability to change the spectral mask, which can be on the order of milliseconds when using a conventional spatial light modulator (SLM) or as low as nanoseconds with more advanced devices such as acousto-optical modulators.

The ability to rapidly shape pulses has been previously studied using SLM techniques and applied in CARS schemes [2-5]. One of the simplest adaptations to a traditional SLM based, 4-f shaper is the ability to change phase shapes by scanning the spectrally spread beam in an additional dimension on a two-dimensional (2-D) SLM, transverse to the spectral axis (See Fig. 1 inset). Using a 2-D SLM, Frumker et al have shown that rapid shape selection is possible by imaging a galvanometric mirror on the grating of a 4-f shaper, prior to the Fourier lens, and thus enable one to scan the location of the beam on the SLM and hence address a series of phase patterns). This technique allows for independent phase patterns to be addressed once fixed on the SLM and changed at rates limited by the galvanometer. Using this technique, Frumker demonstrated pulse shaping up to 100Khz. Such use of rapid phase scanning has demonstrated in a CARS and two-photon absorption schemes where the phase was alternated between shapes that maximize the constructive and destructive interference paths leading to population of a vibrational or electronic level respectively. This technique readily allows for rapid acquisition with suppressed background using standard lock-in detection. Although this method has been used to rapidly observe a

single Raman mode, full spectral information could be obtained by encoding the 2-D SLM with phases corresponding to a full range of temporally split pulses and spectral information could be retrieved via real-time Fourier analysis with a spectrum analyzer.

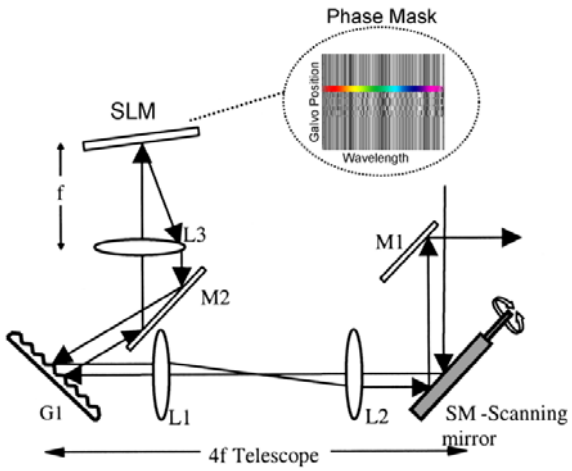

Figure 1. Schematic drawing of a 4-f pulse shaper with a 2-D SLM and corresponding phase pattern (inset) scanned by a galvanometric mirror (SM). The spectral content is dispersed in the horizontal dimension and scanned along the vertical dimension..

Using a similar experimental configuration we have demonstrated 80KHz phase-only shaping for rapid selective excitation measurements with multiplexed detection. In this technique, a series of phase shapes are carefully chosen such that when scanned, the CARS signals from different chemicals are modulated at different frequencies (**Error! Reference source not found.**2 a). This is achieved by first taking full time-domain scans of various pure chemicals and maximizing a cost function that identifies the necessary shapes (shapes corresponding to A-D) leading to the highest contrast between them upon rapid scanning, i.e. lowest frequency correlation (**Error! Reference source not found.**. 2b). The various shapes are then updated on a 2-D SLM and scanned with a galvanometric mirror resulting in the CARS signals modulated at different integer harmonics of the scan frequency, corresponding to the different chemical species (**Error! Reference source not found.**Fig. 2c). The entire CARS signal is chemically discriminated using a dual-harmonic, lock-in amplifier and has been demonstrated with pixel dwell times of 500μs in three dimensional scans. While this technique has proven capable to acquire multiplex measurements of two chemicals, it can be expanded to many more limited by the number of shapes that can be addressed on the SLM as the minimum number of shapes is two to the power of detectable chemicals.

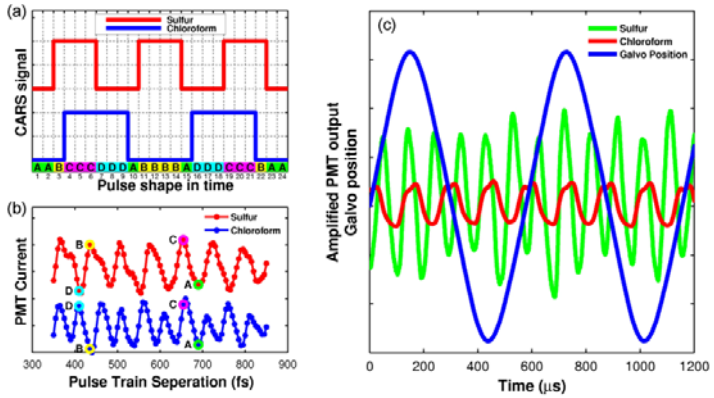

Figure 2. Schematic diagram for rapid multiplexed CARS detection. (a) The desired CARS intensity for sulfur and chloroform, modulated by a series sequentially scanned alternated phase shapes comprised of (b) four independent shapes (A-D). (c) When rapidly scanned, the CARS signal from sulfur and chloroform are modulated at the specified harmonic frequencies of the galvanometric mirror and detected via lock-in detection.

There have also been advances in improving acquisition speeds using techniques that reduce the number of required independent acquisitions. One such technique uses the concepts developed in the field of *compressed sensing* (or compressive sensing). In brief, it has been shown that an N-point signal can be reconstructed from much less than N Fourier measurements, under the assumption of sparse prevalence in the frequency domain. This can be readily applied to the described selective excitation CARS measurements as the number of vibrational spectra of simple molecules are usually sparse, therefore the number of non-zero elements in the spectral domain is low and can be calculated from a similar number of temporal measurements. Using this technique, we demonstrated a 4-fold reduction in the number of temporal measurements necessary to accurately resolve sparse vibrational spectra (Fig. 3)

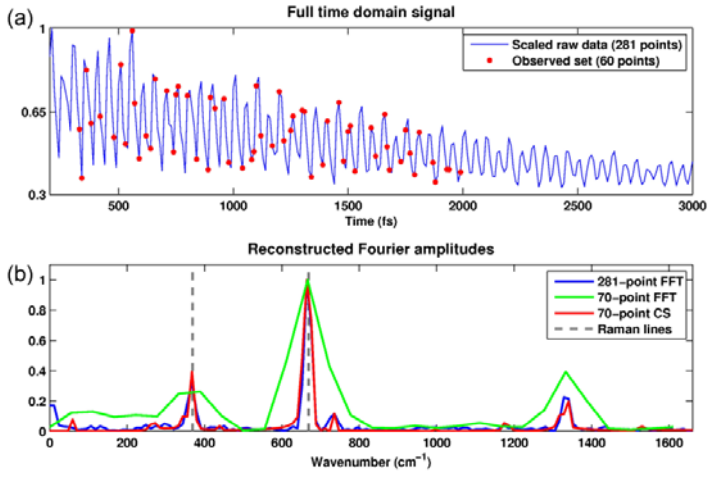

Figure 1

Figure 3. Experimental results of compressive-sensing Fourier transform vibrational spectroscopy using under-sampled time domain data. (a) raw time-domain trace for chloroform, containing 281 points (blue) and the randomly sampled 60 points (red). (b) resolved vibrational spectrum from full data (blue), 60-point data using standard FT (green) and 60-point data using CS reconstruction (red).



Figure 4. Performing standoff detection experiments at distances significantly larger than 10 meters. require some improvisation and special precautions. Experiments at 50 meters were conducted at late hours, in a long corridor that was cordoned off for the duration of the experiment.

IV. Students Involved:

Ori Katz, Postdoc
Jonathan Levitt, Postdoc (Until March 2012).
Hadas Frostig: PhD student
Mor Verbin, PhD student

V. References

[1] Yaron Silberberg 2009. "Quantum Coherent Control for Nonlinear Spectroscopy and Microscopy" , Annu. Rev. Phys. Chem. 2009.60
[2] Frumker, E., D. Oron, D. Mandelik, and Y. Silberberg. 2004. Femtosecond pulse-shape modulation at kilohertz rates. Opt. Lett. 29:890-892.
[3] Frumker, E., and Y. Silberberg. 2007. Femtosecond pulse shaping using a two-dimensional liquid-crystal spatial light modulator. Opt. Lett. 32:1384-1386.
[4] Frumker, E., and Y. Silberberg. 2007. Phase and amplitude pulse shaping with two-dimensional phase-only spatial light modulators. J. Opt. Soc. Am. B 24:2940-2947.
[5] Frumker, E., and Y. Silberberg. 2009. Two-dimensional phase-only spatial light modulators for dynamic phase and amplitude pulse shaping. Journal of Modern Optics 56:2049 - 2054.

SERS Method for Detection of Ultra-Low Levels of Explosives in Complex Matrices

Dr. Radha Narayanan; Chemistry, University of Rhode Island

Objective

The overall objective of my research is to use nanoparticles of different shapes as colloidal SERS substrates for a direct readout and solution-based detection of ultra-low levels of different explosives in different matrices

Summary

We have synthesized dogbone shaped gold nanoparticles of two different sizes. The surface plasmon band of the nanoparticles red-shifts with increasing size of the dogbone shaped gold nanoparticles. We have successfully acquired the SERS spectra for nitrobenzenethiol in water and obtained the calibration curve. We have successfully acquired the SERS spectra of nitrobenzenethiol in other complex matrices such as Sprite and hairspray.

Significance to DHS

The DHS is very interested in being able to detect explosives in actual matrices that travelers would be carrying in their suitcases during a plane trip. We propose to use SERS as a detection method for detecting explosives in liquid matrices that travelers are carrying.

Accomplishments

- Successfully synthesized two different sizes of dogbone shaped gold nanoparticles
- Obtained the UV-Visible spectra of the two sizes of dogbone shaped gold nanoparticles
- Acquired the SERS spectra of nitrobenzenethiol in water
- Obtained the calibration curve of nitrobenzenethiol in water
- Acquired the SERS spectra of nitrobenzenethiol in Sprite and hairspray

Details

The dogbone shaped gold nanoparticles is synthesized using the seed-mediated growth method which consists of two steps: preparation of the gold nanoparticle seeds and growth of the seeds in a growth solution. Systematic variation of the concentration of the different components as well as a variety of different synthetic parameters results in gold nanoparticles of different shapes and sizes. We have synthesized two different sizes of dogbone shaped gold nanoparticles. Figure 1 and 2 show the TEM image and size distribution plot for two different sizes of dogbone shaped gold nanoparticles.

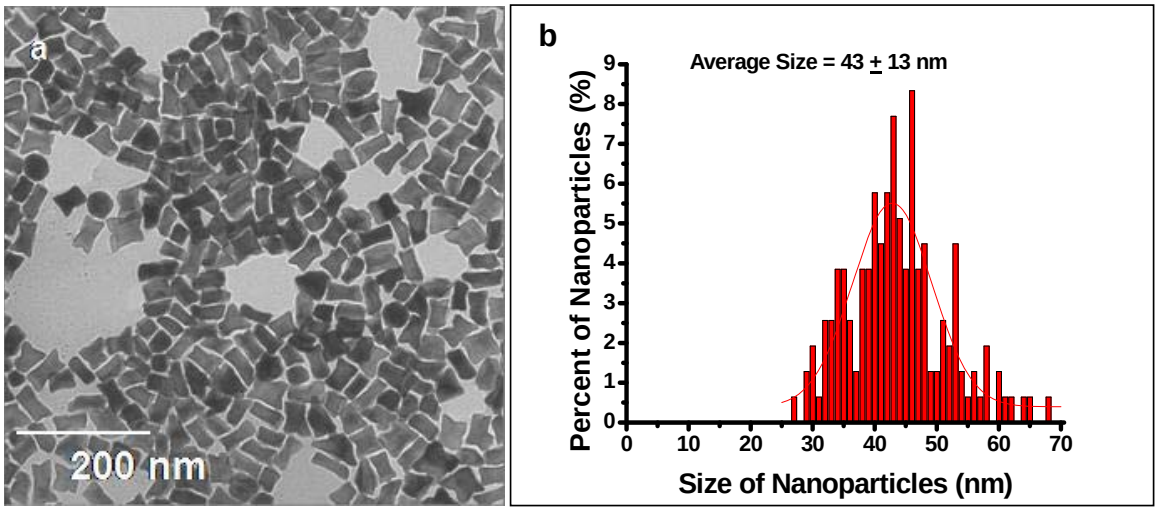

Figure 1. TEM image and size distribution plot of the smaller dogbone shaped gold nanoparticles.

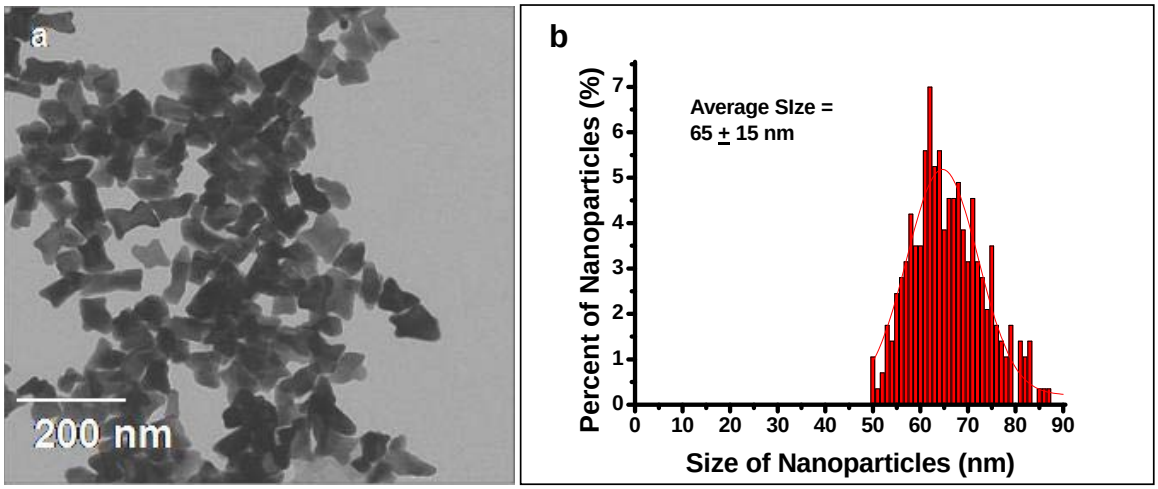

Figure 2. TEM image and size distribution plot of the larger dogbone shaped gold nanoparticles.

We have obtained the UV-Visible spectra of the two different types of dogbone shaped gold nanoparticles. It was observed that the larger dogbone shaped gold nanoparticles result in a higher SPR lambda max which would result in higher SERS enhancements compared to the smaller dogbone shaped gold nanoparticles. Figure 3 and 4 show the UV-Visible spectra of the two types of dogbone shaped gold nanoparticles.

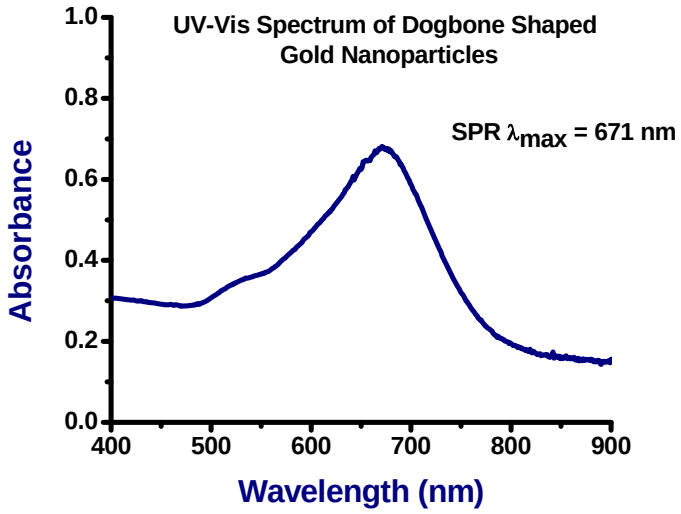

Figure 3. UV-Visible spectra of the smaller dogbone shaped gold nanoparticles

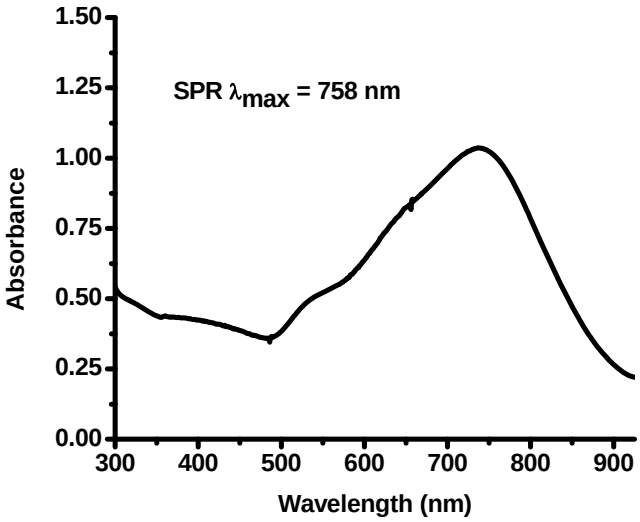

Figure 4. UV-Visible spectra of the larger dogbone shaped gold nanoparticles

We have obtained the SERS spectra of different concentrations of nitrobenzenethiol in water using the larger dogbone shaped gold nanoparticles. Figure 5 shows the SERS spectra of nitrobenzenethiol in water that we have obtained. Figure 6 shows the calibration curve that we have generated for nitrobenzene in water. We also have obtained SERS spectra of nitrobenzenethiol in other complex matrices that would be present in passengers travelling in an airplane. Figure 7 shows the SERS spectra of nitrobenzenethiol in Sprite and Figure 8 shows the SERS spectra of nitrobenzenethiol in hairspray.

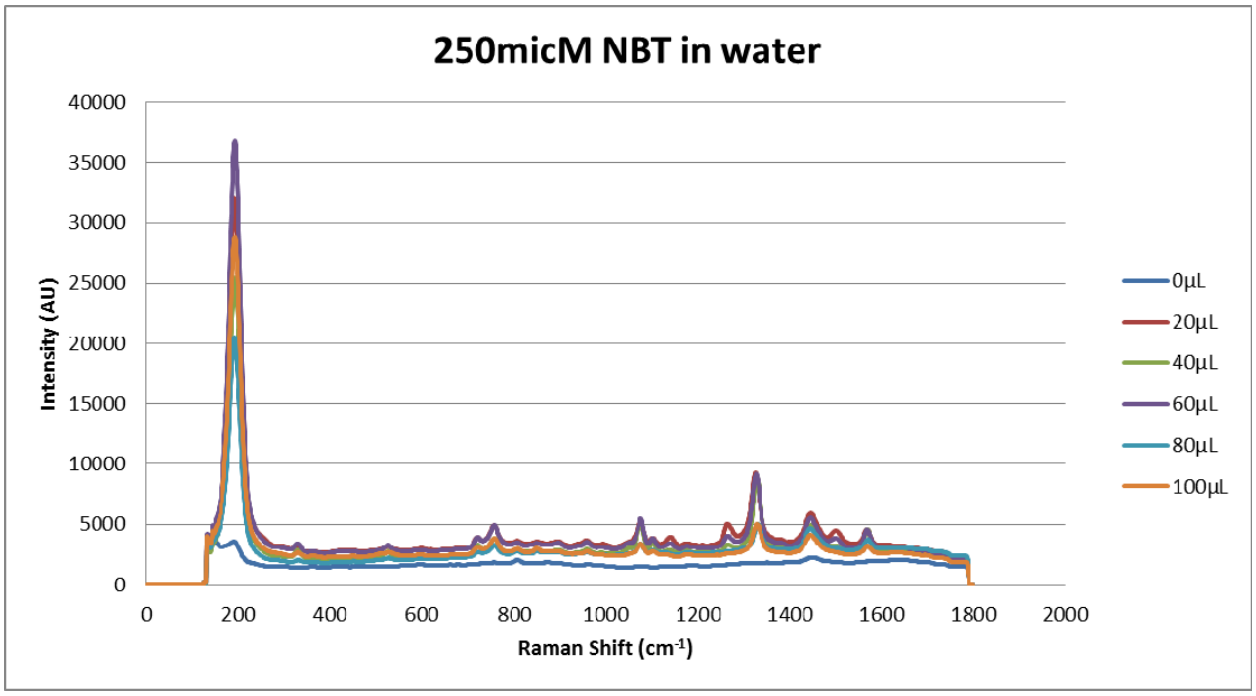

Figure 5. SERS spectra of nitrobenzenethiol in water using the dogbone shaped gold nanoparticles as solution based SERS substrates

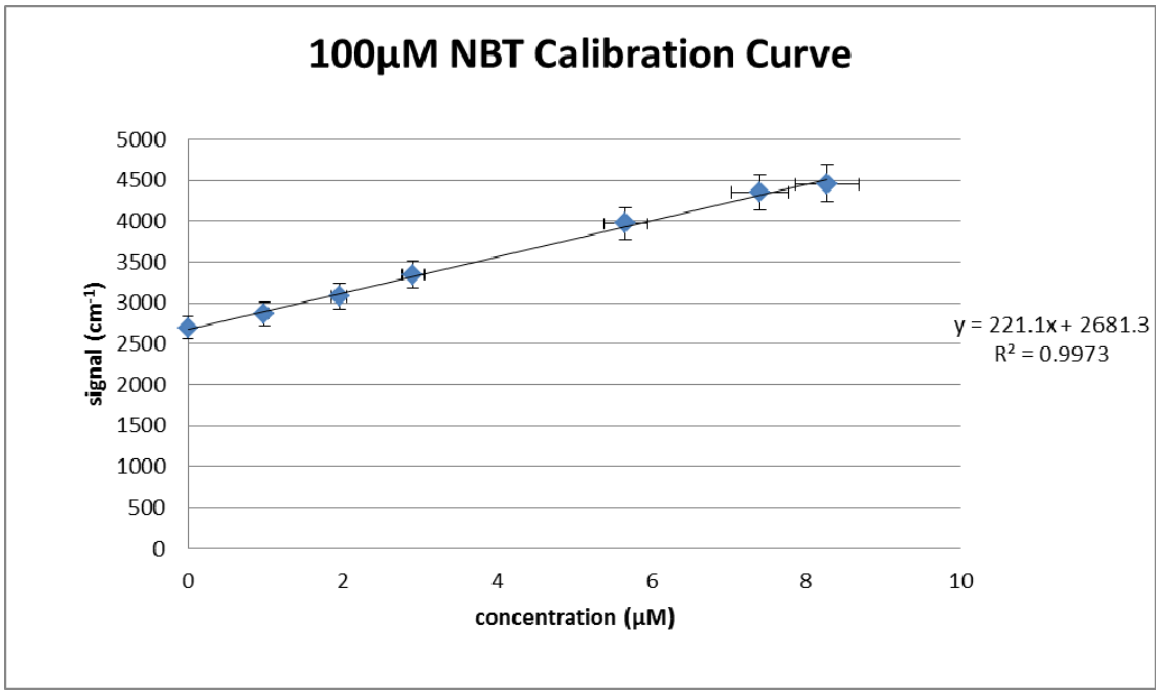

Figure 6. Calibration curve of nitrobenzenethiol in water

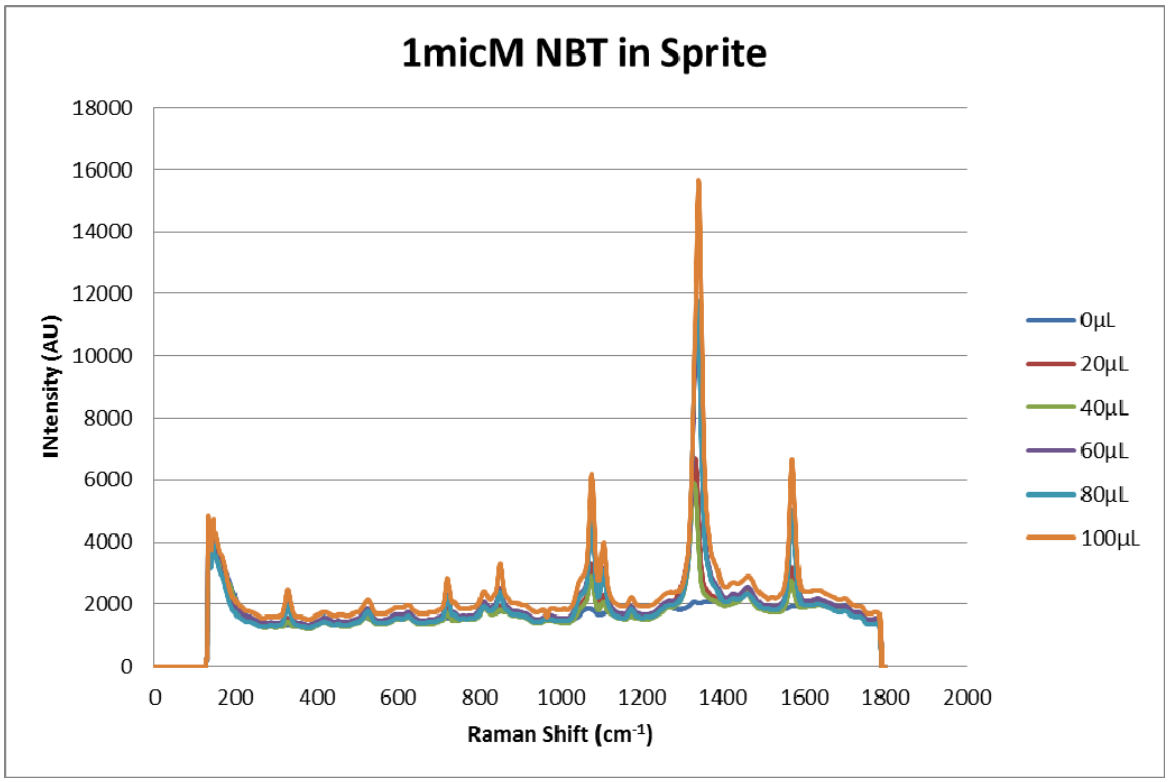

Figure 7. SERS spectra of nitrobenzenethiol in Sprite as the matrice

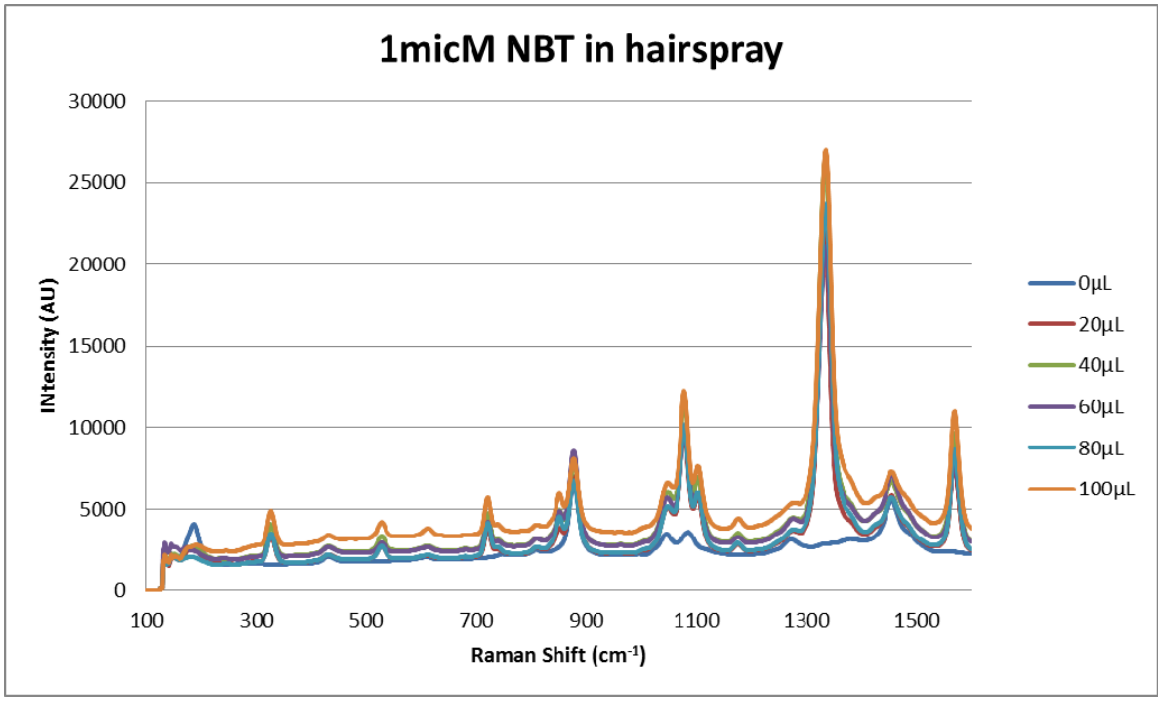

Figure 8. SERS spectra of nibrobenzenethiol in hairspray

Students Supported

Benjamin Saute—Ph.D. student

Allison Alix—undergraduate student

Transition Partners

None.

Publications

1. Saute, B.; Narayanan.R, "Solution-Based Direct Readout Surface Enhanced Raman Spectroscopic (SERS) Detection of Ultra-Low Levels of Thiram with Dogbone-Shaped Gold Nanoparticles", *Analyst*, **2011**, *136(3)*, 527-532.

Prsentations

1. URI Explosives Workshop Poster Session, October 7-9, 2009, Kingston, RI, **Poster**, "Metal Nanoparticles of Different Shapes as Colloidal Substrates for Solution-Based SERS Detection of Environmental Pollutants and Explosives", Benjamin Saute, Nicole Cook, and Radha Narayanan
2. DHS Center Review, March 24-25, 2011, **Poster**, "Nanotechnology for Detection of Ultralow Levels of Explosives", Benjamin Saute and Radha Narayanan
3. DHS Center Review, April 4-5, 2012, Kingston, RI, **Oral**, "SERS Detection of Explosives with Au Nanoparticles", Radha Narayanan

X-ray Bottle Screener Simulant Project

Jimmie Oxley; James Smith; Austin Brown; University of Rhode Island
with Lou Wainwright AS&E

Objective

The original goal of this project is to develop non-hazardous liquids which to x-ray detection instrumentation simulate hazardous (explosive) liquids. Due to the complex nature of x-rays it became apparent that creating simulants that would work for any x-ray system was not feasible. The new goal of the project became the development of an x-ray simulant creation method that could be applied to various x-ray systems.

Relevance to DHS

Airport explosive detection relies heavily on X-ray techniques. Yet, the airport environment is not amenable to calibrating and verifying operability by use of actual explosives. Therefore, we seek to create explosive simulants that can be used for that purpose. However, acknowledging that a simulant for one X-ray instrument may not be appropriate for another, the goal is creating a simulant development method.
the goal shifted from creating simulants to creating a simulant development method.

Background

X-ray scanner response to a compound is based on density (ρ) and effective atomic number (Z_{eff}) of the sample as well as several constants related to the energy of the x-ray used for the scan (eq 1).

$$\text{X-ray response} = \text{gain}*(\rho * Z_{eff}) + \text{offset} \qquad (1)$$

The development of simulants for x-rays was focused on creating simulants that matched both the density and Z_{eff} of the hazardous liquid. The problem with this approach is that it is challenging to match these values, and more importantly the match is only good for the x-ray energy level for which it was created.

Although x-ray response is depends on ρ and Z_{eff} the exact relationship is difficult to define for two main reasons:

1) As can be seen in the plot to the right, the impact of Zeff on x-ray response depends on the x-ray energy.
2) Zeff itself actually changes:

   $$Z_{eff(E)} = (\Sigma(f_i * Z_i^{n(E)}))^{1/n(E)}$$

   Where n(E) is a constant that is dependent on the x-ray energy.

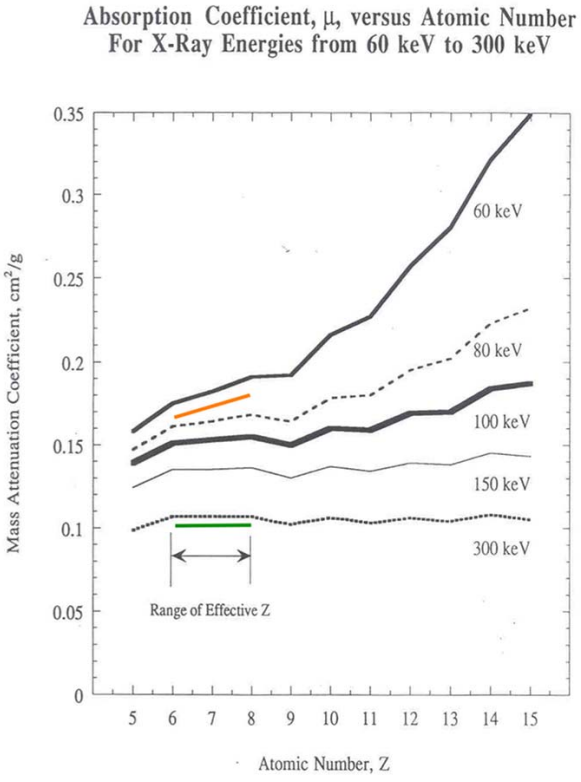

Approach

The instrument used for this project was a bottle screener from AS&E, which measures x-ray response with Scatter Attenuation Tomography Numbers (SAT). Our understanding of the relationship between x-ray response, r, and Zeff (and therefore our approach to simulant development) has gone through several changes as the project has moved forward. An overview of this from our previous summary is:

1) Attempting to create simulants based on the equation:

$$SAT_{(E)} = Gain_{(E)}*(\rho*Z_{eff}) + Offset_{(E)}$$

Where:

$$Z_{eff} = (\Sigma(f_i*Z_i^{4}))^{1/4}$$

2) Through various experiments it was determined that this would not work for the reasons mentioned in the background section. This lead to the examination of more complex equations:

$$SAT_{(E)} = Gain_{(E)}*(\rho^{C1(E)}*Z_{eff}^{C2(E)}) + Offset_{(E)}$$

Where:

$$Z_{eff} = (\Sigma(f_i*Z_i^{n(E)}))^{1/n(E)}$$

3) As many different samples were run through the x-ray screener trends in SAT response based on concentration were identified. These trends were used to estimate the concentrations and components needed to create simulants.

4)

Since the 2011 summary the simulant development method was refined to improve accuracy (*Simulant development for nitric acid in next section*).

Because of the problems described in the background section the goal shifted from creating simulants to creating a simulant development method. This method will involve a specific set of samples that can be run through an x-ray instrument to gather the information necessary to create simulants for that instrument.

Summary of Data Collected and Simulant Development

In our previous summary we presented a simulant for nitrobenzene, simulants for hydrogen peroxide (60, 65, 80, 85, 90%) and nitric acid (40, 50, 60, 70%) have also been developed.

1) Hydrogen peroxide simulants were created using a mixture of $BaCl_2$ and KBr with concentrations ranging from 0.23-0.28% and 0.48-0.85% respectively. These simulants were created based on SAT trendlines for $BaCl_2$ and KBr. This method landed simulants in the right area but each needed refinement resulting in the need to create 25 solutions to make the 5 samples.

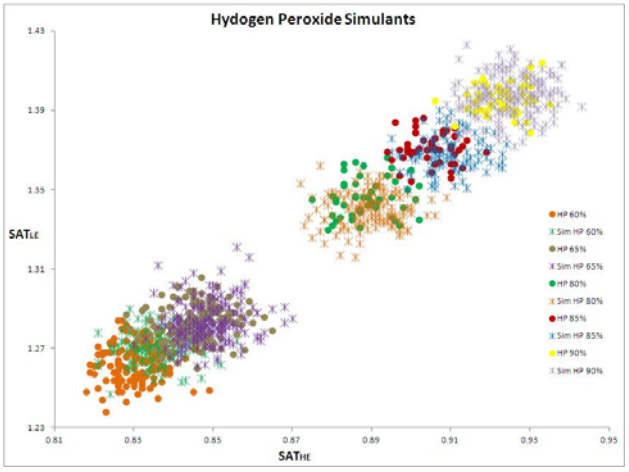

The data collected during the hydrogen peroxide simulant development process was input into Mathematica to develop a more comprehensive simulant development predictive model.

2) Nitric acid simulants were also created using $BaCl_2$ and KBr with concentrations ranging from 0.22-0.30% and 0.40-0.71% respectively. With the improved predictive model only one refinement was needed for the 40% nitric acid simulant, the three others hit on the first try. The most likely reason for the 40% miss was that the concentrations of $BaCl_2$ and KBr fell outside of the range used to create the predictive model.

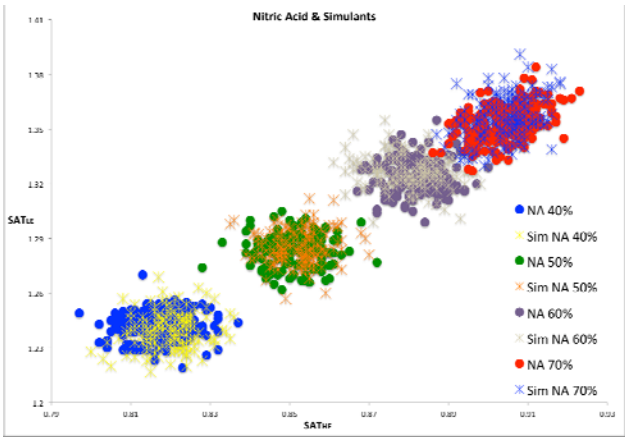

The 60 & 65% hydrogen peroxide simulants was tested to ensure that they could be recreated accurately using the same $BaCl_2$/KBr mix.

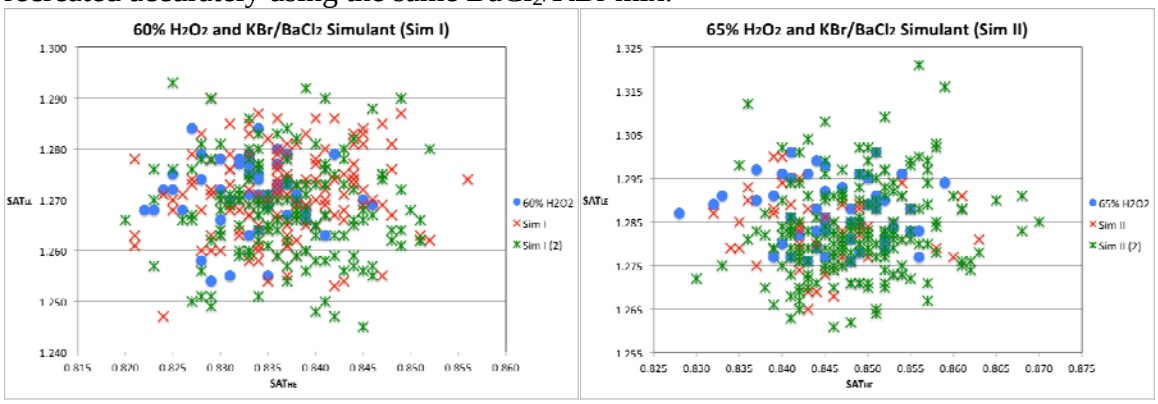

The recreated simulants provided the same results as the original simulants with some expected random scatter variation.

Throughout the course of this project over 120 samples were prepared and run through the bottle screener, many were run multiple times for a total of 273 runs. (Table of samples provided on last page of this summary)

Way Forward

Based on the data collected on the AS&E Bottle Screener a method will be prepared to predict threats and create simulants. The method will involve of a reduced set of samples that best represent the data needed to meet these goals. We are currently working on gaining access to an additional x-ray instrument so that these samples can be run and the method tested.

Salt Samples		
Sample	ρ (g/mL)	$Z_{eff}(4)$
$NaNO_3$ 29%	1.217	8.030
$NaNO_3$ 34.2%	1.262	8.107
$MgSO_4$ 16%	1.09	8.373
K_2SO_4 4%	1.031	8.703
$(NH_4)_2SO_4$ 24%	1.138	8.990
KBr 0.5%	1.002	9.284
$Na_2S_2O_3$ 20.3%	1.177	9.641
K_2CO_3 9.9%	1.087	9.894
$Na_2S_2O_3$ 29%	1.264	10.244
KBr 1%	1.005	10.395
$CaCl_2$ 9.6%	1.079	10.578
KBr 1.5%	1.009	11.219
KCl 16.8%	1.11	11.735
KBr 2% (2)	1.012	11.845
KBr 2%	1.013	11.895
K_2CO_3 26.9%	1.257	12.002
KCl 19.7%	1.131	12.137
$BaCl_2$ 0.5%	1.003	12.847
$CaCl_2$ 20%	1.277	13.422
$ZnSO_4$ 11%	1.119	13.638
KBr 4%	1.028	13.866
KI 1%	1.006	14.982
$BaCl_2$ 1% (2)	1.007	15.046
$BaCl_2$ 1%	1.012	15.116
$ZnSO_4$ 21.9%	1.261	16.079
$BaCl_2$ 1.5%	1.007	16.619
KI 2%	1.013	17.700
$BaCl_2$ 2% (2)	1.016	17.736
$BaCl_2$ 2%	1.016	17.864
KBr 12%	1.09	18.005
$BaCl_2$ 3%	1.025	19.544
KI 4%	1.029	20.959

CHNO Samples		
Sample	ρ (g/mL)	$Z_{eff}(4)$
MeOH	0.792	6.889
iPrOH 40%	0.93	7.151
DMF	0.944	6.535
MeOH 24%	0.964	7.434
MeOH 16%	0.976	7.485
Acetone 15%	0.981	7.444
iPrOH 8%	0.984	7.488
Acetone 10%	0.988	7.501
MeOH 8%	0.989	7.533
iPrOH 4%	0.99	7.527
Acetone 5%	0.993	7.531
iPrOH 2%	0.994	7.547
Water DDDI	0.998	7.566
Benzonitrile	1.01	6.050
Sucrose 4%	1.013	7.550
Sucrose 9%	1.034	7.527
Acetic Acid	1.05	7.096
Sucrose 16%	1.064	7.495
AN 16.8%	1.069	7.553
Sucrose 20%	1.081	7.477
Quinoline	1.09	5.977
AN 23.7%	1.099	7.548
Glycol	1.113	6.992
Diglycol	1.115	6.877
Urea 41.4%	1.115	7.332
Triglycol	1.12	6.832
Formamide	1.129	6.992
AN 31.3%	1.134	7.542
Sucrose 32%	1.137	7.421
Nitrotoluene	1.16	6.608
Sucrose 40%	1.176	7.383
Glycerin	1.264	7.025

Hazards & Simulants		
Sample	ρ (g/mL)	$Z_{eff}(4)$
H_2O_2 60%	1.242	7.687
Sim HP 60%	1.004	11.629
Sim HP 60% R	1.004	11.629
H_2O_2 65%	1.265	7.697
Sim HP 65%	1.004	11.817
Sim HP 65% R	1.004	11.817
H_2O_2 80%	1.338	7.727
Sim HP 80%	1.005	12.095
H_2O_2 85%	1.363	7.737
Sim HP 85%	1.006	12.318
H_2O_2 90%	1.391	7.748
Sim HP 90%	1.007	12.418
HNO_3 40%	1.245	7.635
Sim NA 40%	1.003	11.443
HNO_3 50%	1.308	7.652
Sim NA 50%	1.004	11.889
HNO_3 60%	1.366	7.670
Sim NA 60%	1.005	12.171
HNO_3 70%	1.409	7.688
Sim NA 70%	1.006	12.390
Nitrobenzene	1.2	6.712
Sim NB	0.932	11.398
Hazards Without Simulants		
H_2O_2 30%	1.113	7.626
H_2O_2 35%	1.134	7.637
H_2O_2 40%	1.155	7.647
H_2O_2 45%	1.175	7.657
H_2O_2 50%	1.196	7.667
H_2O_2 55%	1.218	7.677
Nitromethane	1.12	7.286
H_2SO_4 96.5%	1.84	12.291
H_2SO_4 35%	1.261	10.002

Failed Simulants		
Sample	ρ (g/mL)	$Z_{eff}(4)$
$ZnSO_4$/Sucrose Simulants		
Sim A	1.26	8.912
Sim B	1.26	8.797
Sim C	1.26	8.677
Sim D	1.26	8.563
Sim E	1.26	8.433
Sim F	1.26	8.310
Sim G	1.26	8.167
$BaCl_2$ & KBr Simulants		
Sim II +	1.004	11.757
Sim II 2+	1.004	11.734
Sim II 3+	1.004	11.734
Sim II 4+	1.004	11.619
Sim III	1.006	12.335
Sim III +	1.006	12.282
Sim III 2+	1.006	12.262
Sim III 3+	1.006	12.251
Sim III 4+	1.005	12.150
Sim III 5+	1.005	12.038
Sim IV	1.006	12.525
Sim IV +	1.006	12.349
Sim IV 2+	1.006	12.404
Sim IV 4+	1.006	12.318
Sim V	1.006	12.426
Sim V +	1.007	12.469
Sim V 2+	1.006	12.374
Sim V 3+	1.007	12.396
Sim NA 1	1.003	11.522
$BaCl_2$ & iPrOH Simulants		
Sim NB a	0.931	8.950
Sim NB b	0.932	10.973
Sim NB c	0.932	11.149

Development of Novel Composite Materials & Structures for Blast Mitigation

Arun Shukla
with Nate Gardner, Erheng Wang, Puneet Kumar, Jefferson Wright
Mechanical Engineering Dept, University of Rhode Island

Objective

The current investigations aim to develop novel material systems and sandwich structures that can withstand shock wave (air-blast) loadings and effectively mitigate the blast overpressures. The study also focuses on developing a more comprehensive understanding of the shock wave loading process, including the compressibility of gas, as well as creating a model based on one-dimensional gas-dynamic theory to predict the momentum transmitted to the structures.

Summary

A shock tube apparatus was utilized to generate a controlled shock loading on the specimens (Fig. 1a). It has an overall length of 8 m, consisting of a driver, driven and muzzle section. The high-pressure driver section and the low pressure driven section are separated by a diaphragm. By pressurizing the high-pressure section, a pressure difference across the diaphragm is created. When this difference reaches a critical value, the diaphragm ruptures. This rapid release of gas creates a shock wave, which travels down the tube to impart a dynamic loading on the specimen. The driver gas is helium and the driven gas is ambient air.

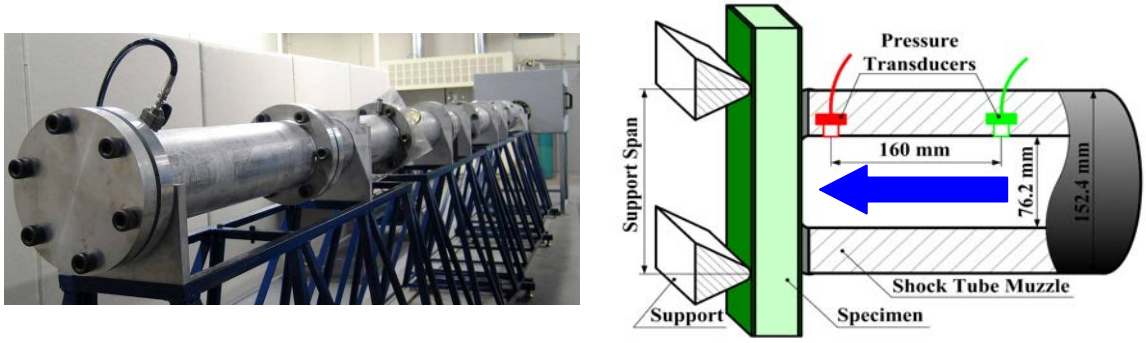

(a) Shock tube (b) Detail dimensions of the muzzle

Fig. 1 Shock tube apparatus

Fig. 1b shows the detailed dimensions of the muzzle and locations of the specimen and the pressure sensors (PCB102A). The sensors are mounted at the end of the muzzle section to measure the incident pressure and the reflected pressure during the experiment. The final muzzle diameter is 0.076 m (3 in). The distance between the two sensors is 0.160 m and the distance between the second sensor and the end of the muzzle is ~ 0.020 m. The specimen was placed in the supports and positioned close to the end of the muzzle. These support fixtures ensure clamped boundary conditions with a span of 0.203 m (8 in) by 0.203 m (8 in). A typical pressure profile obtained from the transducer closest to the specimen (~ 0.020 m away) can be seen in Fig. 2. It should be noted that both pressure transducers were utilized to obtain the shock wave history, i.e. incident / reflected pressure and incident / reflected velocity. However, only the pressure transducer closest to the specimen was utilized to obtain the pressure applied on the specimen.

The Digital Image Correlation (DIC) technique was also used to measure the full-field, in-plane and out-of-plane displacements. The DIC arrangement is shown in Fig. 3. Initially the

camera records an image of the specimen in its un-deformed state. A second picture is then taken after the specimen has deformed. The two images are then compared in order to calculate the in-plane and out-of-plane displacements of the specimen. A random speckle pattern is applied on the specimen and each speckle is individually tracked in order to obtain the in-plane and out-of-plane displacements.

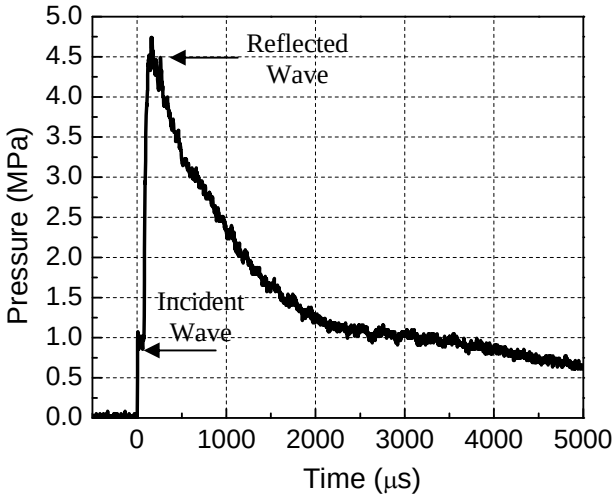

Fig. 2 Typical pressure profile from transducer closest to the specimen

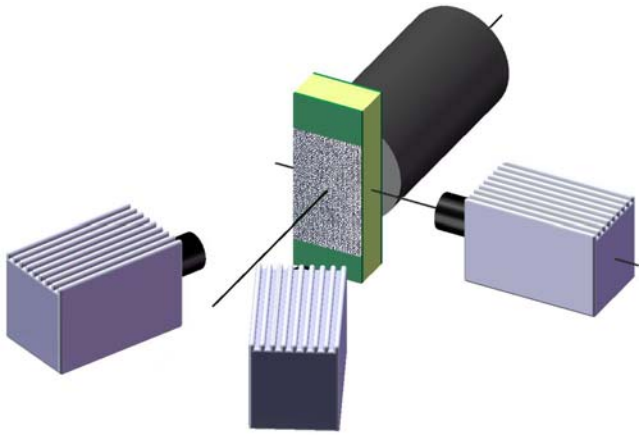

Fig. 3 High-speed photography systems

Accomplishments

Task 1: Gas Compressibility during Air-blast (Shock wave) Loading

A new fluid-structure interaction model that considers high gas compressibility has been developed using the Rankine-Hugoniot relations. The impulse conversion between the gas and the structure was utilized to determine the reflected pressure profile from the known incident pressure profile. The physical parameters of the gas such as the shock front velocity, gas density, local sound velocity, and gas particle velocity, as well as the impulse transmitted onto the structure were also evaluated. A series of one-dimensional shock wave loading experiments on free-standing monolithic aluminum plates were conducted using a shock tube apparatus to validate the proposed model. The momentum was evaluated using high-speed digital imagery. The experimental reflected pressure profile, along with the peak reflected pressure, and the momentum transmitted onto the plate were compared to the predicted results. The comparisons show that the gas's compressibility significantly affects the fluid-structure interaction behavior, and the new model can predict more accurate results that the existing models. The effects of factors, such as the areal density of the plate and the peak incident pressure, on momentum transfer are also discussed using the present model. Moreover, the maximum achievable momentum and the fluid-structure interaction time are defined and calculated.

Task 2: Blast Response Carbon-fiber Composite Panels

Experimental studies were conducted to understand the effect of plate curvature on the blast response of 32 layered carbon-fiber epoxy panels. A shock tube apparatus was utilized to impart controlled shock loading on carbon-fiber panels having three different radii of curvatures; infinite (panel A), 305 mm (panel B), and 112 mm (panel C). These panels with dimensions of 203 mm x 203 mm x 2 mm were held under clamped boundary conditions during the shock loading. A 3-D Digital Image Correlation (DIC) technique coupled with high-speed photography was used to obtain out-of-plane deflection and velocity, as well as in-plane strain on the back

face of the panels. There were two types of dominant failure mechanisms observed in all the three panels: fiber breakage and inter-layer delamination. The fiber breakage initiated from the face exposed to shock loading (front face) and continued to the interior. Delamination occurred on the side of the specimen as well as on the front face. Energy analysis was also performed which showed that panel C had the best energy dissipation property. Macroscopic post-mortem analysis and DIC results showed that panel C can mitigate higher intensity (pressure) shock waves without initiation of catastrophic damage in the panel. Panel B could sustain the least shock wave intensity and exhibited catastrophic failure. Panel A exhibited intermediate blast mitigation capacity.

Task 3: Effect of Equivalent Core Layer Thickness vs. Equivalent Core Layer Mass on Blast Response of Sandwich Structures

The dynamic behavior of sandwich composites made of E-glass Vinyl-Ester (EVE) facesheets and Corecell ^{TM} A-series foam were studied using a shock tube apparatus. The materials, as well as the core layer arrangements, and overall specimen dimensions were identical, with the only difference appearing in the core layers; one configuration utilized equivalent core layer thickness, while the other configuration utilized equivalent core layer mass. The foam core itself was layered based on monotonically increasing the acoustic wave impedance of the core layers, with the lowest wave impedance facing the shock loading. During the shock tube testing, high-speed photography system coupled with the optical technique of 3-D Digital Image Correlation (DIC) was utilized to capture the real-time deformation process as well as mechanisms of failure. Post-mortem analysis was carried out to evaluate the overall blast performance of these two configurations. The results indicated that with a decrease in areal density of ~ 1 kg/m^2 (5%) from the sandwich composites with equivalent core layer thickness to the sandwich composites with equivalent core layer mass, an increase in deflection (20%), in-plain strain (8%) and velocity (8%) was observed.

Task 4: Response of Functionally Graded Sandwich Beams to Blast Loading

The dynamic behavior of sandwich composites made of E-glass Vinyl-Ester (EVE) facesheets and graded Corecell ^{TM} A-series foam was studied using a shock tube apparatus. The foam core was monotonically graded based on increasing acoustic wave impedance, with the foam core layer of lowest wave impedance facing the blast. The specimen dimensions were held constant for all core configurations, while the number of core layers varied, resulting in specimens with one layer, two layer, three layer, and four layers of foam core gradation. Prior to shock tube testing, the quasi-static and dynamic constitutive behavior (compressive) of each type of foam was evaluated. During the shock tube testing, high-speed photography coupled with the optical technique of Digital Image Correlation (DIC) was utilized to capture the real-time deformation process as well as mechanisms of failure. Post-mortem analysis was also carried out to evaluate the overall blast performance of these configurations. The results indicated that increasing the number of monotonically graded foam core layers, thus reducing the acoustic wave impedance mismatch between successive layers, helped maintain structural integrity and increased the blast performance of the sandwich composite.

Task 5: Functionally Graded Corrugated Structures for Blast Mitigation (Collaboration with the University of Connecticut)

Blast loading experiments on graded, corrugated steel sandwich panels were conducted using a shock tube apparatus in combination with high-speed digital photography and pressure sensors. Various combinations of multilayer corrugation cores were experimentally evaluated in order to understand the effects of gradation on the shock response of the corrugated panels. The

results show that a gradual, linearly graded corrugation, from the thinnest corrugation on the front face to thickest corrugation on the back face, mitigates back face deflection of the panel the most, especially when normalized due to areal density. This arrangement leads to a new sequential collapse mode which helped in mitigating the blast and thus reduces back face deflection.

Details in Appendix

Task 6: Collaboration with Industry / Transition to Customer

Novel material systems and sandwich structures, including but not limited to laminated glass panels, corrugated steel armor, and functionally graded foam core composites were designed and fabricated to withstand blast loadings and mitigate blast overpressures. Technical collaboration with XO Armor®, Specialty Products Inc., Gurit SP Technology and TPI Composites will help in facilitating sample preparation. This effort also aligns with the mission of DHS to transition technology and allow for a unified effort to protect our homeland.

Students Supported

1. Nate Gardner (Ph.D)
2. Puneet Kumar (Ph.D)
3. Dan Gracia (M.S)
4. Jefferson Wright (M.S)
5. Payam Fahr (M.S)
6. Chris Shillings (Undergraduate)

Students working on shock tube experiments

Journal Publications

1. E. Wang, N Gardner and A. Shukla, “The Blast Resistance of Sandwich Composites with Stepwise Graded Cores”, International Journal Solid & Structures, 46, 3492-3502, 2009.

2. E. Wang and A. Shukla, “Analytical and Experimental Evaluation of Energies during Shock Wave Loading”, International Journal of Impact Engineering, 1188-1196, 2010.

3. M. Jackson, A. Shukla, “Performance of Sandwich Composites Subjected to Sequential Impact and Air Blast Loading”, Composites: Part B, 42, 155–166, 2011.

4. P. Kumar and A. Shukla, "Dynamic Response of Glass Panels Subjected to Shock Loading", Journal of Non-Crystalline Solids, Vol. 357 (24), 3917-3923, 2011.

5. E. Wang, J. Wright and A. Shukla, “Analytical and Experimental Study on the Fluid Structure Interaction During Air Blast Loading", Journal of Applied Physics, Vol. 110, 114901-1 – 114901-12, 2011.

6. N. Gardner, E. Wang, P. Kumar and A. Shukla, “Blast Mitigation in a Sandwich Composite Using Graded Core and Polyurea Interlayer", Experimental Mechanics, Vol. 52,119-133, 2012.

7. N. Gardner, E. Wang and A. Shukla, "Performance of Functionally Graded Sandwich Composite Beams under Shock Wave Loading", Composite Structures, Vol. 94 (5), 1755–1770, 2012

8. E. Wang and A. Shukla, “Blast Performance of Sandwich Composites with In-Plane Compressive Loading”, Experimental Mechanics, Vol. 52, 49-58, 2012.

9. P. Kumar, J. LeBlanc, D. Stargel and A. Shukla, "Effect of Plate Curvature on Blast Response of Aluminum Panels”, International Journal of Impact Engineering,Vol. 46, 74-85, 2012.

Conference Proceedings

1. E. Wang, N. Gardner and A. Shukla, “Experimental Study on the Performance of Sandwich Composites with Stepwise Graded Cores Subjected to a Shock wave Loading”, SEM Annual Conference and Exposition on Experimental and Applied Mechanics, Albuquerque, New Mexico, June 1-4, 2009.

2. N. Gardner, “Blast Performance of Sandwich Composites with Discretely Layered Core”, SEM Annual Conference and Exposition on Experimental and Applied Mechanics, Albuquerque, New Mexico, June 1-4, 2009.

3. S.A. Tekalur, E. Wang, M. Jackson and A. Shukla, “Failure Behavior and Energy Absorption of Sandwich Composites under Dynamic Loading”, SEM Annual Conference and Exposition on Experimental and Applied Mechanics, Albuquerque, New Mexico, June 1-4, 2009.

4. E. Wang and A. Shukla, “Evaluation of Incident, Reflected and Deformation Energies During Blast Experiments”, SEM Annual Conference and Exposition on Experimental and Applied Mechanics, Albuquerque, New Mexico, June 1-4, 2009.

5. N. Gardner and A. Shukla, “The Blast Response of Sandwich Composites With a Functionally Graded Core”, SEM Annual Conference and Exposition on Experimental and Applied Mechanics, Indianapolis, Indiana, June 7-10, 2010.

6. N. Gardner and A. Shukla, “The Blast Response of Sandwich Composites With a Functionally Graded Core and Polyurea Interlayer”, SEM Annual Conference and Exposition on Experimental and Applied Mechanics, Indianapolis, Indiana, June 7-10, 2010.

7. E. Wang and A. Shukla, “The Blast Response of Sandwich Composites with In-Plane Pre-Loading”. SEM Annual Conference and Exposition on Experimental and Applied Mechanics, Indianapolis, Indiana, June 7-10, 2010.

8. P. Kumar and A. Shukla, “Blast Loading Response of Glass Panels”, SEM Annual Conference and Exposition on Experimental and Applied Mechanics, Indianapolis, Indiana, June 7-10, 2010.

9. E. Wang and A. Shukla, “Core Deformation of Sandwich Composites under Blast Loading”, SEM Annual Conference and Exposition on Experimental and Applied Mechanics, Indianapolis, Indiana, June 7-10, 2010.

10. E. Wang and A. Shukla, “Blast Response of Sandwich Composites using Digital Image Correlation Technique”, 9th International Conference on Sandwich Structures (ICSS9), Caltech, Pasadena, California, June 14 - 16, 2010.

11. E. Wang and A. Shukla, “Performance of Pre-Stressed Sandwich Composites Subjected to Shock Wave Loading”, 14th International Conference on Experimental Mechanics (ICEM 14), Poitiers, FRANCE July 4-9, 2010.

12. N. Gardner and A. Shukla, “The Blast Resistance of Sandwich Composites with a Functionally Graded Core and Polyurea Interlayer”, IMPLAST 2010, SEM Fall Conference, Providence, RI, October 12-14, 2010.

13. P. Kumar and A. Shukla, “Dynamic Response of Glass Panels Subjected to Shock Loading", IMPLAST 2010, SEM Fall Conference, Providence, RI, October 12-14, 2010.

14. N. Gardner and A. Shukla, “The Blast Response of Sandwich Composites with Graded Core: Equivalent Core Layer Mass vs. Equivalent Core Layer Thickness”, SEM Annual Conference and Exposition on Experimental and Applied Mechanics, Uncasville, Connecticut, June 13 - 16, 2011.

15. P. Kumar and A. Shukla, “Dynamic Response of Shock Loaded Architectural Glass Panels", SEM Annual Conference and Exposition on Experimental and Applied Mechanics, Uncasville, Connecticut, June 13 - 16, 2011.

16. P. Kumar and A. Shukla, “Effect of Curvature on Shock Loading Response of Aluminum Panels", SEM Annual Conference and Exposition on Experimental and Applied Mechanics, Uncasville, Connecticut, June 13 - 16, 2011.

17. P. Kumar and A. Shukla, “Blast Response of Architectural Glass Panels", SEM Annual Conference and Exposition on Experimental and Applied Mechanics, Uncasville, Connecticut, June 13 - 16, 2011.

Development of Structural Steel with Higher Blast/Thermal Resistance

Hamouda Ghonem
Mechanics of Materials Research Laboratory
Department of Mechanical, Industrial and Systems Engineering
University of Rhode Island, Kingston RI 028821
ghonem@egr.uri.edu

Objectives

The research work in the Mechanics of Materials Research Laboratory (MMRL), as part of the blast mitigation group of the DHS Center of Excellence, focuses on identifying deformation and damage mechanisms of the reinforcing low carbon steel (LCS) phase of civil structures subjected to combined blast/thermal loadings. These mechanisms govern the post-impact residual life and provide knowledge on material and processing routes required to enhance the steel's blast resistance

The work, carried out June 2011 to June 2012, has dealt with identification of the deformation mechanisms associated with plate impacts, which simulates close range explosive loading. This has been achieved through the use of a newly designed and built light gas gun, capable of delivering impact pressures up to 20 GPa. Results of this work have provided knowledge of the rate controlling parameter associated with blast severity, which has been identified as deformation twins, in particular twin volume fraction. Via microscopy, and through post-impact testing, twins are shown to be sites for internal cracking thus contributing to the progressive failure of steel subjected to blast impacts. The relationship between blast pressure and twin volume fraction has been determined showing a proportional correlation. The post-impact material has been further studied using a newly designed and built Split Hopkinson Pressure Bar (SHPB) in order to determine its high strain rate sensitivity and define the flow characteristics of the mobile dislocations as a function of strain rate and temperature.

The outcomes of these studies which combine the use of the gas gun and the SHPB, are employed to explore microstructure control approaches to enhance the blast resistance of the LCS. This has been investigated by independently examining the influence of alloying and grain refinement on the dynamic strength of the steel. The former approach is being carried out on microalloyed steels, in cooperation with US Steel, while the later involves Equal Channel Angular Pressing (ECAP) techniques, the facilities of which is being built in the Mechanics of Materials Research Laboratory.

A brief review of the research tasks mentioned above and their major outcomes are described in the following sections. Task I has a primary objective of subjecting materials to blast loads and defining microstructure parameters as a function of impact stress. Task II incorporates the SHPB for determining flow characteristics and dynamic stress-strain response. Task III and Task IV both focus on methods to alter the LCS microstructure, in attempts to improve blast properties. In addition, the report gives a brief description of transition to industry, technical publications and students being supported as part of this research program.

Summary of Research

Task I - Blast Deformation Criterion of Low Carbon Steel

The work in this task focuses on identifying microstructural variations in LCS discs subjected to high impacts at pressures comparable to close range explosive loads. This range is defined by stage II loading calculated from simulations of explosive charges using the Jones-Wilkins-Lee Equation of State; see Fig. 1a. The simulated explosive impacts are achieved using a light gas gun system designed and built in the MMRL. This gun has the capability to launch projectiles at 1000 m/s, achieving impact stresses up

to 20 GPa, see Fig. 1b and Fig. 1c. Pre-impact projectile velocities are measured using a set of high power infrared lasers and fast responding photodiodes. Stress in the target material is measured using a piezoresistive manganin stress gauge. Typical stress histories recorded during impacts are shown in Fig. 2a. Examination of steel discs subject to this range of pressures indicated that twin formation is the rate controlling deformation parameter under these conditions. A correlation between impact pressure and twin volume fraction is determined showing an increase in the number of twins with the increase in the pressure; see Fig. 2b. In addition, an analytical model predicting the twin volume fraction as a function of particle velocity and shear stress has been implemented; results are shown in Fig. 2b.

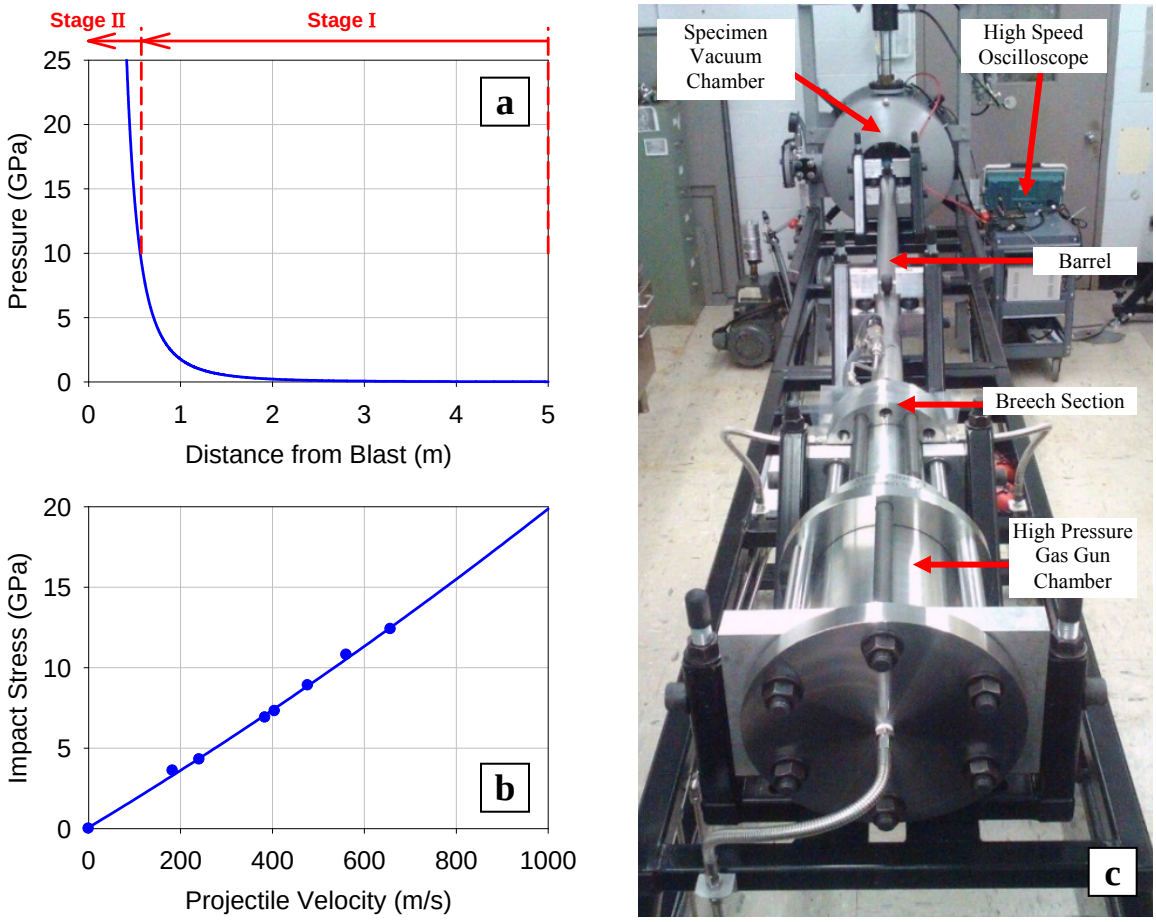

Fig. 1: (a) Blast pressure as a function of distance from an explosive source, calculated for 1000 kg of TNT. Stage I represents "far field" and stage II represents "close range" blasts. (b) MMRL Gas Gun capacity in terms of projectile velocity, up to 1000 m/s, and corresponding impact pressure in steel, up to 20 GPa. (c) Gas Gun built and assembled in the MMRL at URI; includes 10 ft long, 2 in diam. bore barrel, all stainless steel construction.

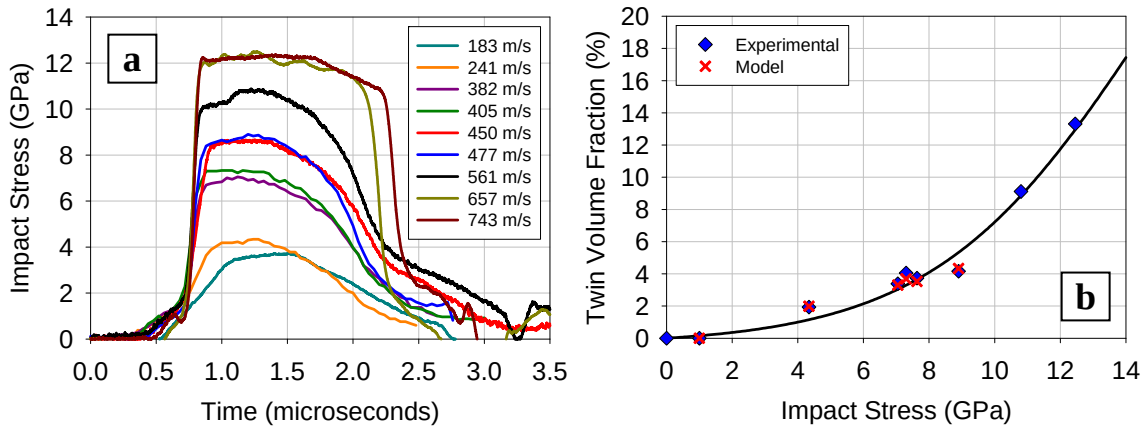

Fig. 2: (a) In plane stress history recorded in low carbon steel with projectile velocities between 180 and 750 m/s. (b) Twin volume fraction as a function of impact pressure.

Further analysis has been carried out on the role of twins and their relation to the residual strength, which is measured as the ratio between the available strain energy in the post-impact material and that of the virgin as-received material; as shown in Fig. 3a. Results show an inverse relationship between residual strength and twin volume fraction. This is interpreted through the hypothesis that twins provide additional interfaces within the ferrite phase. As such, these interfaces, while they represent an important long range entity influencing mobile dislocation flow, they are shown to be nucleation sources of micro cracks, see Fig. 3b, resulting in the embrittlement and rapid loss of material strength.

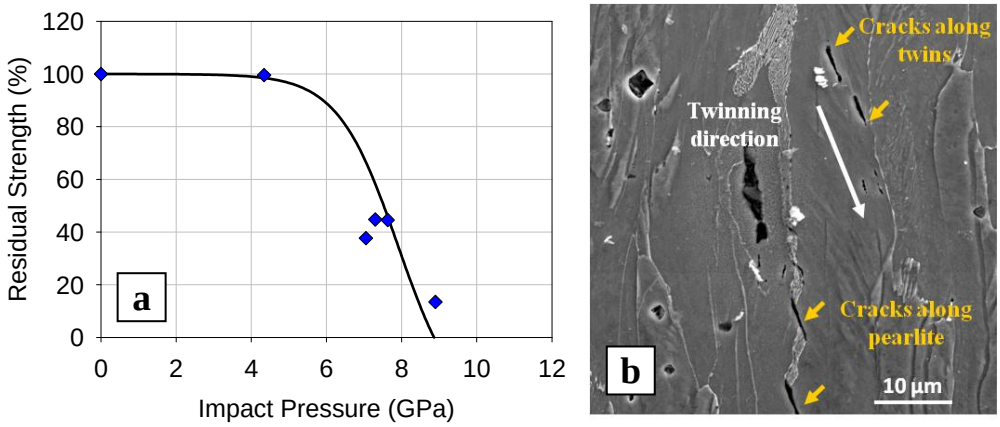

Fig. 3: (a) Residual strain energy as a function of volume fraction of twins. The residual strain energy is measured in reference to the as-received material, and (b) a micrograph of cracking along pearlite and twin interfaces in a quasi-static tension test post-impact loading of 9 GPa.

Task II - Dynamic Deformation of As-Received and Post-Impact Material

The dynamic deformation in terms of the stress-strain response of both as-received and post-impact materials has been examined using a split Hopkinson Pressure Bar (SHPB) which has recently been designed and added to the MMRL, see Fig. 4a. The SHPB has a strain rate capacity up to 10^4 s^{-1} and is equipped with an automated trigger system and a low/high temperature test chamber (-76 to 800°C) (Fig. 4a insert). Typical flow stress versus plastic strain curves produced from the SHPB apparatus for strain rates in the range of 10^3 s^{-1} are shown in Fig. 4b, as compared to that of the quasi static loading condition.

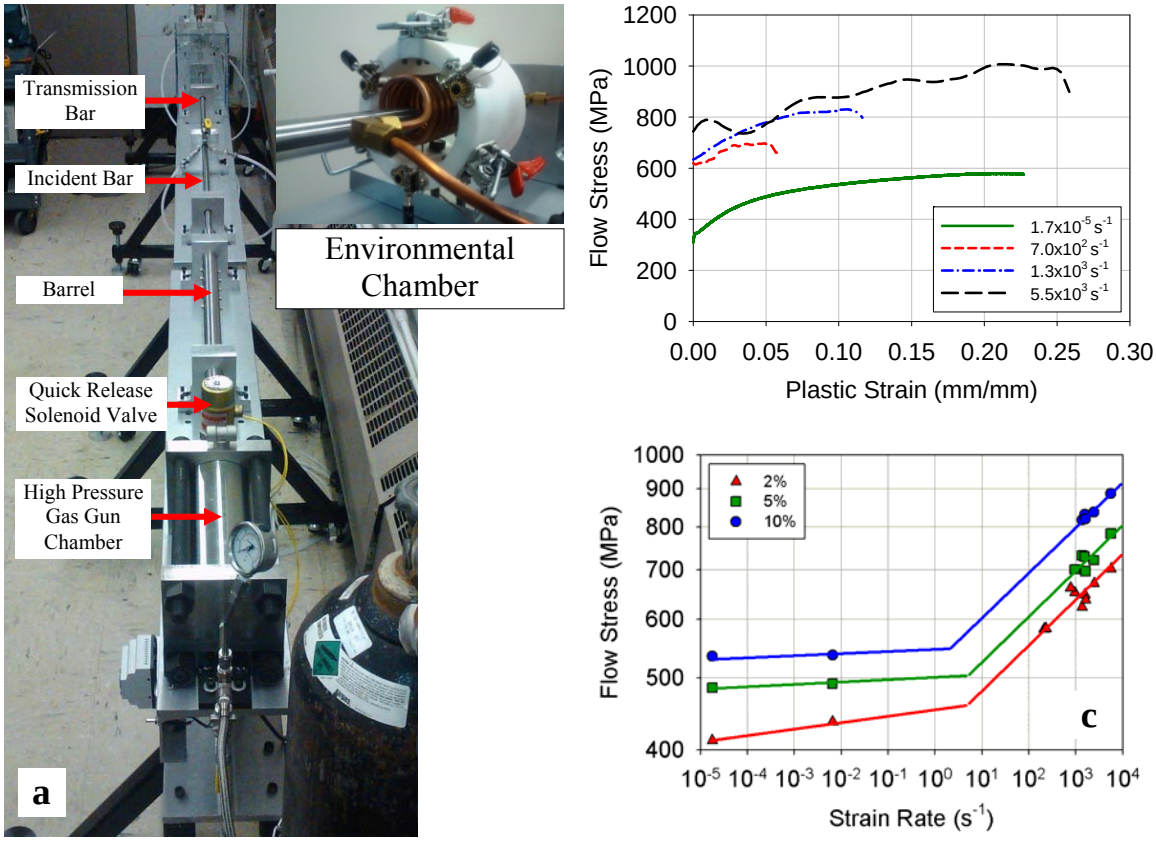

Fig. 4: (a) A newly designed and assembled Split Hopkinson Pressure Bar at the MMRL capable of strain rates up to 10^4 s^{-1} and temperatures ranging from -76°C to >800°C. (b) Dynamic flow stress vs. plastic strain for a range of strain rates, and (c) flow stress vs. strain rate obtained using the SHPB.

The dynamic stress strain curves are critical components in efforts to model the high strain rate response of the steel and associated deformation mechanisms. These efforts include the determination of the strain rate sensitivity; see Fig. 4c, activation volume, dynamic yield and hardening as a function of temperature, all of which can be related to microstructure parameters evolving during dynamic loading. A particular interest in these analyses are the forces acting on the dynamic dislocations, including drag stress and threshold stress, which are used to model short and long range dislocation interactions as a function of post impact evolving microstructure.

Task III - Effects of Pre-straining on Impact Loading

As mentioned in Task I, twin formation has been identified as the rate controlling deformation parameter in the impact test specimens. Therefore, attempts have been carried out to explore the effect of reducing localized deformation during high rate impacts thereby reducing the frequency of twin nucleation, and in turn improve post-impact mechanical strength. Pre-straining the steel prior to impact loading is selected as a route to improve the post-impact strength. By introducing additional mobile dislocations, through pre-deformation by rolling, high rate deformation can be sustained purely by slip without the need for strain accommodation by mechanical twins. The active slip systems allow the impact deformation process to act homogeneously, while still retaining substantial ductility under post-impact

quasi-static loading. Scanning electron microscopy (SEM) analysis provides evidence of the level of pre-strain in which twins are suppressed, without sacrificing substantial strain energy to fracture. As a result of eliminating twins, post-impact microstructure should remain stable for moderate impact loading of as-received material. Also, the reduction in twins will prevent the grains from reorienting to a preferential direction for formation of adiabatic shear bands which generally leads to premature failure. The influence of pre-straining on the impact response in terms of twin volume fraction is demonstrated in Fig. 5 which compares the impact loaded as-received and a 3% pre-strained steel. This figure shows a large volume fraction of deformation twins present in the as-received structure, while the material which has been pre-strained has no twins present.

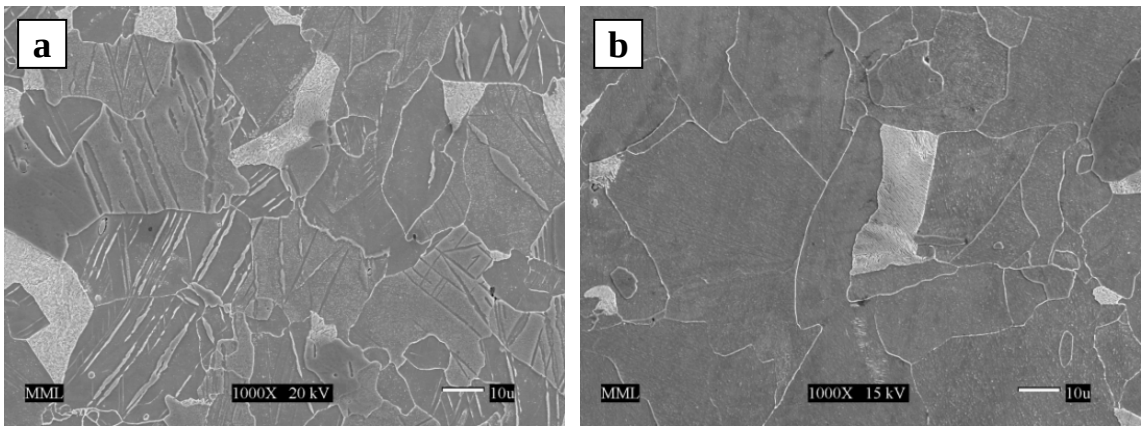

Fig. 5: SEM micrographs of impacted LCS samples (a) as-received impacted at 12 GPa showing formed twins, and (b) 3% pre-strained impacted at 11 GPa free of twins.

Following plate impacts, the SHPB is utilized to obtain the stress-strain relationship of the post-impacted material, with and without twins. From this data the difference in flow stress between as-received and pre-strained material is compared as shown in Fig. 6. These preliminary results indicate that the pre-straining has the ability to restore, or retain properties closer to that of the as-received material even after a 12 GPa impact. The reduction in flow stress also indicates that the material has retained a higher percentage of its original ductility. Further testing the post-impact material at multiple temperatures and strain rates will provide more insight into the blast capabilities as described by the SHPB testing in Task II.

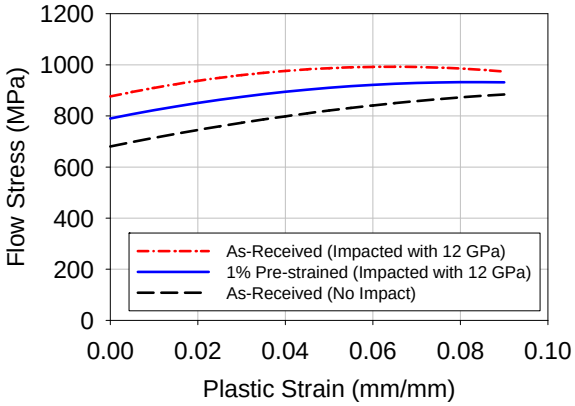

Fig. 6: Dynamic stress-strain curves obtained from post-impact testing using the SHPB at strain rates of $1.2x10^3$ /s.

Task IV - New Steel with High Impact Resistance: Microalloying and Grain Refinement Approaches

Major results obtained from the microstructure analyses low carbon steel subjected to impact loads, points out to the competition between the strength, as defined by the threshold stress of mobile dislocations and ductility, which is determined by the frictional stress of the continuum acting on mobile dislocations and the level of interactions between mobile dislocations and formed microstructure entities such as twins. In our efforts to develop steel, with high blast/thermal resistance, a focus is made on increasing the strength of the steel. This is achieved by microstructure control through two independent routes; alloying and grain refinement. The first route is investigated in cooperation with US Steel using microalloyed steel which contains individual alloying elements (in the range 0.05 to 0.15%) including: niobium, vanadium, titanium, molybdenum, zirconium, boron, and rare-earth metals. These additional elements are used to refine the grain microstructure and/or facilitate precipitation of various nitirides or carbides and result in transformed bainitic microstructure, see Fig. 7. This steel is currently under examination in order to determine its microstructure changes as a function of impact loading, using the gas gun, and to calculate its strain rate sensitivity at both room and high temperature using the SHPB facilities.

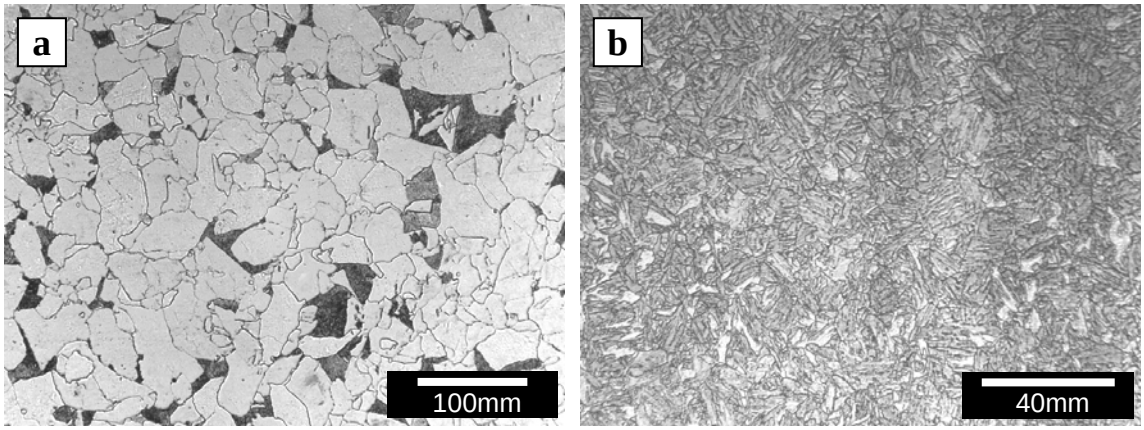

Fig. 7: Optical micrograph of (a) A572 low carbon steel ferrite-pearlite structure and (b) (US Steel) A2 microalloyed steel composed of bainitic structure.

The second approach to increase the steel impact resistance depends on altering the mean free path of intergranular dislocations and provides strength though coarsening of the grain boundaries. These two factors can be achieved by mechanically reducing the grain size of the steel to the ultra fine grain (UFG) range (<10 μm). The grain refinement is carried out through Equal Channel Angular Pressing (ECAP) of the as-received coarse grained (40-50 μm) steel. The ECAP facility, which is established in the MMRL, utilizes shear deformation to rearrange dislocations into thick boundary cells, effectively subdividing the existing grains into the ultra-fine scale resulting in a high strength microstructure, Fig 8a. Work on this track is progressing by the procurement of a 100 ton press, Fig. 8b, and design and fabrication of the ECAP die, see Fig. 8c. The die is designed to press 1/2" and 1" square billets, of which the larger can produce up to 6 in^3 of UFG material per pass. This volume is sufficient for testing using the gas gun or SHPB at both room and elevated temperature conditions. This approach represents an attractive route to industry since it is cost effective in producing a high strength material, which cannot be produced by heat treatment methods, while still retaining its chemical composition. Transition to industry is also viable due to the simple design and ease of incorporation into existing steel rod extrusion techniques.

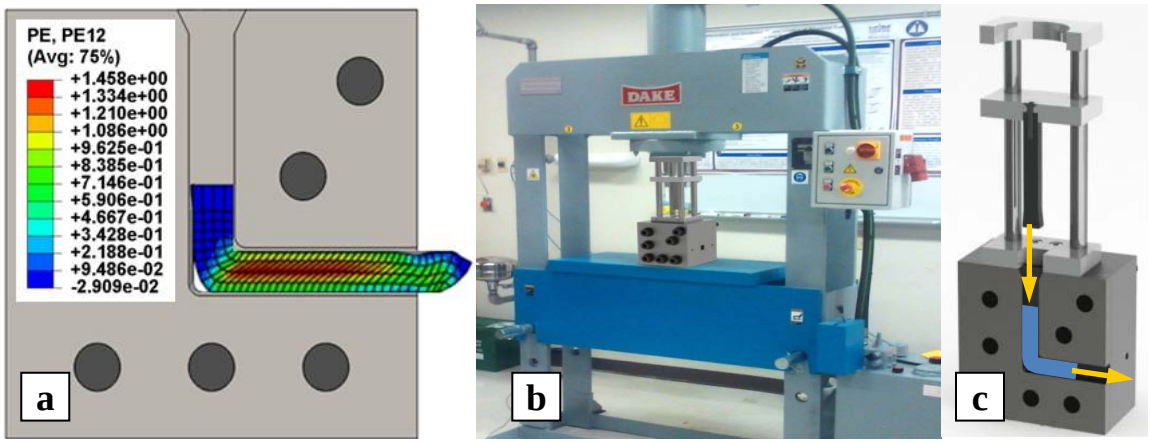

Fig. 8: (a) Finite element analysis showing the plastic strain distribution caused by severe plastic deformation through the 90 degree channel, (b) a 100 ton electro-hydraulic press in the MMRL with ECAP die inserted on pressing platform, and (c) a cross sectional view of the ECAP die design and direction of billet passage.

Accomplishments

The work being carried out in the Mechanics of Materials Research Laboratory at URI aims at developing steel with superior resistance to blast/thermal loadings. Efforts carried out in the period June 2011-June 2012 toward this goal, have the following accomplishments:

- Developed an advanced light gas gun to extend the impact study of low carbon steel to pressures equivalent to close range explosive loading. The gun has been used for impacts reaching 13 GPa, >600 m/s.
- Identified deformation twins as the rate controlling phenomenon during impact loading of low carbon steel. A correlation between the twin volume fraction and impact pressure has been established
- Successfully isolated and suppressed deformation twins during impact loading through the concept of pre-straining. The significance of this outcome is that while providing higher impact strength in the pre-strained material, the suppression of twins eliminated potential crack initiation sites. In addition, heat treatment procedures were carried out to convert ferritic-pearlitic phase structure in the low carbon steel to a single ferritic phase in order to redistribute carbide uniformly into the bulk phase. This was carried out to explore the influence of pearlite colonies on the long range interactions of mobile dislocations during impact loading.
- Developed and built a Split Hopkinson Pressure Bar for the MMRL equipped with environmental chamber. The SHPB system is capable of performing tests in the strain rate range of 10^2 - 10^4 s^{-1} at temperatures in the range -76°C to >800°C. This system has been used to identify the basic dynamic stress-strain relationship characteristics including, strain rate sensitivity, activation volume, drag stress and critical shear stress for twin formation.
- Designed and built a 100 ton Equal Channel Angular Press (ECAP) for producing a steel with ultra-fine grains (<10um) through extreme shear forming. The press is capable of producing 1/2" and 1" square rods. Combined with heat treatments, this material offers superior strength and ductility while still retaining original phases and chemical composition.

Transition to Industry

The cooperation with industry is manifested in joint work performed with FM Global and US Steel. These are as follows:

- The first part of the program was jointly supported by FM Global and DHS Center of Excellence to develop a numerical model to predict time dependent response of structural steel under quasi-static thermal loading. Collaboration continued with FM Global to examine the deformation behavior of loaded steel I beams subjected to pool fires (1440°F) which simulate extreme thermal exposure conditions. Fig. 9 shows stages of these tests including the beam arrangement prior to the fire, the extent of the pool fire and the appearance of the beam post fire indicating the extensive creep condition. These tests have been documented by BBC.

I Beam Before Pool Fire | During Pool Fire | After Fire

Fig. 9: Various stages of deformation of an I-beam subjected to a pool fire carried out by FM Global.

- A second industrial research collaboration is carried out with US Steel Corp investigating the impact response of microalloyed steels. As mentioned above, microalloyed steel is a cost-effective class of high-strength structural steel which has a bainitic phase characterized by high quasi static strength. US Steel has supplied slabs of microalloyed steel which are currently being tested in the MMRL to identify its potential as a high impact/thermal resistant steel.

Publications / Presentations

- Simulation of Viscoplastic Deformation of Low Carbon Steel Structures at Elevated Temperatures, Y. Sun, K. Maciejewski and H. Ghonem, *J. MEP, DOI 10.1007/s11665-011-0023-0*, 2011

- Deformation Characteristics of Low Carbon Steel Subjected to Dynamic Impact Loading, W. Visser, Y. Sun, G. Plume, C.E. Rousseau, O. Gregory and H. Ghonem, *J Material Science and Engineering A, V 528, Issue 27, 2011.*

- Time-Dependent Deformation of Low Carbon Steel at Elevated Temperatures, K. Maciejewski, Y. Sun, O. Gregory and H. Ghonem, *J Material Science and Engineering A, Volume 534, 2012.*

- Effects of Pre-Strain on Impact Deformation of Low Carbon Steel, W. Visser, J. Spirdione, K. Maciejewski and H. Ghonem, *J Material Science and Engineering, August 2012*

- Strain Rate Sensitivity and Flow Characteristics of Low Carbon Steel at Elevated Temperatures, J. Spirdione, K., W. Visser, Maciejewski and H. Ghonem, *J Material Science and Engineering, August 2012*

- Twin Influence on Post-Impact Deformation of Low Carbon Steel, SEM Annual Conference, W. Visser and H. Ghonem, Mohegan Sun, Uncasville, CT, June 16, 2011.

- High Strain Rate Response of Low Carbon Steel at Elevated Temperatures, J. Spirdione, K. Maciejewski and H. Ghonem, Material Science and Technology Conference, Pittsburgh, PA, October 2012.

- Influence of Pre-Strain on Impact Deformation of Low Carbon Steel, W. Visser, J. Spirdione and H. Ghonem, Material Science and Technology Conference, Pittsburgh, PA, October 2012.

- Dynamic Deformation Mechanisms of Post Impacted Low Carbon Steel, W. Visser, J. Spirdione, K. Maciejewski and H. Ghonem, International Conference on Structural Safety and Reliability, Columbia University, New York, NY, June 2013.

- Dynamic Deformation of Ultra-Fine Grained Low Carbon Steel, J. Spirdione, W. Visser and H. Ghonem, International Conference on Structural Safety and Reliability, Columbia University, New York, NY, June 2013.

Students Supported

- William Visser, PhD Candidate
- Justin Spirdione, Masters Student
- Marcus Allen, Undergrad Student
- Kimberly Maciejewski, PhD Candidate

Structural Response to Non-ideal Explosions

Joseph E. Shepherd with J. Damazo, N. Bitter, J. Odell; California Institute of Technology

Objective and Summary of Activities

Experiments and numerical simulations were performed in the Explosion Dynamics Laboratory at Caltech to investigate the effect of internal explosions on surrounding structures. Gaseous detonations were used as a model to simulate non-ideal explosions. Our objective is to develop the capability to predict the degree of damage as measured through plastic deformation and crack propagation induced by a non-ideal explosion in metal tubes and to investigate methods to mitigate the extent of this damage.

Two experimental facilities were used to investigate differing aspects of the structural loading and damage caused by non-ideal explosions. The first facility is a fixture installed in the GALCIT 288-mm diameter detonation tube and instrumented with pressure gauges, heat transfer measurements, and using schlieren imaging to study the gas dynamics of reflected shock and detonation waves. This investigation was motivated on our observations in the previous years of this project, which showed substantial discrepancies in pressure signals from inviscid one-dimensional gas dynamic models as compared to our experimental data. We had speculated that this was due to reflected shock bifurcation (the splitting of the reflected shock into a set of oblique shocks in the near wall region) and a highly non-uniform flow field created behind the reflecting shock. Tests carried out in the last year with schlieren imaging reveals that reflected shock wave bifurcation does not occur with many detonations although the discrepancies between pressure and wave speed are also observed in our new tests. The observations with reflecting detonation waves are dramatically different from the known results for non-reacting shock wave reflection, for which reflected shock waves bifurcate over a wide range of initial conditions and gases. We have carried out tests comparing cases with and without reflected wave bifurcation by operating the detonation tube as a combustion-driven shock tube. Comparing the pressure signals behind a bifurcating to non-bifurcating wave reveals notable differences in the measured wall pressure indicating that bifurcation may significantly affect the damage caused when a blast wave is incident on a structure.

The second facility is designed to significantly extend the range of loading conditions used in our previous studies and quantify the thresholds for rupturing tubes through ductile failure. The planned experiments will build on earlier plastic deformation studies performed in our laboratory using tubes of 127 mm diameter to achieve radial deformations with hoop strains up to 20%. In those studies, we were able to show that with careful control of initial and boundary conditions, that we could obtain very good agreement between experimental measurements and finite-element model predictions when using material models that account for strain-rate hardening. We aim to achieve the same level of repeatability and predictability for tube rupture in our follow-on work although we anticipate that there will be much more scatter in the ductile rupture tests.

As in our earlier studies, the loading will be created by the detonation of a stoichiometric ethylene-oxygen of suitable initial pressure to produce the desired deformation or tube failure. The new facility is similar in concept to that used our earlier study with three key differences: 1) much

higher initial pressures will have to be used in order to obtain rupture; 2) the test fixture will have to be located in our blast room and remotely operated to protect the laboratory and personnel from shock waves and fragments; 3) the test fixture will have to be smaller in order to limit the amount of explosive mixture and blast amplitude to acceptable value. The test specimens will be thin-walled (1.5 mm) small diameter (25 mm) metal tubes constructed of 3003 aluminum, 6061-T6 aluminum, or 304L stainless steel. An extensive safety analysis has been carried out as part of the design of the new test fixture and a number of engineering safety features are incorporated into the design. In addition to studying ductile rupture, we plan to carry out validation experiments on elastic motion and plastic deformation. Preliminary data in the plastic deformation regime show a periodic deformation mode in the tube wall consistent with early observations and the theory developed for the larger diameter tubes. In addition, we have preliminary visualization of a characteristic crack propagation mode for detonation loading in a tube without deliberate pre-existing flaws.

Highlighted Accomplishments

1. Carried out non-ideal explosion experiments examining the gas dynamics of reflected shock and detonation waves inside tubes with closed end.

2. Developed a focused schlieren visualization system to observe reflected shock wave bifurcation without the image being subjected to the turbulence in the boundary layers present on the viewing windows.

3. Applied analytical boundary layer theory to the case of a propagating detonation and compared predictions to heat flux measurements.

4. Determined that gaseous detonation inhibits bifurcation and results in a very different flow than reflected shock conditions into a mixture that was not combusted.

5. Designed a new facility and performed preliminary investigations using internal detonation loading of high pressure mixtures to rupture thin-walled metal tubes.

Details

The goal of the detonation tube experiments is to measure the wall pressure and heat flux loading caused by either a reflecting shock or detonation wave. We anticipate that the flow behind a reflected wave may be substantially affected by the interaction between the reflected shock wave and the boundary layer created by the incident wave. To observe this flow, we use a schlieren imaging system to visualize the incident and reflected waves as well as the boundary layer ahead and behind the waves. The speed of the detonation waves is 2-3 km/s and the boundary layer is on the order of 1 mm; these factors imply that the exposure time of the schlieren images must be on the order of 10 ns. One of the main activities in the past year has been building and testing imaging systems to reach this goal. Although high-speed imaging systems have been extensively used in the previous detonation tests in this facility, all of the key components had become inoperable or

obsolete and had to be replaced.

The experiments are carried out in the GALCIT detonation tube (Figure 1), a special-purpose facility which was designed and built at Caltech specifically to carry out experimentation on detonation waves. The facility consists of a 288-mm diameter tube with a special ignition system at one end and square (150 x 150 mm) test section with optical access at the other end. The ignition system uses a combination of electrical (capacitor discharge into an exploding wire) and chemical (a short section of an acetylene-oxygen mixture) energy to create a nearly planar detonation wave. The detonation propagates away from the point of ignition towards the test section at the constant theoretical Chapman—Jouguet (CJ) velocity. The Taylor—Zel'dovich (TZ) expansion wave trails the detonation and gradually brings the fluid to rest. Once the detonation impinges upon the test section's closed end, a reflected shock wave propagates into the TZ expansion at a non-constant speed. The detonation facility is 7.6 m in length implying that the effects of the TZ expansion are small and we may approximate the reflected shock as propagating into a steady flow.

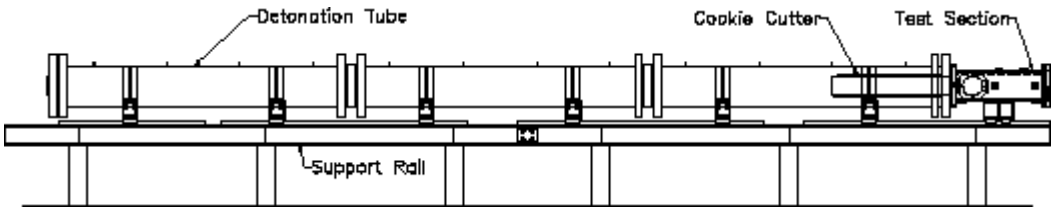

Figure 1. Diagram of experiment used in detonation experiments; the tube and test section are 7.6 m in length.

Details of the test section are given below in Figure 2. A "splitter" plate parallel to the horizontal walls of the test section and with a sharp leading edge is inserted into the test section to raise the location of the boundary layer into the center of the windows. This splitter plate was instrumented with 12 PCB 113B26 pressure transducers and 12 surface junction thermocouples identical to those employed by Sanderson and Sturtevant (Rev Sci Inst 73(7), 2781-7, 2002) for measuring heat flux inside the test section. The thermocouple signals are amplified by a TrikTek Model 205B instrumentation amplifier with a response time of 7.5 μs to a unit step input. The spectral method employed by Sanderson and Sturtevant is used for reducing the heat flux data. A Z-type schlieren system is used to visualize the incident detonation and shock wave reflection. The schlieren system consists of a pulsed EverGreen 70 PIV laser with a pulse width duration less than or equal to 10 ns and a Cooke PCO.2000 digital 14 bit CCD camera system. This allows two images to be taken in quick succession and was used to visualize the incoming detonation and the reflected shock wave for each test. The relative location of the viewing window to the measurement gauges and end wall is shown in Figure 2.

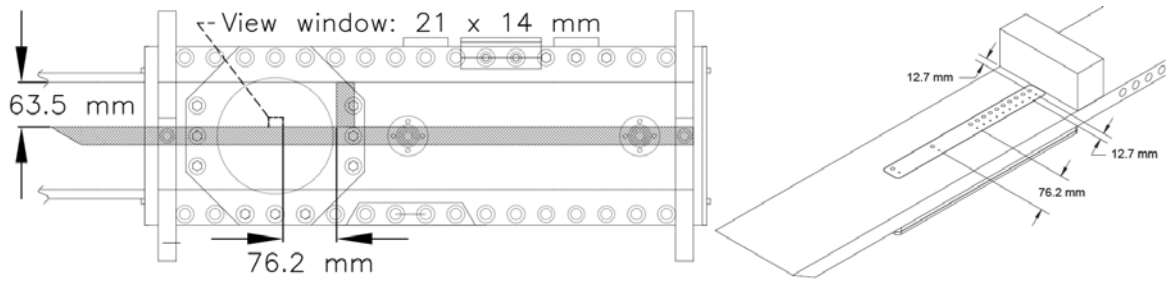

Figure 2. Test section detail. The 14 by 21 mm box is the viewing window used in subsequent schlieren images.

Stoichiometric hydrogen-oxygen, ethylene-oxygen, and hydrogen-nitrous oxide mixtures of various initial pressure and argon dilutions were used to study the effects of composition on the dynamics of the reflected shock. In Figure 3 are shown results for stoichiometric hydrogen-oxygen with an initial pressure 25 kPa and 0% argon dilution. Examining Figure 3(a) we see the incident detonation and reflected shock wave as viewed by pressure measurements of gauges placed at varying distances from the reflecting end. The modeled pressure is predicted by one-dimensional gas dynamic theory using equilibrium post-detonation properties as computed by Cantera. These measurements confirm the preliminary results observed in our laboratory wherein one-dimensional theory was insufficient to predict both the speed and the strength of the reflected shock wave. Figure 3(b) shows the measured heat flux compared to heat flux results obtained from classical laminar boundary layer theory applied to the detonation loading case; this figure shows general agreement between the experiment and model, but a better comparison is obtained by viewing the results on a non-dimensional (Reynolds number-Stanton number) plot, shown in Figure 4.

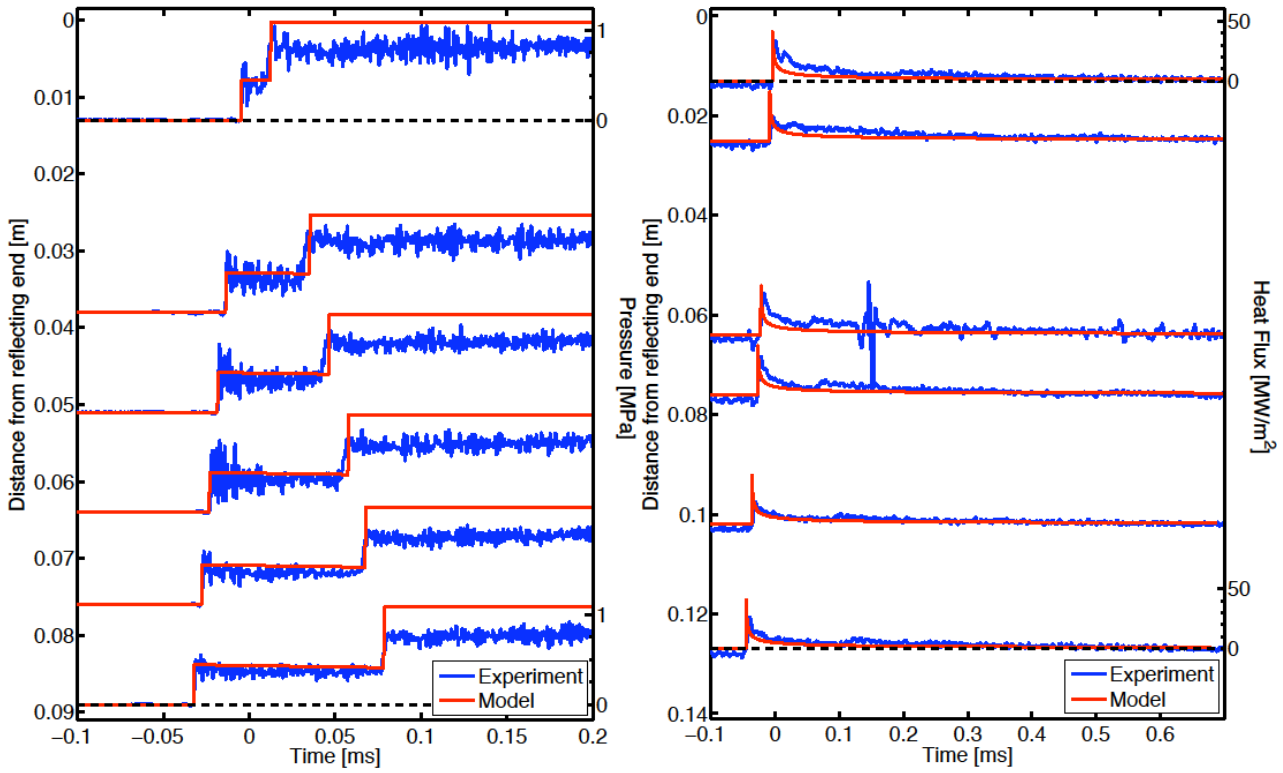

Figure 3. (a) Pressure and (b) heat flux measurements of a reflected detonation in stoichiometric hydrogen-oxygen of initial pressure 25 kPa. The time axis is shifted such that $t = 0$ occurs when the detonation impinges on the end wall. The location of the gauges is given by the intercept of the signal with the left hand ordinate of each plot.

Figure 4 shows the data in terms of Reynolds (*Re*) and Stanton numbers (*St*) as well as comparison with previous empirical fits to shock tube data. In the present study, we define the non-dimensional numbers as

$$Re = \frac{\rho_2 u_2 (t - t_{det})}{\mu_2} \qquad St = \frac{\dot{q}}{\rho_2 u_2 (h_t - h_w)}$$

where ρ is fluid density, u is fluid velocity, t is time, t_{det} is the time when the detonation arrives, $\dot{q}$ is heat flux, h_t is total enthalpy and h_w is the enthalpy at the wall. The subscript 2 represents computed post-detonation conditions. Also plotted on Figure 4 are empirical predictions from Hartunian (J. Aero Sci. 27, 587-94, 1960) based on power-law fits to laminar and turbulent shock tube data. This plot shows that the measured heat flux follows a power law similar to Hartunian's laminar fit. Using a turbulent transition Reynolds number of 6×10^5, it is perhaps not surprising that transition does not occur before the arrival of the reflected shock (which corresponds to a Reynolds number of 9×10^5). An important difference between shock and detonation waves is the presence of transverse waves behind detonations so it is surprising that our results are so consistent with

Hartunian's. There is also a substantial difference between the classical boundary layer predictions and both experimental data as well as the Hartunian correlation. These results are quite unexpected and will be further investigated in the next phase of the study. Transition from laminar to turbulent flow in boundary layers has been extensively investigated in steady flows and it is well known that there are many mechanisms of transition and external factors such as free-stream turbulence levels, pressure gradient, wall roughness, particulates, etc that can influence the transition process. The nonsteady boundary layers induced by moving shock or detonation waves have been much less extensively studied but we expect that similar considerations will be important in determining the transition from laminar to turbulent flow.

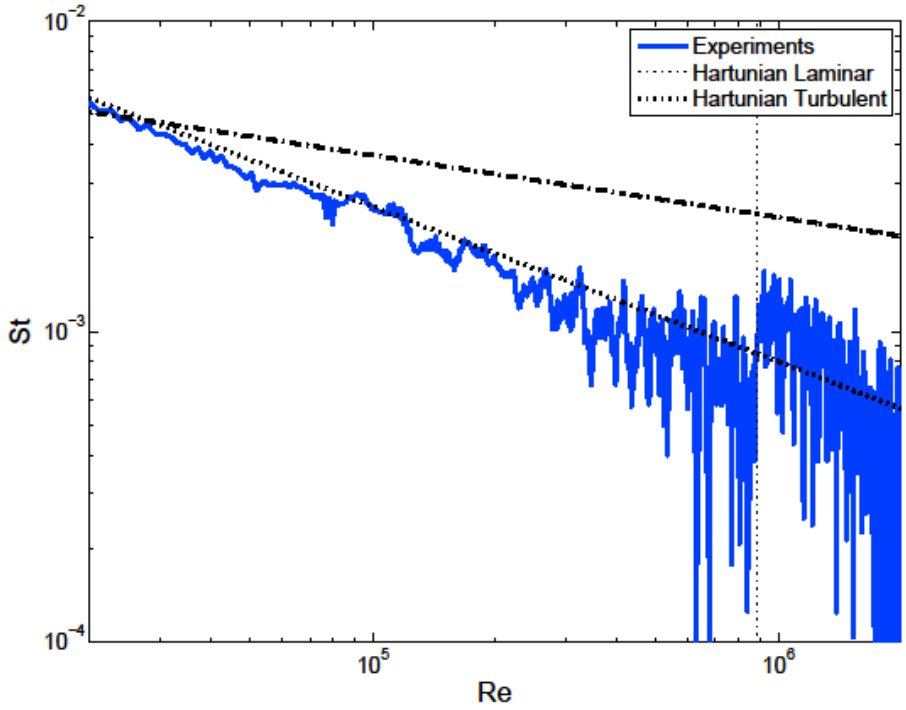

Figure 4. Reynolds—Stanton number plots for heat flux data. The dashed vertical line represents the arrival of the reflected shock wave and indicates when the heat flux models are no longer valid.

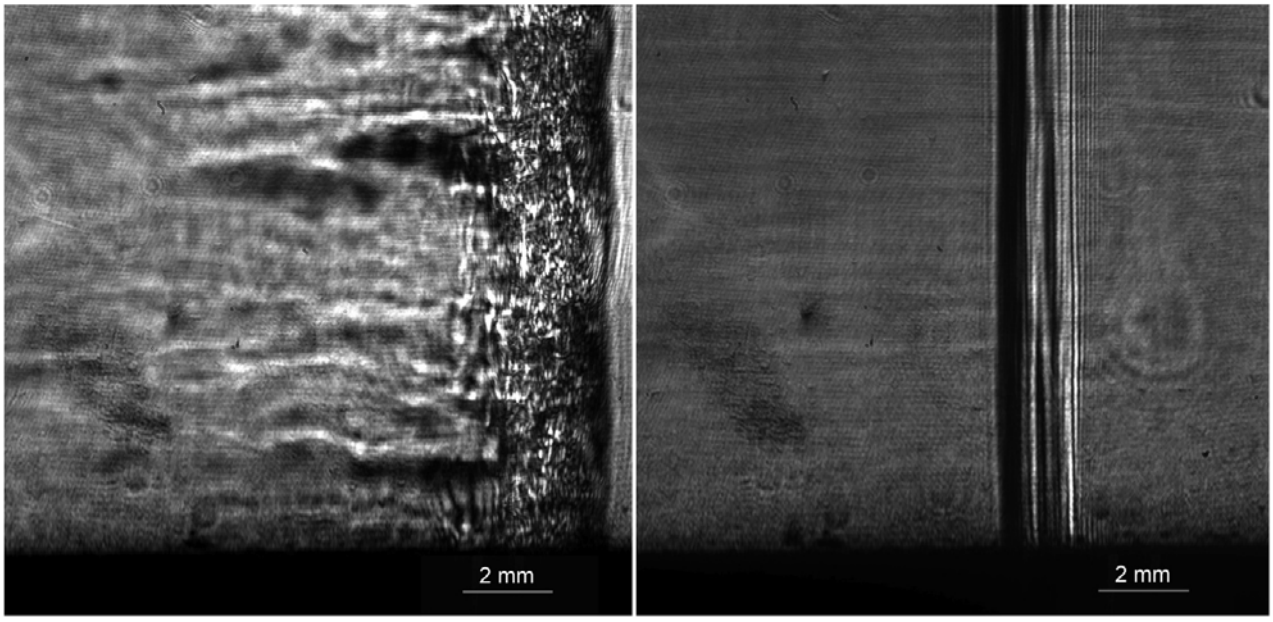

(a) (b)

Figure 5. Schlieren image of (a) the incident detonation propagating to the right and (b) reflected shock wave propagating back to the left. The test section floor is visible at the bottom of the images. The location of this image relative to pressure and heat flux measurements is given in Figure 2.

Figure 5 shows the schlieren images of incident detonation and reflected shock wave for the case of stoichiometric hydrogen-oxygen case plotted in Figures 3 and 4. The detonation is seen propagating to the right and the reflected shock is propagating back towards the left of the image. From this image it is clear from the planar shockwave that bifurcation of the reflected shock did not occur. However, we still observe an inconsistency between one-dimensional gas dynamic models based on measured shock speeds and the observed pressure measurements (Figure 3a). The source of these discrepancies and improved models are under continuing investigation.

The goal of the new facility and experiments examining plastic deformation is to increase the loading pressure so that the detonation ruptures the specimen tube. Figure 6 shows a preliminary result for a 3003 aluminum tube of internal diameter 25.4 mm and wall thickness 1.5 mm with rupture caused by a stoichiometric ethylene-oxygen detonation reflecting from the closed end of the fixture. The butterfly shape created by the crack propagation is one mode that is often observed for test specimens failing under this loading condition.

Figure 6. Tube constructed of 3003 aluminum with internal diameter 25.4 mm and wall thickness 1.5 mm ruptured due to reflected stoichiometric ethylene—oxygen detonation.

Future Work

In the next year, we will continue experimentation and modeling on detonation reflection and the structural response to incident and reflected detonation. The long term goal is to develop a comprehensive understanding and predictive engineering models of plastic deformation, rupture, and blast wave generation for both detonation and deflagration loading.

The goals for our research program in the coming program year (July 2012-June 2013) are:

1. Complete the experimentation in the gaseous detonation tube facility and document visualization, pressure, and heat flux measurements for a range of mixture compositions and initial pressures.
.
2. Use the data obtained in the detonation tube experiments to improve empirical model of the loading pressure distribution.

3. Complete our new experimental facility for high pressure detonation loading. This enable

carrying out experiments on ductile rupture of commodity steel and aluminum specimens.

4. Compare results of elastic and plastic deformation in the new facility with previous results as well as finite-element simulations based on the improved empirical models of the loading pressure.

5. Perform tests examining tube rupture and blast wave generation due to internal gaseous detonation.

6. Carryout finite element simulations of plastic deformation for the ductile rupture tests and compare the failure conditions to existing models of failure thresholds.

Publications and Presentations

1. J. Damazo, J. Ziegler, J. Karnesky, and J. E. Shepherd "Shock Wave Boundary Layer Interaction from Reflecting Detonations" Proceedings of the 28th International Symposium on Shock Waves, University of Manchester, July 17-22, 2011.

2. J. Damazo, J. E. Shepherd, K. Chow-Yee, J. Karnesky "Deformation of Coated Stainless Steel Tubes from Reflected Detonation" 23nd International Colloquium on the Dynamics of Explosions and Reactive Systems, July 24-29, 2011, Irvine, USA. Extended Abstract 257.

3. J. Damazo, J. Odell, and J. E. Shepherd "Boundary Layer Profile Behind Gaseous Detonation as it Affects Reflected Shock Wave Bifurcation" Proceedings of the 42nd AIAA Fluid Dynamics Conference, New Orleans, June 25-28, 2012.

4. J. Karnesky, J. Damazo, K. Chow-Yee, A. Rusinek, J. E. Shepherd "Plastic Deformation due to Reflected Detonation" Submitted to the International Journal of Solids and Structures on May 16, 2012.

Items 1, 2, and 3 were presentations at international meetings and publications in the associated conference proceedings. Item 4 has been reviewed and the requested revisions are in progress with resubmission anticipated during August 2012.

Stress Attenuation by Means of Particulates

Carl-Ernst Rousseau
Mechanical Engineering; University of Rhode Island

Objectives:

The objective of this work is to identify effective means of stress wave mitigation. Traditional shielding techniques have consisted in heavy and voluminous metallic barriers that are efficient but cumbersome. The focus has naturally shifted to composites, as they possess lower densities and, though not as effective as metals, have resilience capabilities approaching them. The approach associated with composites has also been highly empirical. For instance, consecutive tests performed on two equivalent types of fibrous composites dictate which is more appropriate to a *specific* shielding task. However, what specific aspect of the material's microstructure ensures this outcome? We endeavor to answer those questions by launching stress waves within these materials and note instances of absorption, reflection, or deflection that reduce or eliminate damage. We aim to do so not only for composites, but also for metals, as we explicitly target the influence of porosity, inclusions, impurities, cell or grain boundaries, and sizes. Finally, complete description of materials for dynamic, stress wave, and shock study or prediction is frequently associated with knowledge of the Hugoniot conditions, which are the results of numerous experimental studies. At present, we hope to be on the verge of developing a technique whereby the Hugoniot can be obtained from the amalgamation of data pertaining to a single experiment. Comprehensive dynamic materials characteristics can thus be readily obtained.

Significance to DHS:

The work performed, its extension and future ramifications are highly relevant to DHS' aim of protection of infrastructure and citizenry. Indeed full comprehension of mechanisms of failure and of its prevention, will allow engineers working in the security field to base choices on sound scientific grounds, and be better able to combine materials characteristics in order to fabricate more effective shields. Also, experimental techniques developed during the course of this study will allow for the application of speedier and more efficient gathering of experimental outcomes, both for ourselves and others in the broader scientific community who elect to use similar techniques.

Accomplishments:

This year, we have authored two papers associated with this work, and we are plan to submit four others during this coming cycle. This year, we have made but one presentation, and have collaborated with the Lawrence Livermore National Lab on identifying the sources of failure initiation in metals. One high school physics teacher, three undergraduate students, two Master's, and one Ph.D. student have worked on DHS related materials in our lab this year.

Details:

Most experiments undertaken for this study were conducted using plate impact within an evacuated chamber, with the use of a single stage helium driven gas gun. The impactors and tested specimens were 45 mm in diameter and, respectively, 5 mm and 10 mm thick. Appended

to the specimens were thick polycarbonate backing windows. Planarity was ensure by impacting the specimens before the sabot fully exited the barrel of the gun.

50 Ω manganin stress gages were embedded between the back surfaces of the test samples and 20 mm thick polycarbonate backing windows. A simple cutoff time criterion for the experiments was estimated under the assumption that the specimen is in a state of one-dimensional strain until radial release waves originating from the sides interact at the center of the specimen. (A schematic explaining the planning of each experiment is adjacent).

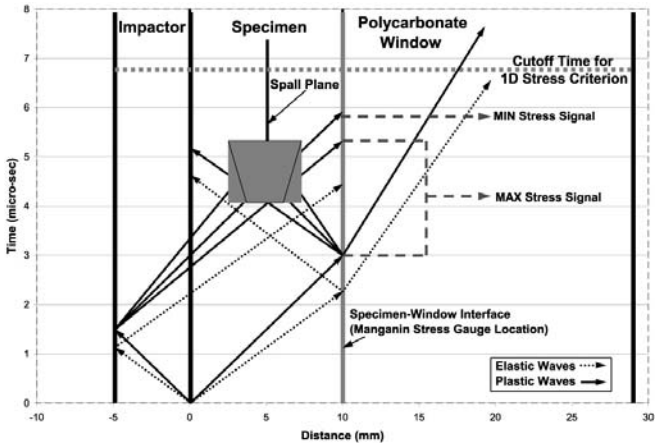

Complete stress history within the impacted specimens were recorded by the gages, providing attenuation and dynamic strength criteria. The impacted specimens were also captured for post mortem analysis utilizing a soft recovery technique by means of clay bricks coupled with a shock absorbing catch box. Recovered specimens were cut through the thickness in order to expose the spall plane for analysis. Cut specimens were sanded and polished to a 3 micron finish for clearer viewing under optical microscope and SEM. Spall planes were categorized into 3 groups: micro-failure start, micro-failure and partial macro-failure, and complete spall fracture. A sample diagnostic image is shown in the adjacent figure, where clusters of fine inclusions (right) are identified as the first location of failure initiation, while regions with larger inclusions (left) remain unaffected.

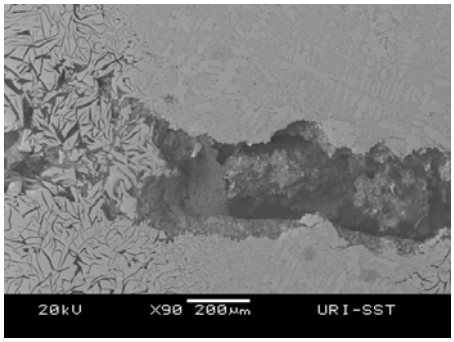

Papers Published:
Plume & Rousseau; "Investigation into the Spall Strength of Cast Iron;" International Journal of Nonlinear Science & Simulations; 2012; 13(2); 195-199

Visser, Sun, Gregory, Plume, Rousseau, Ghonem; "Deformation characteristics of low carbon steel subjected to dynamic impact loading;" Materials Science & Engineering; 2011; 528, 7857-7866.

New Collaboration
Effect of porosity on the performance of cast iron with Lawrence Livermore National Laboratory

Graduate Students
Gifford Plume (2012); Miguel Goni (2013); Michael Franzblau (2013)

Undergraduate Students
Christian Mejia; Jose DeFaria; Sameer Saran

Self Healing Materials for Autonomic Mitigation of Blast Damage

Nancy R. Sottos and Scott R. White
with Jason F. Patrick
Beckman Institute for Advanced Science & Technology; University of Illinois

Objective

This document summarizes research conducted at the University of Illinois over the past three years, in regards to the development of self-healing materials for autonomic mitigation of blast-induced damage. The goal of this project is to develop self-healing composite systems for mitigation of blast damage over a variety of platforms including civil based infrastructure and aerospace vehicles. The intended outcome of this research will not only address issues directly related to protection and recovery of blast-induced damage but also contribute to scientific advancements in the realm of polymer composites. A concise list of research accomplishments motivated by the aforementioned objectives is provided below:

Tasks Accomplished

Prior (Aug. 2009 - July 2011)

- Selection of ideal composite sandwich panel system with regards to blast mitigation performance and realistic integration of self-healing technology.
- Incorporation of bio-inspired microvascular networks into cellular materials to deliver expansive foam healing chemistries suitable for rapid, macro-scale blast damage recovery in polymeric foam sandwich core materials.
- Demonstration of self-healing in a commercial, polyisocyanurate (PIR) foam core using a 3-pt. Single Edge Notched Bend (SENB) mode-I fracture test under quasi-static loading conditions (*Published manuscript* [1]).
- Development of "sacrificial fiber" technology for fabrication of microvascular, fiber-reinforced polymer (FRP) composites (*Published manuscripts* [2, 3]).

Recent (July 2011 - Aug. 2012)

- Extension of the "sacrificial fiber" vascularization (VaSC) procedure to encompass conventional 2D woven FRP composite laminate systems (*Details I*).
- Development of a mechanical testing protocol for evaluation of self-healing performance in 2D woven microvascular composites (*Details II*).
- Demonstration of repeatable in-situ recovery of mode-I interlaminar delamination resistance in 2D woven FRP composites via microvascular delivery of a two-part healing chemistry. (*Details II, manuscript in preparation*).

Summary

Our first milestone was to develop initial specifications for a self-repairing material system based on modern structural requirements for blast resistant composite structures. We completed a

comprehensive survey of state-of-the-art materials and potential failure modes for blast resistant composite structures [4-9]. Based on our review of the literature in this area, we identified 3D woven composite sandwich structures as primary candidates for integration of microvascular, self-healing functionality [10-14]. The unique architecture of 3D woven sandwich panels is favorable for seamless integration of current self-healing technology with little impact on initial mechanical properties. Novel composite sandwich panel configurations such as Transonite® make use of 3D woven E-glass composite skins separated by a polymeric foam core and rigidly connected by through thickness fiber insertions. These panels have been shown to withstand 5 lbs of C4 explosive detonated at a mere 3 ft standoff distance. Depending on the through thickness fiber stitching density, primary failure modes after shock loading include delamination of the face sheets from the core, microcracking in the 3D woven composite face sheets, and fracture proliferation throughout the foam core.

In our initial work [1], we focused primarily on core damage and the development of a self-healing polymeric foam. Blast events predominantly cause the foam core to fracture, significantly reducing structural stiffness and sandwich efficiency of the composite system [9]. Self-healing of core damage will enable recovery of mechanical integrity and result in enhanced resistance to multiple blast events. Conventional polyurethane (PUR) and polyisocyanurate (PIR) foam cores are condensation materials prepared from organic polyisocyanates, polyols, catalysts, surfactants, and a foaming or blowing agent [15]. In typical foam formulations, the polyisocyanate compound is referred to as Part A whereas the remaining materials constitute Part B. Our strategy was to incorporate a vascular network in a closed-cell PIR foam, whereby Parts A and B were sequestered in separate channels of a 3pt. single edge notch bend (SENB) specimen. Upon quasi-static loading and subsequent crack propagation, the healing agents were released and polymerized on contact to regenerate the foam scaffold. Healing efficiencies exceeding 100% were realized through proper selection of the material system and optimization of delivery parameters. The reactive nature of the PUR foam chemistry provided for rapid healing kinetics, with over 75% recovery in both stiffness and fracture toughness in 1 hr at room temperature. Another attractive feature of this system was the volumetric expansion of the healing chemistry, demonstrating the ability to repair macro-scale fractures comparable to damage induced by blast events. Additionally, multiple damage-healing cycles were attained without sacrifice to healing efficiency or structural integrity.

During the second phase of this project, we developed a technique [2, 3] for vascularizing (VaSC) fiber-reinforced polymer (FRP) composites to provide a means for circulation of liquid healing agents throughout the structural composite sandwich panel face sheets. This novel "sacrificial fiber" technology is capable of producing complex vascular networks in a variety of FRP composite reinforcements, providing a conduit for bioinspired dynamic functionality in a multitude of engineering applications. While the initial VaSC demonstration was performed in 3D woven composites, we decided to first pursue self-healing in more conventional 2D woven FRP laminate systems to gain a deeper understanding of the viscous fluid mixing dynamics and healing reaction kinetics involved. A mechanical evaluation procedure based on mode-I interlaminar delamination in a Double Cantilever Beam (DCB) specimen geometry has been developed to accurately assess healing performance. Through careful selection of a two-part epoxy based healing chemistry, improved fluid distribution to the fracture plane via network design, and pressure-based active delivery procedures, multiple damage-healing cycles at nearly

full recovery have been achieved.

Upon completion of the current research efforts pertaining to self-healing in 2D woven systems, investigation into the damage mechanisms and microvascular based recovery in 3D woven FRP composites will commence. Subsequent work will focus on the total integration of microvascular foam core and composite face sheet components into a state-of-the-art self-healing structural sandwich panel.

Students Supported

PhD candidate in Civil Engineering at UIUC
(emphasis in mechanics & materials)

Jason F Patrick

Undergraduate in Aerospace Engineering at UIUC
(interest in structural aircraft design)

Laura K Richardson

Transition Partners

3TEX Inc.

Industrial weaving of "sacrificial fibers" to produce 3D non-crimp orthogonal (3WEAVE™) microvascular composite textile preforms.

Patents

1. Esser-Kahn, H. Dong, P.R. Thakre, J.F. Patrick, N.R. Sottos, J.S. Moore, S.R. White, "Micro-Vascular Materials and Composites for Forming the Materials", UIUC TF 10047, **US Patent Application** 13/416,002 *filed* March 9, 2012.

2. J.F. Patrick, K.R. Hart, N.R. Sottos, J.S. Moore, S.R. White, "A Microvascular Based Self-Healing Fiber Reinforced Polymer Composite", University of Illinois at Urbana-Champaign **Invention Disclosure** *submitted* April 2, 2012.

Publications

1. A. Esser-Kahn, P. Thakre, H. Dong, J. Patrick, V. Vlasko-Vlasov, N. Sottos, J. Moore, and S. White, Three-Dimensional Microvascular Fiber-Reinforced Composites, *Advanced Materials*, **23**, 3654-3658 (2011).

2. H. Dong, A. Esser-Kahn, P. Thakre, J. Patrick, N. Sottos, S. White, J. Moore, Chemical Treatment of Poly(lactic acid) Fibers to Enhance the Rate of Thermal Depolymerization, *Applied Materials and Interfaces*, **4**, 503-509 (2012).

3. J. Patrick, N. Sottos, S. White, Microvascular Based Self-Healing Polymeric Foam, *Polymer*, DOI: 10.1016/j.polymer.2012.07.021 (2012).

4. J. Patrick, K. Hart, N. Sottos, S. White, Self-Healing in a 2D Woven Composite via Bioinpsired Microvascular Networks, *In Preparation.*

Presentations

1. J. Patrick, D.J. Fairfield, N. Sottos, S. White, Microvascular Based Self-Healing Polymeric Foam. 3rd International Conference on Self-healing Materials, Bath, UK, June, 2011.

2. J. Patrick, K. Hart, S. White, N. Sottos, J. Moore, Microvascular Based Self-Healing 2D Woven Composites. American Society of Composites 27th Technical Conference, Arlington, TX, *scheduled* October 2012.

Details I: Vascularization of Fiber-Reinforced Polymer Composites

The recently developed process (Figure 1) designated 'Vaporization of Sacrificial Components' (VaSC), integrates a commercially available biopolymer fiber into existing textile composite reinforcement manufacturing techniques to imbue FRP composites with three-dimensional vasculature.

In VaSC a robust, chemically treated [2, 3] thermoplastic monofilament deemed 'sacrificial fiber' is directly woven into composite textile reinforcement (Fig. 1a). Upon subsequent epoxy resin infusion (Fig. 1b), vacuum/pressure compaction, and elevated temperature post-curing, the fibers sublimate via thermal depolymerization leaving behind high fidelity, inverse replica vascular features (Fig. 1c). The resulting vascularized composite permits the circulation of fluids (Fig. 1d) through its internal structure, providing a conduit for dynamic functionality. In addition to self-healing capability, vascular composites also accommodate multiphysical properties such as thermal regulation and electromagnetic modulation via a simple substitution of fluids.

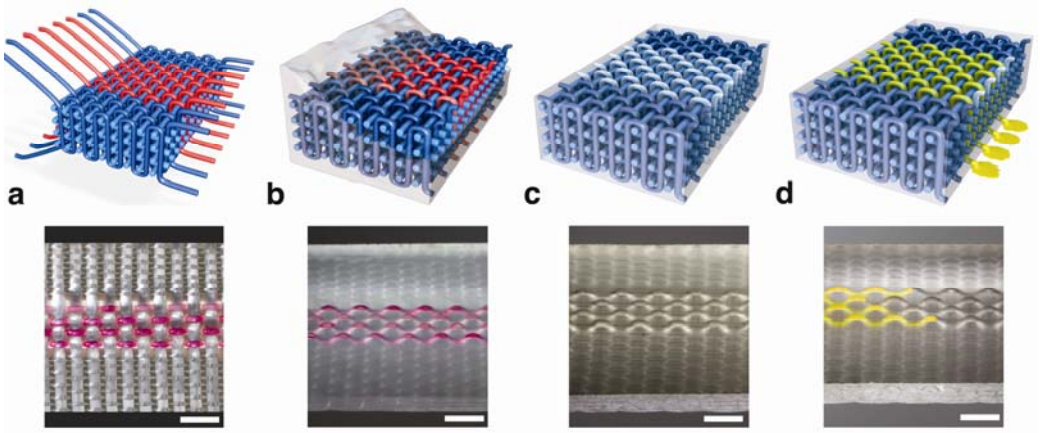

Figure 1. VaSC fabrication procedure. **(a)** 'sacrificial fibers' (red) woven into glass reinforcing fabric; **(b)** infiltration of polymer resin into composite preform; **(c)** matrix solidification and subsequent thermal depolymerization resulting in vascularized structural composite; **(d)** fluid filled (yellow) microchannels (scale bars = 5 mm). Image from Esser-Kahn et al. [2].

The initial VaSC demonstration was performed in 3D woven fiber reinforced composites (FRC), mainly to showcase the commercial practicality and complex geometric possibilities in vascular design [2, 8], although the technique is amendable to alternative reinforcement. Over the past year, we successfully applied the VaSC technique to develop self-healing 2D woven composites for blast applications.

Details II: Self-healing in 2D Woven Microvascular Composites

In order to assess microvascular-based healing performance in a 2D woven FRC laminate, the Double Cantilever Beam (DCB) mode-I interlaminar fracture test was selected with relevant experimental parameters depicted in Figure 2a [16-18]. An 8-harness (8H) satin weave (9 oz./yd^2, E-glass) fabric reinforcement was chosen due its prevalence in composite structures, and more importantly the stable crack growth resistance (R-curve) behavior (Figure 2b) exhibited during DCB testing under displacement controlled loading [17-19]. The predominantly constant R-curve provides a suitable basis for using the tensile opening (mode-I) strain energy release rate (G_I) as a metric to quantify healing efficiency [20, 21] according to:

$$G_I = \frac{3P\delta}{2ba} \tag{1}$$

where P is the applied load, δ is the load-line displacement, b is specimen width, and a is delamination length.

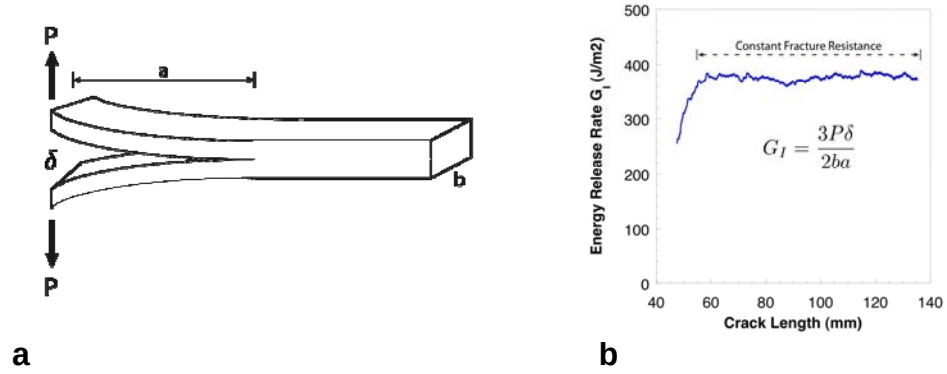

Figure 2. **(a)** Schematic of Double Cantilever Beam (DCB) mode-I fracture specimen; **(b)** Experimental crack growth resistance (R-curve) behavior for 2D woven 8-harness satin (9 oz./yd^2) E-glass composite (Note: fracture along warp direction).

DCB samples were quasi-statically loaded under displacement (δ) control at a rate of 5 mm/min. Illuminating the translucent, E-glass composite samples from below enhanced visual observation of crack propagation using both top and side mounted CCD cameras. Delamination length measurements were determined in 5 mm increments, per ASTM D-5528, from images taken every 2 seconds. Corresponding mode-I strain energy release rates (G_I) were calculated according to Equation (1).

Based on the success of self-healing in polymer systems via microvascular delivery of a two-part epoxy [10-14], a dual-channel 2D woven fiber-reinforced composite DCB specimen was designed (Figure 3). Equipped with new capabilities in network architecture as a result of the VaSC technology [2], undulating through-thickness microchannels were incorporated via stitching to ensure rupture and fluid release upon interlaminar crack advance. The longitudinally 'parallel' channels were placed in close proximity (5mm) to accommodate diffusive mixing of actively delivered (pumped) liquid healing agents. As an extension of the 'parallel' design, a more complex 'herringbone' vascular architecture was constructed to further promote in-situ mixing of reactive healing agents and increase delamination recovery (Figure 4).

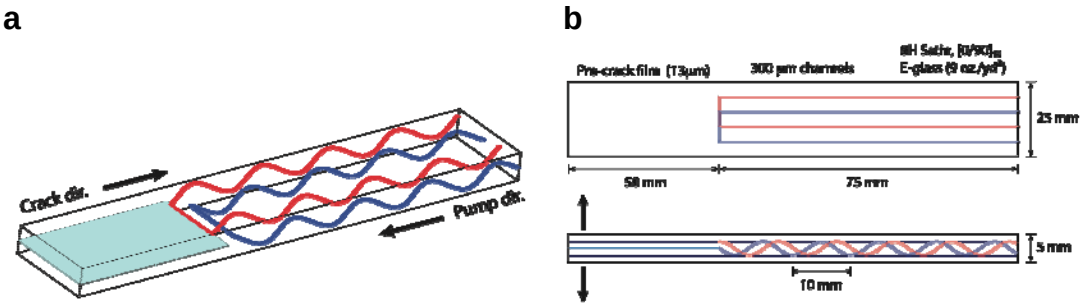

Figure 3. **(a)** Dual channel (red/blue) self-healing microvascular DCB concept; **(b)** Physical sample dimensions and layup details for composite fabrication.

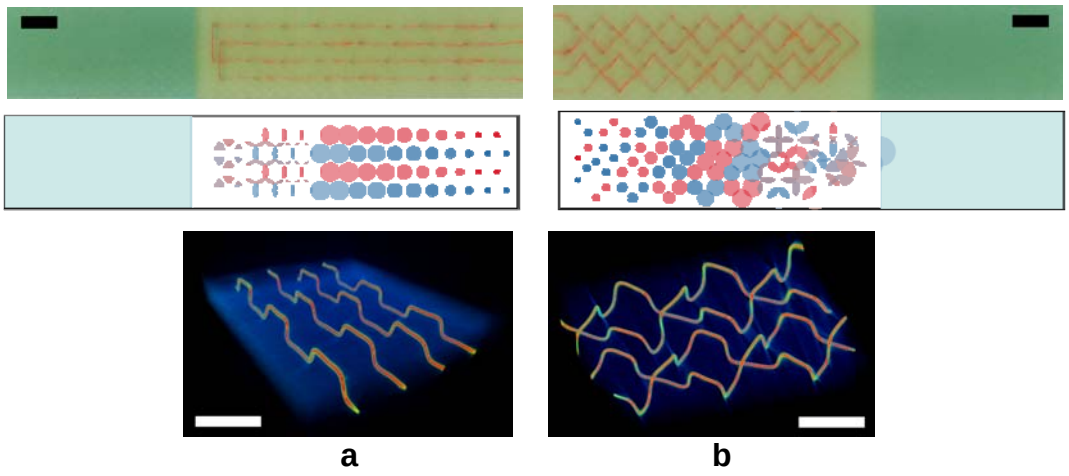

Figure 4. Microvascular network configurations investigated **(a)** Parallel **(b)** Herringbone; (Top): pre-vascularized composite samples showing embedded 300 μm "sacrificial fibers"; (Middle): idealized two-part liquid healing agent distributions on fractured surfaces; (Bottom): post-vascularized x-ray computed tomographic (μCT) images of liquid gallium-indium filled networks revealing internal channel structures (scale bars = 10mm).

In a series of healing experiments, two-part liquid epoxy components were precisely delivered using a computer controlled syringe pump. Initially, each microvascular channel was prefilled with the desired healing agent by pumping through one channel opening and subsequently connecting at the second aperture resulting in a closed system (Figure 5a). Next the 'virgin' self-healing DCB samples were loaded to propagate the pre-crack and fracture through the channels (Figure 5b) resulting in fluid release. Healing agents were concurrently delivered (1:1) at a rate of 50 μL/min until a delamination length of 40mm was reached. With the pumping stopped, the samples were then unloaded while the delivered portions of healing agents dispersed across the fractured surface to promote mixing. The samples were allowed to heal in a 30°C oven for 48 hours (same conditions in [10-11, 13-14] for consistency).

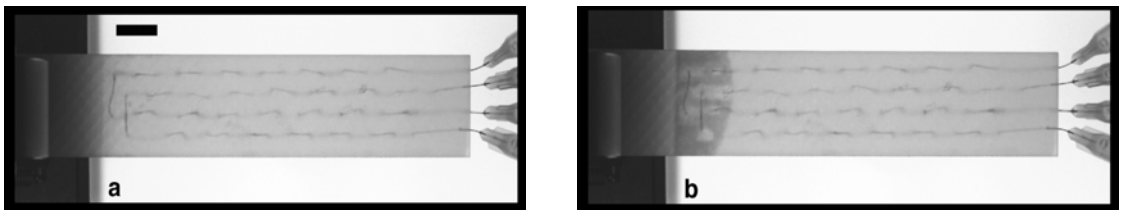

Figure 5. Overhead CCD images captured during DCB (parallel) loading sequence **(a)** intact micro-channels; **(b)** crack (shaded region) has ruptured both networks releasing healing agents; (scale bar = 5 mm).

Healing efficiency (η_G), or recovery in mode-I strain energy release rate, was appropriately quantified in this study by [16, 20-22]:

$$\eta_G \equiv \frac{G_I^{Healed}}{G_I^{Virgin}} \tag{2}$$

Representative healing efficiencies versus crack length for both 'parallel' and 'herringbone' specimens using the syringe pump delivery procedure are provided in Figure 6a. While a relatively constant delamination propagation region characterized the 'virgin' R-curves (Figure 2b), the 'healed' crack growth resistance behavior was more erratic as a result of non-uniform in-situ mixing/polymerization, reflected in the fluctuating healing efficiency behavior. The 'herringbone' channel design exhibited higher average healing efficiencies (89% ± 15.2) compared to the 'parallel' (40% ± 1.7) configuration (3 samples each), which is partially attributed to enhanced in-situ mixing as a result of improved fluid interspersion on the fractured surfaces (Figure 4, 6b). Although, only a single heal cycle (for both sample types) was achieved via syringe pump delivery due to cross-contamination and ensuing polymerization inside the microchannels, thereby obstructing additional fluid delivery to the fracture plane.

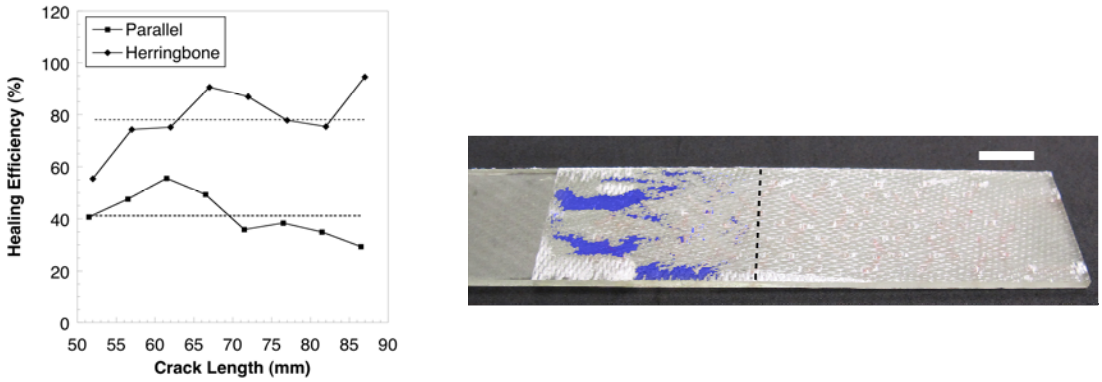

Figure 6. **(a)** Representative healing efficiency (η_G) results for 'parallel' and 'herringbone' patterns after delivery of a two-part epoxy (1:1) at 50 µL/min over a 40 mm delamination length and allowed to heal for 48 hrs at 30°C (dashed lines indicate average values). **(b)** healed fracture surface of a 'herringbone' DCB sample indicating the sparse regions (blue color overlay) of unpolymerized material due to enhanced fluid mixing as a result of improved channel design; (scale bar = 10 mm).

While the latest experimental findings mark the first true demonstration of in-situ microvascular self-healing in a FRC via active delivery of a two-part epoxy, additional investigations are required to unravel the governing physics and reach full self-healing potential. Another immediately relevant research objective is to determine the effect of vascular features and/or VaSC processes employed to create these dynamic composites, on the mechanical integrity of the native structural material [23, 24]. A series of standardized mechanical tests [18, 25-26] will be conducted in order to develop a comprehensive understanding of the material response.

Once the 2D FRC vascular self-healing systems have been well characterized, our research efforts will move towards developing similar damage-healing protocols for 3D woven microvascular composites. The ultimate goal of our anticipated research and development program is to combine the stand alone microvascular FRC and polymer foam self-healing technologies into a single composite structural sandwich panel capable of unprecedented, autonomic blast protection.

REFERENCES

1. J. Patrick, N. Sottos, S. White, Microvascular Based Self-Healing Polymeric Foam, Polymer, DOI: 10.1016/j.polymer.2012.07.021 (2012).
2. A. Esser-Kahn, P. Thakre, H. Dong, J. Patrick, V. Vlasko-Vlasov, N. Sottos, J. Moore, and S. White, Three-Dimensional Microvascular Fiber-Reinforced Composites, *Advanced Materials*, **23**, 3654-3658 (2011).
3. H. Dong, A. Esser-Kahn, P. Thakre, J. Patrick, N. Sottos, S. White, J. Moore, Chemical Treatment of Poly(lactic acid) Fibers to Enhance the Rate of Thermal Depolymerization, *Applied Materials and Interfaces*, **4**, 503-509 (2012).
4. J. Baucom, M. Zikry. Evolution of Failure Mechanisms in 2D and 3D Woven Composite Systems under Quasi-static Perforation. Journal of Composite Materials, **45**, 1651-1674 (2003).
5. J. LeBlanc, A. Shukla, C. Rousseau, A. Bogdanovich. Shock Loading of three-dimensional woven composite materials. *Composite Structures*, **79**, 344-355 (2007).
6. J. Grogan, S. Tekalur, A. Shukla, A. Bogdanovich, A. Coffelt. Ballistic Resistance of 2D and 3D Sandwich Composites. *Journal of Sandwich Structures and Materials*, **9**, 283-302 (2007).
7. J. Patrick, "Fundamental Characteristics of 3-D GFRP Pultruded Sandwich Panels." *M.S. Thesis*, Department of Civil and Environmental Engineering, North Carolina State University, Raleigh, NC (2007).
8. A. Bogdanovich, M. Mohamed, Three-Dimensional Reinforcements for Composites, *SAMPE Journal*, **45(6)**, 2-20 (2009).
9. S. Tekalur, A. Bogdanovich, A. Shukla. Shock loading response of sandwich panels with 3-D woven E-glass composite skins and stitched foam core. *Composites Science and Technology*, **69**, (2009).
10. A. Hamilton, N. Sottos, S. White, Pressurized vascular systems for self-healing materials, *Journal of the Royal Society Interface*, **9(70)**, 1020–1028 (2012).
11. A. Hamilton, N. Sottos, S. White, Self-healing of internal damage in synthetic vascular materials, *Advanced Materials*, **22**, 5159–5163 (2010).
12. C. Hansen, S. White, N. Sottos, J. Lewis, Accelerated Self-healing via ternary interpenetrating microvascular networks, *Advanced Functional Materials*, **21**, 4320-4326 (2011).
13. C. Hansen, W. Wu, K. Toohey, N. Sottos, S. White, J. Lewis, Self-healing materials with interpenetrating microvascular networks, *Advanced Materials*, **21**, 4143–4147 (2009).
14. K. Toohey, C. Hansen, N. Sottos, J. Lewis, S. White, N. Sottos, Delivery of two-part self-healing chemistry via microvascular networks, *Advanced Functional Materials*, **19**, 1399–1405 (2009).
15. M. Kapps, S. Buschkamp, The production of rigid polyurethane foam, Technical Report, Bayer Material Science, (2004).
16. M. Kessler, S. White, Self-activated healing of delamination damage in woven composites, *Composites A*, **32**, 683–699 (2001).
17. J. Whitney, C. Browning, W. Hoogsteden, A Double Cantilever Beam Test for Characterizing Mode I Delamination of Composite Materials, *Journal of Reinforced Plastics and Composites*, **1**, 297-313 (1982).

18. ASTM International, ASTM D5528: Standard Test Methods for Mode I Interlaminar Fracture Toughness of Unidirectional Fiber-Reinforced Polymer Matrix Composites (2007).
19. N. Alif, L. Carlsson, L. Boogh, Effect of weave pattern and crack propagation direction on mode I delamination resistance of woven glass and carbon composites, *Composites Part B*, **29**, 603-611 (1998).
20. S. White, N. Sottos, P. Geubelle, J. Moore, M. Kessler, S. Sriram, E. Brown, S. Viswanathan, Autonomic healing of polymer composites, *Nature*, **409**, 794–797 (2001).
21. E. Brown, Use of the tapered double-cantilever beam geometry for fracture toughness measurements and its application to the quantification of self-healing, *Strain Analysis for Engineering Design*, **46**, 167–186 (2011).
22. J. Rule, E. Brown, N. Sottos, S. White, J. Moore, Wax-Protected Catalyst Microspheres for Efficient Self-Healing Materials, *Advanced Materials*, **17**, 205-208 (2005).
23. A. Kousourakis, A. Mouritz, M. Bannister, Interlaminar properties of polymer laminates containing internal sensor cavities. *Composite Structures*, **75**, 610–618 (2006).
24. A. Kousourakis, M. Bannister, A. Mouritz, Tensile and compressive properties of polymer laminates containing internal sensor cavities, *Composites A*, **39**, 1394-1403 (2008).
25. ASTM International, ASTM D3039: Standard Test Methods for Tensile Properties of Polymer Matrix Composite Materials (2008).
26. ASTM International, ASTM D7264: Standard Test Methods for Flexural Properties of Polymer Matrix Composite Materials (2007).

Self-Healing Concrete

Anjii Bose; University of Rhode Island

1. Objective: Develop a class of concrete that has autonomous healing properties – self-healing concrete

2. Summary: Polyurethane microcapsules containing a sodium silicate solution are encapsulated in concrete. Upon crack initiation, the capsules break. The sodium silicate solution is released into the crack by capillary action, and reacts with the calcium hydroxide to form a C-S-H gel that partially heals the crack.

3. Accomplishments: (i) Samples with capsules located only in regions where concrete experiences tension recover flexural strength more than in samples where capsules are distributed throughout. (ii) Water containing capsules appear to be as efficient as those containing sodium silicate solution (iii) Capsules do not break during mixing, but only upon crack initiation.

4. Details:

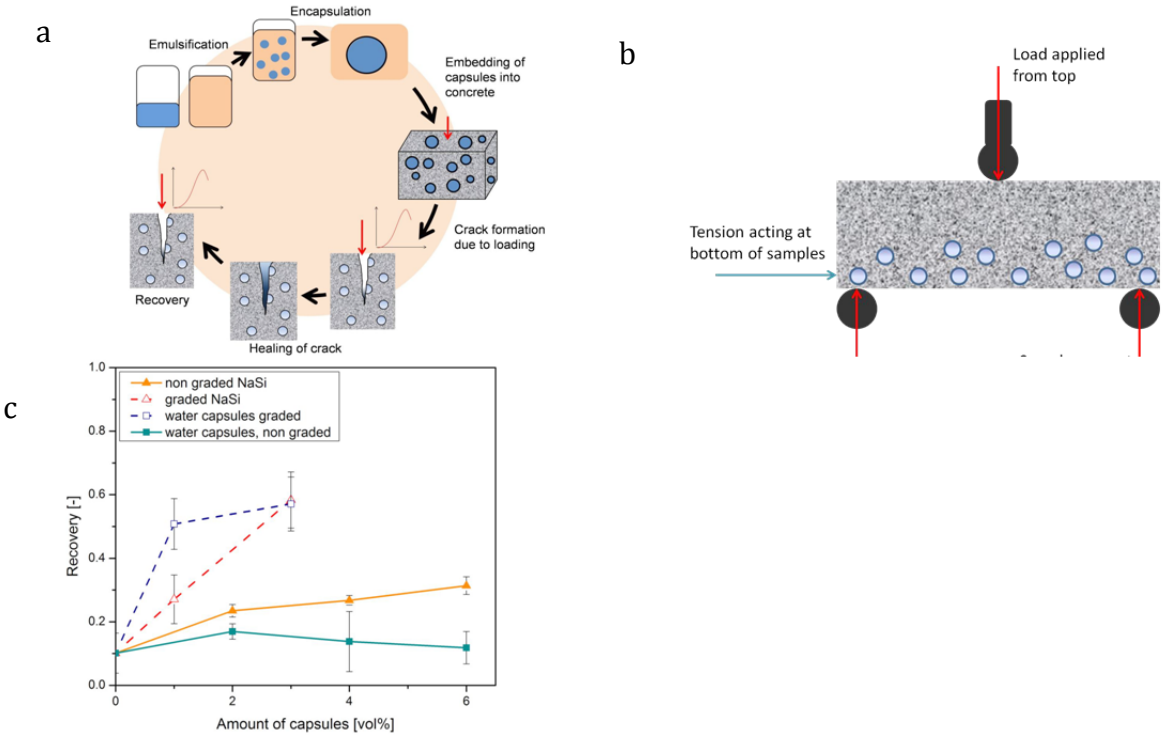

Figure 1. (a) Overall scheme and principle of self-healing concrete (b) Flexural strength test (c) Comparison of results from graded and non-graded samples. The graded samples show better recovery than those that are not.

5. Students Supported: Triparna Bhattacharya, Svenja Reinke, Lindsay Lozeau

6. Transition Partners: CEMEX – Brugg, Switzerland

7. Publications: (i) Self-healing Concrete, M. Pelletier, T. Bhattacharya, A. Bose, submitted to **Journal of Concrete Research,** submitted (2012). (ii)Optimization of Autonomous Healing Properties of Concrete Using Microcapsules with Healing Agents, S. Reinke, L. Lozeau, A. Shukla, R. Brown, A. Bose, **Journal of Concrete Research**, submitted (2012)

8. Presentations: (i) Self-healing Concrete, M. Pelletier, T. Bhattacharya, A. Shukla, R. Brown, A. Bose, RIDOT Annual Meeting, Providence, October 2011 (ii) Self-healing Concrete, S. Reinke, T. Bhattacharya, A. Shukla, R. Brown, A. Bose, DHS Center Annual Review, Kingston, April 2012.

Water Blast Mitigation

S. F. Son (PI), A. J. Zakrajsek, L. J. Groven, and D. R. Guildenbecher

School of Mechanical Engineering, Purdue University

West Lafayette, Indiana

September, 2012

1. Objective

The purpose of this study is to investigate the effectiveness of water as a blast mitigant. Water blast mitigation is being investigated in multiple configurations including: solid water barriers, water sprays and water sheets. An explosion yielding a blast wave can cause catastrophic damage to a building and its personnel. This threat defines an immediate importance for understanding blast mitigation techniques via readily available materials. Specific blast mitigation techniques using water are being studied with the motivation of protecting high-risk targets from damage. An initial understanding of the mitigating mechanisms, along with the experimental results from each configuration is presented here.

2. Summary

Since 1968, bombing has accounted for nearly half of international terrorist attacks [1]. A Department of Homeland Security (DHS) brief on the treat of domestic improvised explosives devices (IEDs) indicated that there is increased terrorism intent on attacking high risk targets [2]. Overall a blast wave from a nearby explosive can cause catastrophic damage to an intended target [3]. These simple findings present the immediate importance of protecting high risk structures by being able to mitigate incident blast waves.

For the purpose of this research, water is being studied as a readily available mitigant. Four different water configurations have been designed and tested to provide a detailed overview of the different mitigating mechanisms associated with each configuration. Specific formations of water may be able to protect high risk targets during an elevated warning level, or when a visible threat is detected.

3. Accomplishments

Four different water configurations have been designed, and tested to date. These configurations include solid water barriers, water sprays, and water sheets. Each water configuration provided different insight into different mitigating principles. These blast mitigating principles can not only be applied to water blast mitigation, but other forms of blast mitigation. Overall the water sheet performed the best, mitigating the peak overpressure and impulse of the blast up to 82%, and 77% respectively. These results point out possible advantages of using an unconfined sheet of water as a blast mitigant. This has also motivated consideration of a non-contact water filled barrier and some initial experiments were performed with this. This work motivated collaboration with other Purdue University researchers that have developed blast/impact pads. This work was leveraged with internal funding to obtain data for this and a patent disclosure was submitted. The student supported by this work successfully completed his MS work and is now working for the Air Force Research Laboratory. A visiting professor partially supported by this work is now employed at Sandia National Laboratory.

4 Details

This past year our focus has been mainly on water barriers and these results were reported in a journal submission. They also appear in Andrew Zakrajsek's 2012 M.S. thesis. This work is summarized in the Appendix that follows. In addition to this we built a small-scale water sheet experiment using a shock tube and also did some exploratory experiments. We also did some initial stand off water barriers that show promise. This configuration may be more practical than water sheets.

A new pad system was tested using internal funding and leveraging this effort. Figure 1 shows a summary of those results and comparison with a water filled pad.

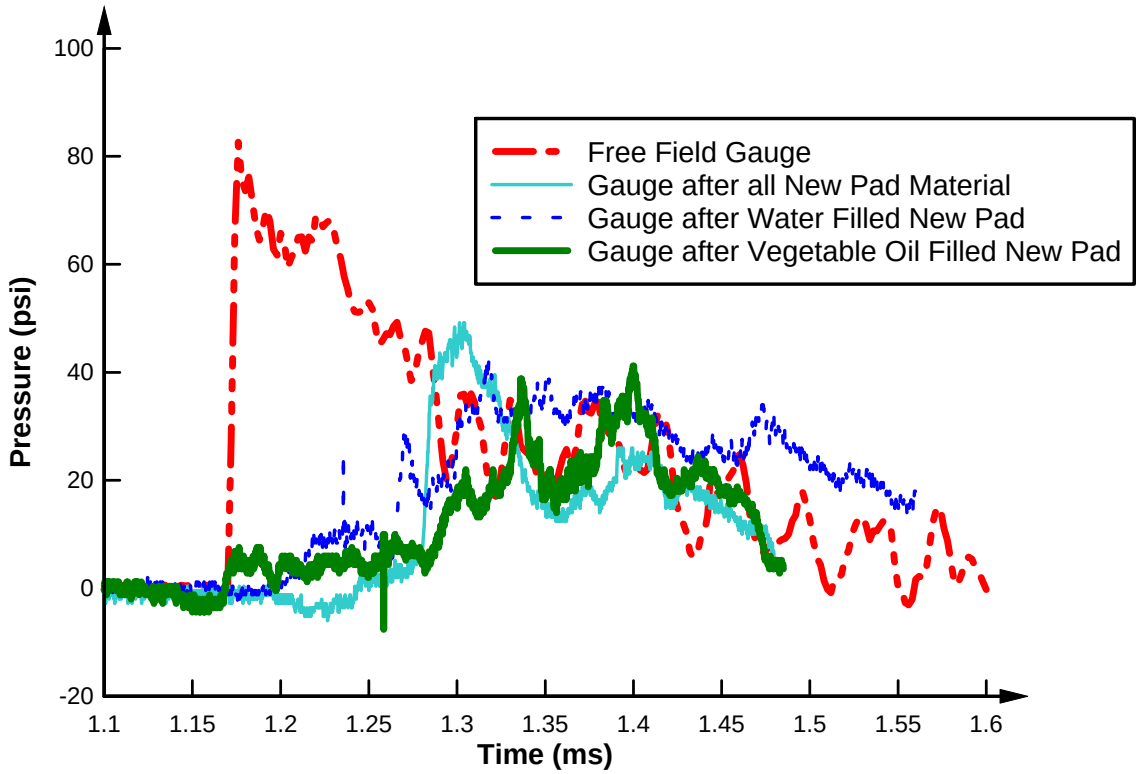

Fig. 1. Pad mitigation results.

5. Students Supported

Andrew Zakrajsek (graduated)

6. Conference and Journal Publications

- We submitted results to the Journal of Shock Waves within the next few months.
- Leverage internally funded work and submitted a patent disclosure on new pad materials.
- A poster was presented at DHS Review Meeting for ALERT research projects.

7. Future Work

This work will not continue this next year.

8. Acknowledgements

We would like to thank the Department of Homeland Security and the Center of Excellence for Explosive Detection, Mitigation and Response, Sponsor Award No. 080409/0002251.

9. Appendix: Submitted Paper.